RELIABILITY ANALYSIS OF EXTERNALLY BONDED FRP STRENGTHENED BEAMS CONSIDERING EXISTING CONDITIONS: APPLICATION OF STOCHASTIC FE AND CONDITIONAL PROBABILITY

by

Connor Petrie

Submitted in partial fulfillment of the requirements
for the degree of Master of Applied Science

at

Dalhousie University
Halifax, Nova Scotia
August 2022

DEDICATION PAGE

I would like to dedicate this thesis to my mother, Rita Larose, and father, Joseph Petrie, for their endless support and push to pursue my passions in higher education. To my two best friends Justin and Mitch, without you two being in my life throughout this journey I would not have been as successful as I have been. Support is everything.

TABLE OF CONTENTS

LIST OF TABLES

LIST OF FIGURES

ABSTRACT

The use of externally bonded (EB) fiber reinforced polymer (FRP) to strengthen existing reinforced concrete (RC) flexural members is becoming a more heavily used practice in North America due to the advantages FRP has shown over conventional reinforcing in rehabilitation. This has led to a large field of research into the design and optimization of EB FRP, in which several design standards in North America have been issued to guide the design, including CSA S806, ACI 440.2R, and provisions in CSA S6 and AASHTO LRFD. Existing design standards lack guidance on accounting for the existing conditions of the member before strengthening. The existing condition in this context can refer to either the condition of loading or resistance of the member prior to strengthening that can affect the reliability. For loads, this is the type and magnitude of the loads seen to date. For resistance, this could represent the spatial change in physical properties of the concrete or steel reinforcement before strengthening.

In this research, several reliability-based frameworks are developed to investigate the effect of accounting for the existing conditions of an existing beam on its strengthened reliability. Each chapter is a standalone paper starting with the literature review. Based on identified research gaps in the literature review, the work is divided into three topic chapters: i) Stochastic FE (SFE) Monte Carlo simulation (MCS) reliability analysis of flexural strengthened RC beams considering random fields for concrete and bond strength, ii) Optimization of the computation of SFE reliability analysis through clustered active-learning kriging (AK-cluster) MCS, and iii) Reliability analysis considering load type and history of existing members for strengthening RC flexural members. Several FRP design standards are considered in the analysis.

Summary tables of EB FRP random variable input statistics used in literature are provided as a reference point for calibration, as no agreement on a unified set of statistics has been shown. An LS-DYNA-Python-MATLAB interphase has been proposed to conduct automated SFE-MCS analysis. A total of 4,066 stochastic FE strengthened beam models have been generated and evaluated to establish the resistance statistics using the proposed interface. Results show that the spatial variation of the concrete can be captured through SFE, but calibration of the stochastic inputs is needed for proper representation of the random field. Reduction in the number of calls to SFE models has been shown possible using AK-cluster techniques. Design aids have been produced to consider the load history of the existing beam. Results show that optimization of EB FRP design is possible considering both the existing conditions of loads and spatial variability of concrete. Further optimization could be possible by considering reliability-based strain limits on the FRP.

LIST OF ABBREVIATIONS AND SYMBOLS

ACI	American Concrete Institute
AK	Active-learning Kriging
ASHTTO	American
CFRP	Carbon fiber reinforced polymer
CHBDC	Canadian Highway Bridge Design Code
COV	Coefficient of Variation
CSA	Canadian Standards Association
DLS	Durability Limit State
EB	Externally-bonded
EB FRP	Externally-bonded Fiber Reinforced Polymer
EM	Element Mesh (FE)
FE	Finite Element
FLS	Fatigue Limit State
FORM	First-Order Reliability Analysis
FOSM	First-Order Second Moment
FRP	Fibre-Reinforced Polymer
GPa	Giga-pascal (Unit)
GFRP	Glass Fibre-Reinforced Polymer
IFC	Intermediate Crack De-bonding (FRP)
IS	Importance Sampling
LHS	Latin Hyper Cube Sampling
LRFD	Load and Resistance Factor Design
MCS	Monte Carlo Simulation
MPa	Mega-pascal (Unit)
MP	Mid Point
MPP	Most Probable Point (Design Point)
NBCC	National Building Code of Canada
OLE	Optimal Linear Estimator
PSO	Particle Swarm Optimization

PPD	Polynomial Dimensional Decomposition
PDF	Probability Density Function
RC	Reinforced Concrete
RV	Random Variable
SLS	Serviceability Limit State
SF	Shape Function
SA	Spatial Average
SSFEM	Spectral Stochastic Finite Element Method
SAR	Structural Assessment and Retrofit
SEM	Stochastic Element Mesh
SFE	Stochastic Finite Element
TV	Time Variant
UR	Utilization Ratio
ULS	Ultimate Limit State
$3D$	Three-dimensional
$2D$	Two-dimensional
β	Reliability index
β_t	Target reliability index
β_{frp}	Angle of FRP strips (shear)
ε_{frpu}	FRP ultimate tensile strain
ψ_L	Measured-to-design-live-load ratio
ψ_D	Measured-to-design-dead-load ratio
μ_{M_u}	Mean Ultimate Moment Resistance
$\mu_{f_c'}$	Mean Concrete Strength (Random Field)
ζ_{cr}	Corrosion model error
ζ	FRP resistance model error
ρ_{ij}	Correlation function
σ	Standard deviation
σ_{norm}	Program calculated normal stress (LS DYNA)
σ_{shear}	Program calculated shear stress (LS DYNA)

ε_{cu}	Maximum strain in concrete
λ	Bias (Experimental/Nominal)
ϕ_s	Material resistance factor for steel (CSA).
ϕ_c	Material resistance factor for concrete (CSA).
ϕ_{frp}	Material resistance factor for EB FRP (CSA).
ϕ	Overall strength reduction factor (ACI).
A_b	Cross-sectional area of a steel reinforcing bar.
A_s	Area of steel (Tension)
A'_S	Area of steel (Compression)
A_{frp}	Total cross-sectional area of GFRP reinforcement in a given section
b	RC beam width
C_S	Chloride concentration
$COV_{f'_c}$	Coefficient of variation of concrete compressive strength
C_{th}	Corrosion threshold
C_{pit}	Corrosion coefficient
C_{yy}'	Covariance matrix
d/h	Depth to height ratio of the concrete section
D/L	Dead-to-live-load ratio
DL	Dead load
D_{cl}	Chlorine diffusion coefficient
E_c	Concrete modulus of elasticity
E_{frp}	FRP modulus of elasticity
E_s	steel modulus of elasticity
f'_c	ultimate concrete compressive strength
f_{frp}	FRP ultimate tensile strength
f_y	yield strength of steel
$G(X)$	Performance (limit state) function of X
G_f	Fracture energy to initate EB FRP debonding.
h	RC beam height
$\widehat{H}(Y,\theta)$	Matrix of random field realizations

k_{eff}	EB FRP anchorage efficiency factor
L_{pit}	Pitting length
$L(X)$	Load effect model (demand) of *X*
LL	Live load
M_u	Ultimate moment resistance (unfactored)
M_R	Ultimate unstrengthened moment resistance (factored)
M_S	Ultimate strengthened moment resistance (factored)
M_S/M_R	EB FRP strengthening factor
M_{err}	LS DYNA model error (EXP/FE)
N	Number of trials in MCS.
$NFLS$	Normal failure limit stress
P_f	Probability of failure
Q	Representation quality factor (random field)
$R(X)$	Resistance model (capacity) of *X.*
RH	Relative humidity
S_{frp}	Spacing of FRP strips (shear and flexure)
$SFLS$	Shear failure limit stress
$T2L$	Transformation to load effect
t_{frp}	FRP laminate thickness
w_{frp}	FRP laminate width
w/c	Water cement ratio
W_{cr}	Surface crack width

ACKNOWLEDGEMENTS

I would first like to acknowledge my supervisor, Dr. Oudah, for his insights, opportunities, and knowledge shared with me during my degree. I would also like to acknowledge the moral and academic support from my peers in the structural assessment and retrofit (SAR) research group. In particular, thank you to Koosha and David for their support in developing and debugging what seemed like endless scripts. Finally, I would like to thank MITACS and NSERC for the financial support, and Norlander Oudah Engineering Limited (NOEL) for both the financial support and guidance, during my research internships.

CHAPTER 1 INTRODUCTION

1.1 GENERAL

Aging existing infrastructure in North America is becoming an increasing issue for civil engineers. It has become essential to find economical ways to extend the service life of these structures in the most environmentally friendly way possible. Fiber-reinforced polymer (FRP) has become a prominent alternative to conventional steel to accomplish this task. FRP is a composite reinforcing material commonly used to strengthen reinforced concrete (RC) structural components, such as beams, columns, and walls (Bakis et al. 2002). Compared with conventional reinforcing materials FRP offers several advantages such as its strength-to-weight ratio, non-conductivity, and non-corrosiveness when exposed to harsh environments (Wu et al. 2014). To strengthen existing infrastructure, FRP can be used through externally bonding (EB) the material to the existing member that may be deficient, or in need of an upgrade. EB FRP strengthening techniques have gained popularity as an alternative to conventional strengthening techniques and research is being conducted into the calibration and optimization of FRP related design standards. A safe design will be one that considered the *existing condition* of the in-service member prior to strengthening in the design of the strengthening upgrades. In this context, the term *existing condition* refers to any condition that changes the ability of the in-service member to resist loads.

The following thesis considers beams designed to three North American design standards; the CSA Design and Construction of Buildings Structures with Fiber Reinforced Polymer (CSA S806:17, 2017), the CSA Canadian Highway Bridge Design Code (CHBDC), Chapter 16 (CSA S6:19, 2019), and the ACI Guide for the Design and Construction of Externally Bonded FRP Systems for Strengthening Concrete Structures (ACI 440.2R:17, 2017). The work considers the design of EB FRP strengthening for beams in flexure, considering the existing condition of the in-

service member prior to strengthening and investigates how it can improve the efficiency of the structural upgrade while meeting target safety limits prescribed by design standards. A literature review on the existing reliability-based work has shown that both the *load history*, and the *spatial variability* of the concrete, in the RC beam are not considered by any of the design codes. Reliability-based frameworks are developed to assess the safety of a set of strengthened beams considering the two existing conditions identified, and its effect on the strengthened reliability of the member.

The following chapter is an introduction to the thesis topic; background on the design of EB FRP strengthened beams, research motivation, and a summary of the thesis structure are provided.

1.2 DESIGN OF EB FRP RC BENDING MEMBERS

The use of EB FRP for the strengthening of RC flexural members can be an effective way to accomplish the need for upgrading the capacity of a deficient member. This is achieved in beams by increasing the capacity of members within the structure through rehabilitation, by bonding EB FRP to the tension face using an epoxy (M4 ISIS, 2004). Figure 1.1 shows a typical cross-section of an RC beam strengthened in flexure at its tension face with EB FRP bonded to the concrete substrate (EB FRP shown in blue). The linear strain and internal force profiles are also shown for the strengthened section, with the components of the steel, concrete, and EB FRP shown. The assumption that plane sections remain plane is employed to maintain strain compatibility through the linear strain profile, where $h, b, d,$ and d' are the height, width, depth to tensile reinforcement, and depth to compression reinforcement, respectively, of the RC beam, ε_{cu} is the strain in the extreme compression fiber of the concrete, ε'_s is the strain in the reinforcement in compression, ε_s is the strain in the internal tensile reinforcement, and ε_{frp} is the strain in the FRP.

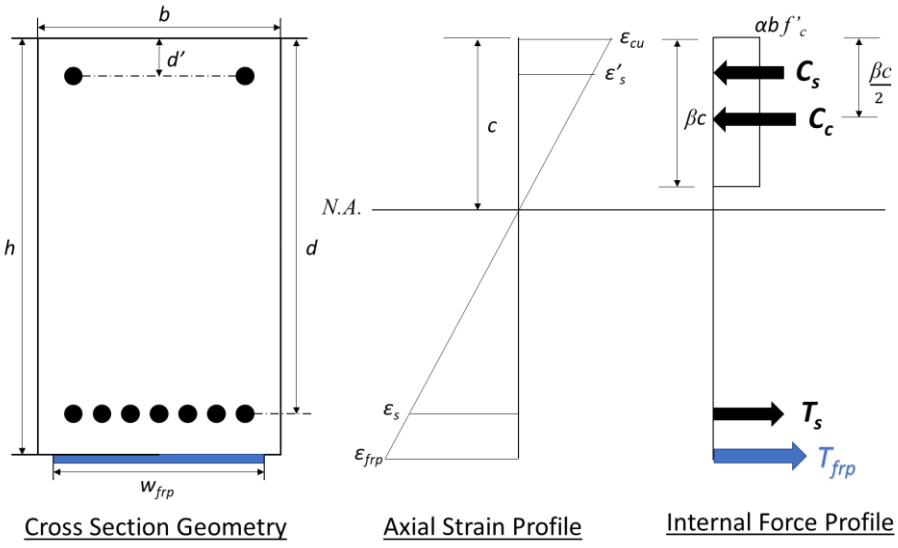

Figure 1.1. Cross-section of strengthened beam; strain, stress, force profiles.

The FRP will have a width, w_{frp}, and a thickness, t_{frp}. Each material will form a force during flexural bending, which is represented by an arrow in the internal force profile. The steel and concrete in compression will form C_s and C_c, respectively, while the tension forces from the steel and FRP will form T_{frp} and T_S, respectively. Depending on if the structure is designed to be tension controlled, or compression controlled, will determine the strain limit used to control the design. For compression-controlled sections, a maximum concrete compressive strain, ε_{cu} = 0.0035 mm/mm, is used for the Canadian FRP design standards (CSA S806:17; CSA S6:19), whereas for the American code the strain is set to ε_{cu} = 0.0030 mm/mm (ACI440.2R:17). If the section is tension-controlled, CSA S806:17 and CSA S6:19 design standards stipulate fixed values for the strain limit on the maximum tensile strain in the EB FRP, ε_{frpu}. ACI440.2R:17 stipulates an equation with an upper bound instead. Table 1.1 shows the strain limits of both CSA and ACI design standards. It should be noted that both CSA code/standard permits the design of sections using tension controlled failure given the factored moment resistance, M_r, be larger than the

factored moment demand, M_f, by a given factor. Clause 16.8.2.2 of CSA S6:19 and Clause 8.2.2 of CSA S806:17 state that if the ULS design of the section is governed by FRP rupture, M_r shall be greater than 1.5 and 1.6 times, respectively, the value of M_f. These factors were not considered in the reliability analysis in this project as the inclusion would increase the reliability index of the strengthened beams to be much greater than even a target reliability index for new construction, as discussed in Section 3.7.4.

Table 1.1. Specified maximum tensile strain in EB FRP, $\varepsilon_{frp.}$ in design standards.

Code / Standard / Guideline	Strain Limit, ε_{frpu} (mm/mm)
CSA S6:19	0.006
CSA S806:17	0.007
ACI 440.2R:17	$0.41\sqrt{\frac{f_c'}{nE_{frp}t_{frp}}} \leq 0.9\varepsilon_{frpu}$

The design equations used to calculate the ultimate moment resistance of the three design standards are summarized in Appendix A. It provides the resistance and load factors, and design equations. Two different approaches are taken by the North American code/standard to calibrate the load and resistance factors based on the aforementioned strain limits on the concrete and FRP. The CSA standards calibrate material factors for the resistance ($\phi_c, \phi_s, \phi_{frp}$) based on the statistics of each material. The American codes on the other hand, calibrates an overall strength reduction factor (ϕ) that is calibrated for a specific component action (i.e., flexure, or shear). Both approaches can be calibrated to meet the same target reliability index value and are typically calibrated for a similar target range.

Several failure modes exist for EB FRP strengthened RC beams in flexure as shown in Figure 1.2. Some of these failure modes such as debonding are unique to EB FRP strengthened members over conventional RC beams with the addition of external reinforcing bonded using epoxy. Figure 1.2 shows the four predominant failure modes considered by the CSA standards and ACI guideline with end debonding not included as it is typically mitigated with end anchorage and proper anchorage length. Rupture of the FRP (Figure 1.2a) and crushing of the concrete (Figure 1.2b) are common failure modes, these will occur after the internal steel reinforcing has yielded, in practice. With the addition of bonded FRP on the tension face of the concrete substrate, additional debonding failure modes are documented in literature (Smith and Teng 2002a, b). Debonding is shown to happen pre-maturely to the concrete crushing, or FRP rupture, and can cause a sudden lost of strength as the FRP peels off the concrete as the bond is broken due to cracks in the concrete reaching the tension face. Critical diagonal cracks (Figure 1.2c) and flexural cracks (Figure 1.2d) reaching the surface of the FRP-concrete bond initiate the debonding.

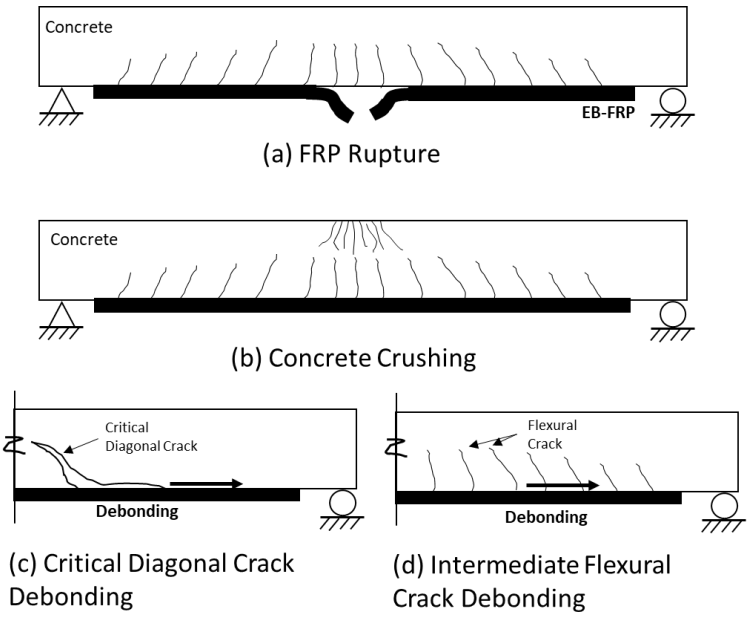

Figure 1.2. Failure modes of EB FRP Strengthened RC Beams in Flexure.

1.3 RESEARCH GAP AND MOTIVATION

Three decades of research in the topic of reinforcing civil structures with FRP has given a breadth of knowledge on the use of EB FRP using reliability-based methods for assessment, optimization of design, and calibration of design standards (CSA S6:19; CSA S806:17; ACI 440.2R:17). These design standards have been developed to deal with the design of FRP, both as internal and external reinforcing, similarly to other CSA or ACI load and resistance factor design (LRFD) design codes (CSA A23.3:19; CSA S16:19; ACI 318:19), using calibrated resistance and load factors. These standards/codes, in the current cycle of revision, have been shown to provide simple designs for flexural members, and can be cost-prohibitive in the amount of EB FRP strengthening prescribed to meet a pre-determined level of safety in some cases (Petrie and Oudah 2021).

Several reliability studies have been conducted on the application of FRP strengthening in flexure (Atadero and Karbhari 2008; Bigaud and Ali 2014; Huang et al. 2019, 2020; Okeil et al. 2002; Plevris et al. 1995; Wang et al. 2010; Wieghaus and Atadero 2011, Wang and Ellingwood 2015), but none addresses the following two considerations, for exiting structures, that impact the structural safety evaluations for EB FRP strengthened RC members designed per the respective standards (CSA S6:19; CSA S806:17; ACI 440.2R:17):

a. The standards/codes do not account for the impact of the spatial variability of the concrete and the bond at the FRP-concrete interface on the structural safety of beams designed per the standards. For example, the CSA S806 and CSA S6 standards stipulate that the existing concrete substrate plays a key role in the effectiveness of the EB FRP strengthening due to the bond (CSA S6:19; CSA S806:17). Though neither standard gives guidance on how to evaluate the effect of the spatial variation of the concrete, as it degrades before strengthening, on the structural safety of beams strengthened by the respective standards.
b. The standards do not consider the effect of satisfactory past performance of existing structures prior to strengthening on updating the load and resistance models for the safety evaluation of the EB FRP retrofit. The satisfactory past performance can be considered by accounting for the load history (type and magnitude) applied to the beam, and reducing the uncertainty around the beam capacity if it is service-proven (Hong 1998).

1.4 OBJECTIVES AND SCOPE

The objective of the thesis is to investigate the effect of considering the aforementioned two predominant existing conditions identified on the design of EB FRP strengthening of RC beams

using reliability-based methods for CSA S806:17, CSA S6:19, and ACI 440.2R:17. The two existing conditions considered are: i) the spatial variation in the concrete strength throughout the member, and ii) existing load type and load history experienced by the existing beam prior to strengthening.

To investigate the first identified existing condition, a reliability-based framework of analysis that utilizes stochastic finite element (SFE) models to capture the spatial variability in existing concrete strength and FRP bond is developed in Chapter 3. The use of SFE models is costly to compute when conducting reliability analysis. To limit the calls to the SFE models, an optimization technique called active-learning kriging (AK) reliability is investigated in Chapter 4, using a surrogate metamodel to predict the limit state. Chapter 5 investigates the second existing condition of load type / history on the strengthened beam. It presents reliability-based design aids, in the form of charts, to aid practicing engineers with the flexural design of EB FRP strengthened beams using CSA S806:17 by accounting for the load history and type experienced by the existing RC beam prior to strengthening.

1.5 THESIS STRUCTURE

This thesis consists of six chapters, a bibliography, and appendices. This thesis is paper based and is a conglomeration of 4 research papers (Chapters 2, 3, 4, and 5), an introduction (Chapter 1), and conclusion (Chapter 6). Chapter 2 is currently being reviewed by the Journal for Composite Construction as a state-of-the-art review. Chapter 5 has been presented and included as part of the ACMBS 2021 conference proceedings (Petrie and Oudah, 2021). Chapter 3 and 4 will be submitted for review in the coming months. The content and description of the comprising chapters are given below:

Chapter 1. *Introduction*. Provides a general introduction into the research topic and describes the need for the project. It also provides a general background into the main aspects of the research while also detailing the objectives and scope of work.

Chapter 2. *Literature Review*. Literature review into the reliability-based work done on EB FRP strengthened members. It discusses the background of the principle of reliability, available literature relevant to the research topics, and provides summary tables of the descriptive statistics (Bias, COV, and Distribution Type) used in reliability analysis. Research gaps around the design of EB FRP strengthening are identified.

Chapter 3. *SFE Reliability Analysis of EB FRP Strengthened RC Beams Considering Random Fields for Concrete and Bond Strength.* Novel framework proposed for conducting SFE reliability analysis using the non-linear FE software LS DYNA. Reliability of strengthened beams designed to CSA S6:19, CSA S806:17 and ACI 440.2R:17 investigated considering the effect of spatial variation of the concrete strength on EB FRP bond. Parametric analysis on several stochastic input parameters is presented. Sensitivity analysis on the effect of the code stipulated strain limit of the FRP is also presented.

Chapter 4. *Stochastic FE Reliability Analysis of EB FRP Strengthened Beams using Active-learning Kriging.* Reliability-based framework presented to assess the strengthened beams from chapter 3 to assess the optimization of computation of AK-SFE-MCS as compared to SFE-MCS. Parametric analysis on the stopping criteria is presented.

Discussion of the AK configuration, clustered learning, and comparison of proposed reliability methods is presented.

Chapter 5. *Reliability-Based Charts Based on Load Type / History for EB FRP Strengthening of Existing RC Flexural Members as per CSA S806:17*. Framework for conduction reliability analysis considering a service proven member is presented. User-friendly design charts are presented for the flexural strengthening of existing RC beams using EB FRP, as per the CSA S806 standard, considering load type and history. A design example is provided for a sample beam.

Chapter 6. *Conclusions and Recommendations*. Provides summary of the steps taken to deliver on the project objectives, presents the significant results from the performed reliability analyses. This chapter presents the final conclusions and design recommendations regarding the project and recommended future research.

CHAPTER 2 LITERATURE REVIEW

2.1 EXECUTIVE SUMMARY

The chapter presents a comprehensive state-of-the-art review of reliability-based analysis of RC structures strengthened using EB FRP. The objective of the chapter is to provide readers with a single-point-of-reference for the *descriptive statistics* (bias, COV, and distribution type), along with the progress in the field. The scope of the chapter includes: i) synthesize the existing research, ii) provide summary tables of the descriptive statistics of the random variables used in reliability analysis, and iii) identify research gaps and recommend future research directions. Review of the principals of reliability is provided as background. A collection of forty-five reliability-based papers on the external strengthening of RC members using FRP have been reviewed herein. These papers cover a wide variety of topics on EB FRP reliability on the different limit states, using various reliability methods to assess the safety of the strengthened members probabilistically. Summary tables on the descriptive statistics and a discussion of current literature are provided. From the literature review, ten primary research directions have been proposed based on the gaps identified: proposing unified reliability input parameters for code calibration, reliability-based calibration of design strain limits of FRP in codes, reliability analysis of FRP anchorage systems, reliability analysis for material resistance factor calibration, reliability analysis for shear and torsion limit states, consideration of time-dependent reliability analysis in design, reliability-based durability limit state, consideration of adaptive reliability methods, consideration of load history in reliability-based optimization of FRP design, and the spatial distribution of FRP properties in the reliability analysis. The last two identified research gaps relate to the existing conditions of the deficient member prior to strengthening. These two research gaps will be the topics of Chapter 3, 4, and 5.

2.2 PRINCIPLES OF RELIABILITY ANALYSIS

A safe design is one that accounts for variations expected from the applied loads, structural resistance, and the method of analysis. To properly account for these variations, reliability-based analysis is conducted to evaluate the structural safety and compare to target values set by standards. The three key components to reliability analysis are briefly described in this section: establishing the performance function; synthesizing the applicable statistical parameters; and the choice of reliability method used for analysis.

Let $G(X)$ be the performance function describing the ultimate limit state (ULS) design of a reinforced concrete (RC) beam strengthened using EB FRP. The ULS in this context can be related to flexural or shear behavior. The limit state function, $G(X)$, can be written as a linear combination of the resistance, $R(X_R)$ and load, $L(X_L)$, as shown in Eq.[2.1], where the vector X is composed of random variables related to the structural resistance (X_R) and the applied loads (X_L).

$$G(X) = R(X_R) - L(X_L) \geq 0 \qquad [2.1]$$

The random variables considered in X_R and X_L should be comprehensive and cover a large design space to ensure the values are representative. For the ULS design of RC members strengthened using EB FRP, X_R typically includes concrete strength, f'_c, steel yield strength, f_y, FRP ultimate strength, f_{frpu}, and correction random variables to account for variation between experiments and prediction, while X_L includes load effects resulting from dead, live, wind, seismic, blast loads, or a combination of loads. Three descriptive statistics are required per random variable for the reliability analysis: bias, coefficient of variation (COV), and distribution type. The choice of load and resistance input statistics are both equally important in calibration. These statistics are obtained from statistical analysis of experimental tests and/or field measurements.

Once $G(X)$ is established and the descriptive statistics are obtained, the reliability index, β, is calculated. The reliability index is indicative of the probability of failure, P_f. The probability of failure is described as having the load exceeding the resistance as expressed in Eq. [2.2]. The accuracy of the calculated β depends on the accuracy of the formulation of $G(X)$. For highly non-linear formulation of $G(X)$, choice of reliability method used in the reliability analysis can also affect the accuracy, if the limit state is approximated. Reliability analysis can be performed using the First Order Reliability Method (FORM), First-order Second-moment (FOSM) method, Monte Carlo Simulation (MCS), or a combination of multiple methods. For the case where $R(X)$ and $L(X)$ in Eq. [2.1] have Gaussian distributions, the joint distribution $G(X)$ will be Gaussian and β can be found using FORM (Nowak and Collins 2000). The use of FORM has been shown to be adequate in some instances where $G(X)$ is linear, but will provide less accurate results when $G(X)$ becomes more non-linear, like in the case of an EB FRP strengthened beam in flexure (Huang et al. 2019).

$$P_f(G(X) < 0) = \Phi\,(-\beta_t) \qquad [2.2]$$

The efficiency of the reliability method can be improved by using adaptive techniques or system-based reliability. Adaptive techniques in this paper refer to methods of reducing the computational cost of the reliability analysis or improving the accuracy of solution. It should be noted both methods are not used predominantly in code calibration. Some examples of methods used are importance sampling (IS) (Melchers 1989); MCS with augmented sampling using IS (Huang et al. 2020); finite-element (FE) based model to evaluate the limit state with Latin hyper cube sampling (LHS) (Helton and Davis 2003); FE based surrogate model with active-learning kriging MCS (Khorramian et al., 2020); FE model to evaluate the limit state with polynomial dimensional decomposition (PDD) to reduce the number of calls to the FE during MCS (Rahman

2008); or, particle swarm optimization (PSO) using LHS and system reliability (Poli et al. 2007). Moreover, system reliability in this context refers to evaluating a collection of structural members and failure modes by treating them in a series, parallel, or a combination system. This technique allows for the redundancy of the structure to be accounted for by considering several` members in a system rather than each member individually.

Two approaches are generally taken by the North-American codes to obtain the factored resistance (R in Eq. [2.1]) : Method 1) apply reliability-based material resistance factors to the specified material strength (CSA S6:19; CSA S806:17), or Method 2) apply a reliability-based member strength reduction factor to the nominal strength based on the mode being examined (flexure, shear, etc.) (ACI 440.2R:17; AASHTO 2014) (Adam and Oudah 2022). Method 2 facilities the use of a two-step reliability approach to perform the calibration in which MCS can be used to obtain the distribution characteristics of the capacity (R in Eq. [2.1]) and then use FORM or other techniques to evaluate $G(X)$. The most accurate reliability method for Method 1 is MCS where $G(X)$ is evaluated for a sufficient number of times, N (number of trials), to obtain the probability of failure (number of failed trials divided by N) and the associated reliability index can be found. This can be difficult when the probability of failure is small, meaning that N must be in the hundreds of millions or more to achieve a reliable prediction of the probability of failure.

2.3 Summary of Research Progress

The reliability-based studies completed to date on the use of EB FRP strengthening of RC members are summarized in Figure 2.1 and Table 2.1. Figure 2.1 is presented per the method of reliability analysis: FORM/FOSM, MCS, adaptive methods, and system reliability; and by limit state: ultimate limit state (ULS), serviceability limit state (SLS), durability limit state (DLS), and fatigue

limit state (FLS). Two additional categories of anchorage and extreme loads have also been included due to the number of papers investigating these topics.

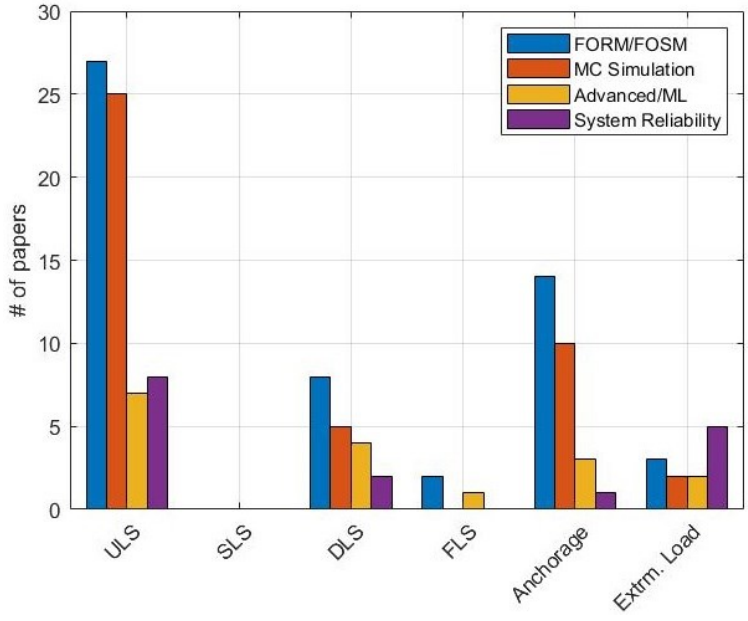

Figure 2.1. Type of reliability method used by research category.

In Table 2.1, research is categorized by author, year, and research category. Six research categories are identified: ultimate limit state (ULS); serviceability limit state (SLS); time-variant (TV) reliability; anchorage and bond; extreme loading; and reliability method. Within each research category, studies are further broken down by research topic. The first column of the table also looks at the type of load and resistance factor design (LRFD) code investigated. Material reduction refers to the Canadian CSA code (CSA A23.3:19, 2019, CSA S6:19, 2019; CSA S806:12(17), 2017) type of analysis where material resistance factors are applied to the respective materials (ϕ_c, ϕ_s, ϕ_{frp}), and member strength reduction refers to the American code (ACI440.2R:17, 2017; ACI 318:19, 2019; ASHTTO:19, 2019) type of analysis where an overall member reduction factor (ϕ_u) is applied to the member nominal capacity.

It can be observed that most of the research has examined the reliability of EB FRP at ULS employing FORM/FOSM, or MCS, to conduct the analysis. Reliability research at ULS is further divided into four categories: flexure, shear, torsion, and confinement. From the review of Table 2.1, it can be concluded that investigation of the ULS of flexure members has been the major focus of the available research, while other research areas like SLS and Torsion have received little to no attention yet. Experimental work that does not have a reliability component has not been considered in this table. Work in the TV domain is starting to be investigated, with the long-term effects of EB FRP strengthening still not well understood. As the number of in-service strengthened members increase, TV topics like fatigue and durability will need more research. This means new sets of random variables and the need for calibration of their statistics.

Table 2.1. Summary of reliability-based EB FRP studies by research topic.

#	Paper Citation	Material reduction	Member strength reduction	Flexural Strengthening	Shear Strengthening	Torsional Strengthening	Column / Confinment	Bridge Component	Servicability	Durability	Fatigure	Debonding	Anchorage	Seismic	Blast	FORM / FOSM	MCS	Adaptive Methods	System Reliability
	Research Category	LFRD		ULS					SLS	Time-variant		Anchorage		Extrm. Loads	Reliability Method				
1	Plevris et al. 1995		X	X											X	X			
2	Deniaud and Cheng 2001	X			X			X							X				
3	Monti and Santini 2002	X		X											X	X			
4	Okeil et al. 2002		X	X				X							X	X			
5	Ellingwood 2003		X	X	X		X					X			X	X			
6	Val 2003		X				X								X				
7	Atadero et al. 2005		X	X				X								X			
8	Atadero and Karbhari [2008		X	X				X		X					X	X			
9	Wang et al. 2010		X	X												X			
10	Lima and Barros 2011	X			X							X	X		X				
11	Weighaus and Atadero 2011		X	X						X						X			
12	Zou and Hong 2011	X					X								X				
13	Ali et al. 2012		X	X				X		X		X	X		X	X			
14	Okeil et al. 2013		X		X			X							X	X			
15	Alsayed and Siddiqui 2013		X		X				X			X	X			X			
16	Dehaghani and Fadaee 2014		X			X									X				
17	Bigaud and Ali 2014		X	X				X		X	X	X			X				
18	Wang and Ellingwood 2015		X	X			X	X								X			
19	Shi et al. 2015		X	X								X			X	X			
20	Huang et al. 2016						X									X			
21	Hao et al. 2016						X							X	X	X			X
22	Ali 2017		X				X								X				
23	Liang et al. 2018									X	X	X			X				
24	Taki et al. 2018	X			X				X	X		X				X			
25	Zhang et al. 2018		X									X			X				
26	Zou et al. 2018			X			X							X	X				X
27	Ali et al. 2018	X		X			X							X		X	X	X	X
28	Huang et al. 2019	X	X	X								X	X		X	X	X		
29	Firouzi et al. 2019		X	X	X					X		X			X				X
30	Noel 2019										X								
31	Yang et al. 2019	X	X	X	X			X		X							X		X
32	Omairey et al. 2019	X	X														X		
33	Khorramian et al. 2019		X				X								X				
34	Souza et al. 2019	X				X									X				
35	Bagheri et al. 2019	X	X				X							X	X				X
36	Dias-da-Costa et al. 2019		X	X				X		X					X				
37	Huang et al. 2020	X	X	X								X	X		X	X	X		
38	Zhou et al. 2020	X	X		X							X			X	X			
39	Narváez et al. 2020	X	X		X							X			X	X			
40	Pen and Xue 2020		X	X	X			X							X	X			
41	Shahriari and Naderpour 2020		X		X							X			X	X			
42	Bharil 2020	X								X		X			X				
43	Mahdavipour et al. 2020		X				X						X	X				X	X
44	Oudah et al. 2020	X					X									X			X
45	Petrie and Oudah 2020	X		X												X			

2.4 SUMMARY OF STATISTICAL PARAMETERS

Tables 2.2 to 2.5 provide summary tables of the input statistics used in the reliability studies presented in Table 2.1. Table 2.2 summarizes the descriptive statistics of the random variables of

EB FRP used in literature. Table 2.3 summarizes the descriptive statistics of loads, concrete material, and internal steel reinforcement. Table 2.4 summarizes descriptive statistics of the random variables that deal with the durability of EB FRP strengthened members. Finally, Table 2.5 summarizes the load input statistics used for calibration of the North American codes that deal with FRP.

Looking first at the load statistics, around 90% of studies considered only gravity loads in analysis. In most papers, the dead load input statistics used for calibration of the applicable design standards are typically chosen for analysis, whereas the live load input is typically chosen based on literature values or assumed. The transformation to load effect, $T2L$, random variable used in calibrating the load factors in the National Building Code of Canada (NBCC, 2015) is not incorporated into most studies.

For the resistance statistics of EB FRP, researchers have used code defined input statistics, conducted limited scope experimental testing to propose their own statistics, or assumed values in many cases. Table 2.2 shows the statistics used by various researchers for the random variables related to EB FRP, they are: ultimate tensile strength, f_{frp}, EB FRP modulus of elasticity, E_{frp}, EB FRP thickness, t_{frp}, EB FRP width, w_{frp}, EB FRP ultimate tensile strain, ε_{frpu}, model error for the strengthened resistance model, ζ, spacing of FRP strips, S_{frp}, and angle of FRP strips (shear), β_{frp}. The distribution type, bias and COV in many studies were based on small scale experimental benchmark testing to establish the descriptive statistics completed by several studies (Atadero et al. 2005; Atadero and Karbhari 2008; Huang et al. 2019; Wieghaus and Atadero 2011).

In most experimental studies, the probability density function (PDF) of the variables f_{frp} and ε_{frpu} have been found to follow a weibull distribution. The exception being two studies investigating strengthened columns, where the PDF of f_{frp} was taken to be lognormally distributed

(Val 2003; Zou and Hong 2011). With the bias and COV varying depending on the member type (beam, column) and depending on the database the statistics were taken from. The variables E_{frp} and t_{frp} have been found to follow a lognormal distribution with a bias of unity and a COV that varies based on type of FRP used. The variables w_{frp}, and shear variables S_{frp} and β_{frp} have been found to follow a normal distribution in most cases.

Table 2.4 summarizes the descriptive statistics that relate to the durability analysis of EB FRP strengthened members. A total of four reliability studies reviewed investigated the durability of strengthening (Ali et al. 2012; Bigaud and Ali 2014; Firouzi et al. 2019; Taki et al. 2018). Due to the small number of experimental tests around the long-term durability of these members, most statistics used are in agreeance on the distribution, bias, and COV used in the reliability analysis.

Table 2.2. Summary of descriptive statistics for EB FRP in flexure and shear.

Reference	Parameter	f_{frp}	E_{frp}	t_{frp}	w_{frp}	ε_{frpu}	ζ	s_{frp}	β_{frp}
	Distribution Type					Extreme Type III			
Plevris et al. 1995	Bias					1.32			
	COV					0.24			
	Distribution Type	Not Listed							
Monti and Santini 2002	Bias	1.00							
	COV	0.06							
	Distribution Type					Weibull	Normal		
Okeil et al. 2002	Bias					1.10	1.01		
	COV					0.02	0.05		
	Distribution Type	Lognormal					Normal		
Val 2003	Bias	1.00					1.00		
	COV	0.15					0.08		
	Distribution Type	Not Listed							
Ellingwood 2003	Bias	1.12							
	COV	0.13							
	Distribution Type	Weibull	Lognormal	Weibull					
Atadero et al. 2005	Bias	1.18	1.18	0.92					
	COV	0.13	0.10	0.04					
	Distribution Type	Weibull	Lognormal	Lognormal					
Atadero and Karbhari 2008	Bias	1.00	1.00	1.00					
	COV	0.10	0.10	0.05					
	Distribution Type						Normal		
Wang et al. 2010	Bias						1.05		
	COV						0.06		
	Distribution Type	Weibull	Lognormal	Lognormal					
Weighaus and Atadero 2011	Bias	1.00	1.00	1.00					
	COV	0.10	0.10	0.05					
	Distribution Type	Lognormal							
Zou and Hong 2011	Bias	1.33							
	COV	0.15							
	Distribution Type	Weibull	Logmornal				Normal		
Ali et al. 2012	Bias	1.00	1.00				1.00		
	COV	0.15	0.20				0.20		
	Distribution Type		Lognormal	Lognormal		Weibull		Normal	
Alsayed and Siddiqui 2013	Bias		1.00	1.00		1.10		1.01	
	COV		0.10	0.05		0.02		0.10	
	Distribution Type	Weibull							
Souza et al. 2013	Bias	1.00							
	COV	0.04							
	Distribution Type	Weibull	Lognormal				Normal		
Bigaud and Ali 2014	Bias	1.00	1.00				1.05		
	COV	0.11	0.11				0.10		
	Distribution Type		Lognormal						
Shi et al. 2015	Bias		1.00						
	COV		0.10						
	Distribution Type						Normal		
Wang and Ellingwood 2015	Bias						1.02		
	COV						0.08		
	Distribution Type		Lognormal	Lognormal			Weibull		
Baji et al. 2016	Bias		1.10	1.00			1.00		
	COV		0.20	0.05			0.42		
	Distribution Type	Weibull		Lognormal			Normal	Normal	
Ali 2017	Bias	1.31		1.00			1.00	1.00	
	COV	0.15		0.05			.25+.018h/ey	0.10	
	Distribution Type		Lognormal		Normal	Weibull		Normal	Normal
Taki et al. 2018	Bias		1.00		1.00	1.10		1.01	1.00
	COV		0.15		0.10	0.02		0.10	0.05
	Distribution Type		Lognormal	Normal					
Zhang et al. 2018	Bias		1.00	1.00					
	COV		0.12	0.02					
	Distribution Type		Lognormal		Normal	Weibull		Normal	Normal
Firouzi et al. 2019	Bias		1.00		1.00	1.10		1.01	1.00
	COV		0.15		0.10	0.02		0.10	0.05
	Distribution Type		Lognormal						
Bagheri et al. 2019	Bias		1.00						
	COV		0.10						
	Distribution Type	Weibull	Lognormal						
Pen and Xue 2019	Bias	1.04	1.00						
	COV	0.06	0.15						
	Distribution Type	Weibull	Normal	Lognormal					
Huang et al. 2019	Bias	1.15	1.00	1.00					
	COV	0.10	0.04	0.05					
	Distribution Type								
Bharil 2020	Bias								
	COV								
	Distribution Type		Lognormal	Lognoral		Weibull			Normal
Shahriari and Naderpour 2020	Bias		1.00	1.00		1.10			1.00
	COV		0.10	0.05		0.02			0.05
	Distribution Type	Weibull	Normal	Lognormal					
Huang et al. 2020	Bias	1.15	1.00	1.00					
	COV	0.10	0.04	0.05					
	Distribution Type	Lognormal	Normal	Lognormal					
Zhou et al. 2020	Bias	1.10	1.00	1.00					
	COV	0.12	0.02	0.05					

f_{frp} = FRP ultimate tensile strength; E_{frp} = FRP modulus of elasticity; t_{frp} = FRP thickness; w_{frp} = FRP width; ε_{frpu} = FRP ultimate tensile strain; ζ = Strengthened resistance model error; S_{frp} = Spacing of FRP strips; and β_{frp} = Angle of FRP strips (shear).

Table 2.3. Summary of descriptive statistics for loads, concrete, and steel parameters.

Reference	Parameter	D	L	f'_c	h	b	f_s	E_s	d	A_s
	Distribution Type			Normal	Normal	Normal	Beta		Normal	
Plevris et al. 1995	Bias			1.00	1.00	1.01	1.08		1.01	
	COV			0.15	0.01	0.01	0.10		0.00	
	Distribution Type			Beta			Beta		Beta	
Monti and Santini 2002	Bias			1.00			1.00			
	COV			0.20			0.15		0.20	
	Distribution Type	Normal		Normal	Normal	Normal	Normal		Normal	Normal
Okeil et al. 2002	Bias	1.05		1.10	1.00	1.00	1.10		1.00	1.00
	COV	0.10		0.18	0.03	0.03	0.13		0.03	0.02
	Distribution Type	Normal	Gumbel				Lognormal			
Val 2003	Bias	1.05	1.00				1.00			
	COV	0.10	0.25				0.10			
	Distribution Type	Normal	Gumbel	Lognormal			Lognormal			
Ellingwood 2003	Bias	1.05	1.00	1.12			1.05			
	COV	0.10	0.25	0.13			0.11			
	Distribution Type	Normal	Not Listed							
Atadero et al. 2005	Bias	1.05	1.55							
	COV	0.10	0.18							
	Distribution Type		Not Listed							
Atadero and Karbhari 2008	Bias		1.10							
	COV		0.18							
	Distribution Type	Normal	Gumbel	Normal			Lognormal		Normal	
Wang et al. 2010	Bias	1.05	1.00	1.00			1.12		1.00	
	COV	0.10	0.25	0.18			0.10		0.4/dn	
	Distribution Type	Normal	Type I	Normal	Normal	Normal	Beta	Normal	Normal	Normal
Weighaus and Atadero 2011	Bias	1.05	1.00	1.10	1.00	1.00	1.08	1.01	1.00	1.00
	COV	0.10	0.25	0.18	0.03	0.03	0.09	0.10	0.03	0.10
	Distribution Type	Normal	*Weibull (a)	Normal			Lognormal			Shifted Lognormal
Zou and Hong 2011	Bias	1.05	0.24	1.16			1.12			1.01
	COV	0.10	0.67	0.14			0.06			0.04
	Distribution Type	Normal	Normal	Normal			Normal		Normal	Normal
Ali et al. 2012	Bias	1.05	1.00	1.00			1.11		0.99	0.97
	COV	0.10	0.40	0.15			0.10		0.02	0.02
	Distribution Type		Type I	Normal		Normal	Normal		Normal	
Alsayed and Siddiqui 2013	Bias		0.90	1.10		1.00	1.10		1.00	
	COV		0.25	0.18		0.03	0.13		0.03	
	Distribution Type			Lognormal			Lognormal			
Souza et al. 2013	Bias			1.22			1.13			
	COV			0.11			0.07			
	Distribution Type	Normal	Normal	Normal			Normal		Normal	
Bigaud and Ali 2014	Bias	1.05	1.00	1.00			1.00		1.00	
	COV	0.10	0.18	0.15			0.10		0.05	
	Distribution Type	Normal	Type I	Normal	Normal	Normal	Beta		Normal	
Shi et al. 2015	Bias	1.05	1.00	1.21	1.01	1.01	1.15		0.99	
	COV	0.10	0.25	0.08	0.04	0.04	0.05		0.04	
	Distribution Type	Normal	Normal	Normal			Lognormal		Normal	
Wang and Ellingwood 2015	Bias	1.05	1.15	1.20			1.12		1.00	
	COV	0.10	0.18	0.18			0.10		0.4/dn	
	Distribution Type									
Baji et al. 2016	Bias									
	COV									
	Distribution Type	Normal	Type I	Lognormal			Lognormal	Normal		
Ali 2017	Bias	1.05	1.00	1.18			1.15	1.00		
	COV	0.10	0.25	0.16			0.10	0.03		
	Distribution Type	Normal	Type I	Normal			Normal	Lognormal		
Taki et al. 2018	Bias	1.05	1.00	1.10			1.10	1.00		
	COV	0.10	0.25	0.18			0.13	0.10		
	Distribution Type	Lognormal	Type I	Normal		Normal				
Zhang et al. 2018	Bias	1.05	1.00	1.24		1.01				
	COV	0.10	0.25	0.15		0.04				
	Distribution Type	Normal		Normal			Normal	Normal		Normal
Firouzi et al. 2019	Bias	1.05		1.15			1.20	1.00		1.00
	COV	0.10		0.10			0.04	0.02		0.13
	Distribution Type		Type I	Normal			Lognormal			
Bagheri et al. 2019	Bias		1.00	1.00			1.05			
	COV		0.25	0.10			0.10			
	Distribution Type	Normal	*Type I (b)	Normal	Normal	Normal			Normal	
Pen and Xue 2019	Bias	1.05	1.23	1.00	1.00	1.00			1.00	
	COV	0.10	0.18	0.10	0.1/h	0.04			0.03	
	Distribution Type	Normal	Type I	Normal	Normal	Normal	Normal	Normal		Normal
Huang et al. 2019	Bias	1.05	1.00	1.25	1.00	1.00	1.10	1.00		1.00
	COV	0.10	0.25	0.15	0.02	0.02	0.08	0.02		0.03
	Distribution Type									
Bharil 2020	Bias									
	COV									
	Distribution Type		Type I	Normal		Normal	Normal		Normal	
Shahriari and Naderpour 2020	Bias		0.90	1.10		1.00	1.10		1.00	
	COV		0.25	0.18		0.03	0.13		0.03	
	Distribution Type	Normal	Type I	Normal	Normal		Normal	Normal		Normal
Huang et al. 2020	Bias	1.05	1.00	1.25	1.00		1.10	1.00		1.00
	COV	0.10	0.25	0.15	0.02		0.08	0.02		0.03
	Distribution Type	Normal	Type I		Lognormal	Normal			Normal	
Zhou et al. 2020	Bias	1.05	1.00		1.00	1.00			1.00	
	COV	0.10	0.25		0.01	0.02			0.02	

D = Dead Load; L = Live Load; f'_c = Concrete strength; h = Section height ; b= Section width; f_s = Steel yield strength; E_s = Steel modulus of elasticity; d = Diameter of bar (steel); A_s = Area of steel reinforcing
*(a) – Point-in-time live load; (b) – Live + impact load

Table 2.4. Summary of descriptive statistics for EB FRP durability

Reference	Parameter	C_s	C_{th}	ζ_{cr}	w/c	L_{pit}	C_{pit}	D_{cl}	w_{cr}	RH
Ali et al. 2012	Distribution Type	Lognormal	Uniform	Normal	Normal	Uniform				
	Bias	1.00	1.00	1.00	1.00	1.00				
	COV	0.50	0.19	0.20	0.05	0.39				
Bigaud and Ali 2014	Distribution Type	Lognormal	Uniform	Normal			Gumbel	Lognormal	Normal	
	Bias	1.00	0.90	1.00			1.00	1.00	1.00	
	COV	0.50	0.19	0.20			0.17	0.75	0.20	
Taki et al. 2018	Distribution Type	Lognormal	Uniform		Lognormal		Gumbel	Lognormal		Normal
	Bias	1.00	0.90		1.00		1.00	1.00		1.00
	COV	0.50	0.19		0.05		0.22	0.20		0.10
Firouzi et al. 2019	Distribution Type	Lognormal	Uniform		Lognormal		Gumbel	Lognormal		Normal
	Bias	1.00	0.90		1.00		1.00	1.00		1.00
	COV	0.50	0.19		0.05		0.22	0.20		0.10

C_s = Chloride concentration; C_{th} = Corrosion threshold; ζ_{cr} = Corrosion model error; w/c = Water-to-cement ratio; L_{pit} = Pitting length; C_{pit} = Corrosion coefficient; D_{cl} = Chloride diffusion coefficient; w_{cr} = Surface crack width; RH = Relative humidity

Table 2.5. Input statistics for load used in code calibration.

Code / Standard	Governing Load	Description	DL	LL	$T2L$
CSA S806:17	$1.25DL + 1.5LL$	Dist.	Normal	Gumbel	Normal
		Bias	1.0500	0.9000	1.0000
		COV	0.1000	0.1700	0.2060
CSA S6:19	$1.2DL + 1.7LL$	Dist.	Normal	Normal	Normal
		Bias	1.0400	1.1680	1.0200
		COV	0.0360	0.0686	0.0900
ACI 440.2R:17	$1.2DL + 1.6LL$	Dist.	Normal	Normal	N/A
		Bias	1.0500	1.0000	
		COV	0.1000	0.1800	

DL = Dead load; LL = Live load; and $T2L$ = Transformation to load effect

2.5 DISCUSSION OF RELIABILITY-BASED LITERATURE

In-depth discussion regarding the reported research progress is provided in this section. The discussion is provided per research category reported in Table 2.1.

2.5.1 Ultimate Limit State (ULS)

Discussion regarding the research progress on ULS is provided in this section. Flexure, shear, torsion, and confinement are covered.

Flexural (ULS): The topic of flexural strengthening of RC members with FRP is the most widely researched topic in the reliability-based literature on EB FRP. Flexural strengthening typically consists of prefabricated (or in-field wet layup) FRP plates bonded with epoxy to the tension face of the RC member. Early work looked at developing reliability framework to quantify the safety (or, probability of failure) of using EB FRP to reinforce concrete elements, similar to that used in steel RC concrete design (Plevris et al. 1995). This study looked at flexural members, under only concrete crushing and FRP rupture failure modes, as debonding had not been widely observed as a pre-mature failure mode. The framework was to calibrate resistance reduction factors and begin to describe probabilistically these limit states of failure to give practicing engineers confidence to utilize FRP for structural applications, by making the process similar to that of other LRFD design codes (CSA A23.3, 2019; ACI 318, 2019; CSA S6, 2019). At this time, it was typical to use first-order methods to assess the limit state of the member, with common methods used were those proposed by Hasofer-Lind (Hasofer and Lind, 1974), and Rackwitz-Fiessler (Rackwitz and Fiessler, 1978).

This body of work was furthered by several studies in the 2000s (Atadero et al. 2005; Atadero and Karbhari 2008; Ellingwood 2003; Monti and Santini 2002; Okeil et al. 2002). Limited experimental databases were available still at that time for EB FRP, and assumptions were needed on the distribution type of the various random variables of geometry, material strength and loads. Most parameters were taken as deterministic to begin, so that first-order methods could be utilized. For a more general framework to be put forward, only key parameters, such as ultimate FRP strain, ε_{frpu}, ultimate FRP tensile strength, f_{frpu}, concrete strength, f'_c, FRP modulus, E_{frp}, and FRP laminate thickness, t_{frp}, were typically considered as random variables. Distribution types of weibull, weibull, normal, lognormal and weibull, respectively, were assumed for these random

variables for analysis. Summary tables of the descriptive statistics for EB FRP used by each study can be found in Tables 2.2 to 2.4.

A study in 2011 examined the uncertainties around an existing structure before and after strengthening by varying the amount of uncertainty involved with each design random variable, to examine the effect on the calculated reliability using MCS (Wieghaus and Atadero 2011). It was noted in this and other studies that an increased variation (COV) in FRP parameters had less of an effect on reliability than the effects of the existing structure (i.e., the level of corrosion present, or level of deterioration in the concrete before strengthening). A review study was also conducted on the available tools and databases needed to conduct reliability analysis, showing the feasibility of making a framework for analysis similar to that of the existing design guidelines like ACI440.2R (Wang et al. 2010, ACI440.2R, 2017). Research has been done into the use of CFRP laminates in the flexural strengthening of prestressed bridge girders in which MCS-FOSM is employed (Peng and Xue 2019). This work proposed input statistics for the flexural capacity of prestressed beams (shown in Tables 2.2 to 2.4).

A set of studies used importance sampling (IS) to optimize traditional MCS so that the various methods can be compared (Huang et al. 2019, 2020). Three methods (IS-MCS, MCS and FORM) were used to generate reliability index values with the efficiency and accuracy compared for calibrating the various FRP design codes. This process was used to both calibrate partial resistance factors and strength reduction factors for various failure modes using a system approach and included a database with anchored and bonded specimens. The system approach is taken so that no failure mode needs to be assumed a priori. An extensive database of strengthened and un-strengthened beams evaluated at the ultimate in bending, combined with an experimental program to define updated input statistics for the parameters related to external strengthening was

conducted. In particular, new bias, COV and distribution types for concrete strength, f'_c, FRP modulus of elasticity, E_{frp}, and FRP ultimate tensile strength, f_{frpu}, were proposed. It can be noted that the database collected by Huang included both anchored and bonded specimens for comparison of both strengthening systems (Huang et al. 2019).

Shear (ULS): Unlike flexural strengthening, shear interactions of the composite RC-FRP are less well understood, mostly due to the design methods being semi-empirical and also due to the brittle failure mode and added parameters of FRP strip angle and spacing (Zhou et al. 2020). Resistance models for shear are usually empirical in nature as compared with flexural limit states that utilize mechanics to formulate them. This leads to significant variation in prediction models used in unique design codes around the world and gives rise to the need for proper calibration through reliability analysis. For this reason, considerable work related to studying the interaction of FRP strengthened RC beams in shear, numerically and experimentally, has been conducted (Bukhari et al. 2013; Chen and Teng 2003; D'Antino et al. 2016; Khalifa et al. 1998; Khalifa and Nanni 2002; Monti and Liotta 2007; Pellegrino and Modena 2008; Sayed et al. 2013; Täljsten 2003; Triantafillou and Antonopoulos 2000; Triantafillou 1998; Zhang and Hsu 2005).

A study looked at shear strengthening using EB FRP in strip configuration, by evaluating 6 well-known resistance models used for calculating shear capacity of RC beams, V_R, comprised of $V_c + V_s + V_{frp}$ (Deniaud and Cheng 2001), where V_c, V_s, and V_{frp} are the shear resistance of concrete, shear resistance of the internal steel stirrups, and shear reinforcement of the EB FRP reinforcement, respectively. Experimental testing was conducted on sixteen full scale T-Beams and the resistance models were compared with the experimental results to evaluate model accuracy and to obtain the necessary statistical parameters for completion of reliability analysis.

As with flexural designs, debonding in shear strengthening configurations has been observed that limits the capacity of the section. Anchorage has been shown to improve the performance of EB FRP used for shear strengthening (Kalfat et al. 2013). This is why a study in 2013 proposed two expressions for shear design, one for bonded and one for anchored (Okeil et al. 2013). The proposed equations were compared with results of experimentally evaluated eighteen full sized bridge girders twice: once anchored and once bonded. Uncertainty from materials strength, fabrication, loads, distribution factors were included as random variables in the limit state formulation. Results from the 2013 study showed choosing a target reliability index of $\beta_t = 3.5$, the average strengthened beam reliability achieved by the 36 beams tested (18 anchored / 18 bonded) was 3.28 on average, indicating that it is difficult to reach on consistent basis the target reliability index of 3.5 or higher for any configuration (Okeil et al. 2013). The result of the lower than target reliability means existing bridges may have lower reliability than previously thought.

Shear strengthening has additional parameters that need to be considered such as strip angle and fiber orientation. Some studies have looked to quantify the effect these parameters have on the reliability of a member (Alsayed and Siddiqui 2013; Shahriari and Naderpour 2020). These studies used MCS and considered complete wrapping (W), U-jacketing (U) and Side bonding (S) configurations. A key finding was that the level of service load mattered; below 70% of ultimate load saw that most fiber orientation and strip configurations could be used effectively (Alsayed and Siddiqui 2013). It was only when seeing close to ultimate loadings that the certain (U) and (S) configuration failed. Moreover, it was found by the more recent study that increasing loads and decreasing the amount of internal shear reinforcement had a large negative effect on reliability (Shahriari and Naderpour 2020).

Another study conducted a reliability-based analysis of EB FRP strengthened beams, deficient in shear, using modern day LRFD style calibration (Zhou et al. 2020). Using a database of experimental tests on shear strengthened beams, and employing MCS-FORM reliability analysis, calibration of the safety factors based on a target reliability were performed. It was found that most models under-predicted the contribution of EB FRP in shear. More information on each resistance model can be found in the paper (Zhou et al. 2020). It has been shown that the Chen and Teng (Chen and Teng 2003) shear resistance model was the most accurate for predicting side bonding (S) and u-jacketing (U), whereas Khalifa (2002) (Khalifa and Nanni 2002) model was shown to be the most accurate for predicting complete wrapping (W). This result was confirmed by Narváez et al. (Narváez et al. 2020) in which they showed that the Chen and Teng model (Chen and Teng 2003) led to higher reliability for debonding failure mode than that given by the ACI 440.2R guideline (ACI 440.2R:17).

Torsional (ULS): Torsional strengthening using EB FRP is a new application with limited reliability-based research done on the topic. There has been three reliability-based studies on this topic, with the studies focusing on the overall member strength reduction LRFD format (Alabdulhady and Sneed 2019; Dehghani and Fadaee 2014; Souza et al. 2013). The first two works proposed a model error based on experimental data, in addition to a set of resistance factors calibrated for different target index values. In the 2014 study (Dehghani and Fadaee 2014), six variables were taken as random for analysis, based on loads, geometry, and FRP properties. A key result shows that the chosen analytical model was under-conservative, yielding an average strengthened reliability index of 2.82 for a target index of 3.0. A database of 23 experimentally tested specimens was used to establish the bias and variance of 1.07 and 0.265, respectively, based on the method of calculating the variance proposed by Ellingwood (Ellingwood et al. 1980).

A state-of-the-art of torsional strengthening providing a comprehensive review of the body of knowledge around the subject was conducted in (Alabdulhady and Sneed 2019). Databases of available experimental tests available in literature were established in this work for different strengthening configurations tested. Results from experiment show the use of anchorage in applications such as torsional strengthening can increase reliability. As with confinement and shear, full wrap configurations were found to be the most effective. Conversely to shear, it was observed that continuous (longitudinally) full length wraps were more effective than discrete strips due in part to the confinement of the cracks in the concrete struts that form during loading (Alabdulhady and Sneed 2019).

Column (ULS): Early research on confinement aimed to quantify the uncertainty in the confinement effect using FORM by examining both pure axial and combined axial/bending loading, with small eccentricities considered (Val 2003). Zou and Hong in 2011 looked at the reliability of columns through investigation of the resistance and load models from the S806 and NBCC standards (CSA S806:17; NBCC 2015), using FORM to conduct the reliability analysis. The number of FRP layers and internal reinforcement ratio were found to have only a small effect on strengthened reliability. This is due to the observation that once confinement is achieved, the addition of more layers does not increase reliability significantly (Zou and Hong 2011). The same observation was made in another study (Mahdavipour et al. 2020).

Other studies have compiled large databases of axial compression tests of confined FRP-RC columns for calibration (Baji et al. 2016; Huang et al. 2016). New closed-form probabilistic ultimate stress and strain models were proposed, and model error was calculated for the various confinement models (Baji et al. 2016). It should be noted the FRP modulus, E_{frp}, was found to follow a weibull distribution in most cases. A 2016 study investigated the reliability of

strengthened columns within a frame under blast loads considering various strengthening schemes (Hao et al. 2016).

A study in 2017 examined the behavior of short/slender square columns with bi-axial eccentricity of loads that are strengthened with FRP was also conducted (Ali 2017). FORM was used for analysis, and it was found that using a finite difference model (FDM) for the resistance model allowed full derivatives to be found, causing the FORM analysis to converge well. It was observed that only a slight increase in reliability is gained when rounding the columns (Ali 2017).

A more recent study used advanced reliability-based methods to calibrate the reduction factor EB FRP strengthened columns using an extensive database of experimentally tested beams (Khorramian et al. 2019). This study investigated the reliability indices used to calibrate the ACI 440 standard (ACI 440.2R 2017) and found the proposed reduction factor in the ACI standard is adequate to meet target reliability index of 3.5.

2.5.2 Serviceability Limit State (SLS)

To date limited work has been done on the serviceability limit state (SLS). Some studies have considered SLS loadings looking at shear strengthening (Alsayed and Siddiqui 2013; Taki et al. 2018), but with a limited scope from a reliability analysis standpoint. Codes/design guidelines like CSA S6 (CSA S6:19) and ACI 440 (ACI 440.2R:17) give some guidance on SLS analysis of EB FRP strengthened sections but are limited in scope. More work is needed to examine the SLS behavior of EB FRP strengthened members in the same manner as other current LRFD standards.

2.5.3 Time-Variant (TV) Analysis

Time-variant (TV), or sometimes called time-dependent, analysis is of high importance to proper life-cycle designs in civil applications. As loads change or structures degrade overtime, the need for calculating both instantaneous reliability and cumulative probability of failure becomes equally important to optimization (Kroetz et al. 2020). The guidance and research on TV limit states for EB FRP are scattered and can lead to over design making the use cost prohibitive (Bharil 2020). Loss of strength during service-life can pose a serious risk to public safety and the topic is becoming of higher importance, as a growing number of structures strengthened with EB FRP progress into their service life. Fatigue, and more recently durability, are the most common topics studied in time-variant analysis of civil structures. Fatigue refers to the failure mechanism that involve of reduction in material strength overtime due to cyclic loading. A fatigue limit state (FLS) can be formulated to evaluate if a member can sustain an acceptable level of safety under certain loading conditions. Durability refers to a materials capability to resist weathering, chemically harsh environments overtime, while a durability limit state (DLS) looks at maintaining an acceptable level of safety under the mentioned conditions.

As durability deals with the deterioration due to physical and environmental factors, a new set of random variables are needed to be defined. Corrosion of internal reinforcing steel, chloride attack on the concrete is both of concern (Bigaud and Ali 2014). Table 2.4 provides a summary of the input statistics used in the TV durability analysis for EB-FPR related research. Several works have looked into the durability of EB FRP strengthening (Ali et al. 2012; Bigaud and Ali 2014; Firouzi et al. 2019; Taki et al. 2018), and have proposed descriptive statistics for eight durability random variables: chloride concentration, C_s; corrosion threshold, C_{th}; corrosion model error, ζ_{cr};

water-to-cement ratio, w/c; pitting length, L_{pit}; corrosion coefficient, C_{pit}; chloride diffusion coefficient, D_{cl}; Surface crack width, w_{cr}; and relative humidity, RH.

From a computational standpoint, the additional aspect of time adds a layer of complexity that most reliability research does not yet effectively consider. Crude MCS is still accepted as the most accurate method for solving such problems but becomes costly to compute when conducting TV analysis. To address this, there have been several methods proposed in literature for computing TV reliability as an alternative to MCS (Melchers and Beck 2018), namely: the nested FORM (Madsen and Tvedt 1990), the outcrossing (Andrieu-Renaud et al. 2004; Sudret 2008), the fast probability integration (Wen and Chen 1987), the directional simulation (Melchers 1992), and time-integrated approach. More information on these methods can be found in their respective references and in (Kroetz et al. 2020). Survey of the literature on TV reliability of EB FRP studies shows that only conventional MCS (Ali et al. 2012; Taki et al. 2018) and FORM (Dias-da-Costa et al. 2019; Firouzi et al. 2019) have been used thus far to compute reliability. More recently, the use of more complex methods like multi-objective particle swarm optimization (PSO) techniques have been employed to achieve better life-cycle optimization and cost-reduction (Yang et al. 2019). TV research related to the durability and fatigue of RC members strengthened using EB FRP is described in the following sections.

Durability: Early work into durability effects looked at the deterioration models for internal steel rebar to account for the deterioration of existing structures before strengthening (Atadero and Karbhari 2008). The work investigated different parameters around concrete and steel deterioration of T-beam bridge girders to help understand additional uncertainties around strengthening an existing structure. This effect of existing conditions of the member prior to strengthening was further studied by investigating the effect of the input statistics had on the TV

reliability (Wieghaus and Atadero 2011). Results showed that variability (COV) of the remaining area of deteriorated steel was had a larger effect on the reliability, than the variability of the EB FRP. Moreover, in prefabricated laminate, the variability of FRP modulus and ultimate strength were observed to be less than 10% (i.e., did not significantly affect the reliability), and was recommended to be taken as deterministic (Wieghaus and Atadero 2011).

Other studies have also examined the durability of CFRP strengthened bridge girders with the goal of calibrating the AASHTO resistance factors for a range of target reliability indexes (Ali et al. 2012; Bigaud and Ali 2014). Several failure modes were considered by applying three durability factors and accompanying deterioration actions. The results showed that all three deterioration actions have an effect on durability, with the most significant being live load growth initially after strengthening, which then switches to corrosion being more dominant farther into the repaired service life (Ali et al. 2012). It should be noted that FRP anchorage is known to provide better initial reliability to the strengthened beam, since it effectively eliminates debonding as a failure mode (Huang et al. 2019; Kalfat et al. 2018)**.** Though, investigation revealed that durability of the FRP plays a larger role in the reliability of the strengthened beam when anchorage systems are put in place. Overtime is an compression control section that has been designed with anchorage may degrade to switch failure modes, making a rupture failure possible. Rupture strength is directly proportional to the thickness, meaning FRP laminate thickness also will have a greater effect on reliability when anchorage is present.

A systems approach has also been taken to develop reliability-based TV framework to examine the effects of harsh environment on the resistance capacity of strengthened RC beams (Firouzi et al. 2019; Taki et al. 2018). It is necessary in some cases to consider both failure modes (shear and flexure) in a system fashion as deterioration and growth in loads can cause the failure mode to

switch from flexure to a more brittle shear failure over time. This has been shown to occur when steel stirrups are present internally.

A study in 2019 conducted an analysis considering both time- and spatial-variation investigating the use of CFRP to strengthen degraded prestressed bridge girders (Peng and Xue 2019). The spatial variation of pitting corrosion was considered by discretization of the rebar elements. Sensitivity analysis showed that the random variables with the largest effect on reliability will shift through time. Certain variables such as area of steel and concrete cover which are typically taken as deterministic may need to be treated as random to ensure this shift is accurately captured in a TV reliability analysis. Another study in 2019 proposed a novel life-cycle optimization method to account for durability limit state in planning for maintenance of infrastructure by including deterioration models into reliability-based framework (Yang et al. 2019).

Fatigue: Limited reliability-based research has been conducted on the fatigue behavior of EB FRP strengthened members. A 2019 study reviewed the simple fatigue models used in industries such as aerospace and marine transportation, to investigate the validity of using these to model FRP used to reinforce structures (Noël 2019). Engineers in these fields have been studying fatigue long before the popularization of the composite in civil applications, which has given a breadth of knowledge to refer to in the development of fatigue limit state for FRP in civil applications. It should be noted that the study by Noël looked at all types of FRP reinforcing and found for EB FRP specifically, models such as the Sendeckyj model (Sendeckyj 1981) can be used to probabilistically describe static and fatigue loading scenarios using a single closed form equation. It was also observed that when trying to achieve high reliability (low probability of failure) under a high number of loading-cycles (1 million to 10 million), FRP could only sustain as high as 34%

of its ultimate static load indicating that current deterministic design equations, based on mean or 95% confidence intervals, can over-estimate the service-life at fatigue limit state.

Another study remarked that fatigue action slightly affects the reliability of EB FRP strengthened beam, unless combined with corrosion or live load growth, to which an increase of failure at the ultimate is observed (Ali et al. 2012). Considering fatigue in the TV reliability allows for the effects of damage in the compression zone of the concrete on the reliability to be examined. This aids in capturing the change in the ultimate strain in the concrete as it degrades over time. A 2014 study examined the TV effects of combined durability and fatigue on RC bridge girders strengthened in flexure with CFRP (Bigaud and Ali 2014). Three deterioration models were examined with the effects from fatigue added in deterministically, to examine what parameters have the largest effect on reliability and the service life after strengthening.

2.5.4 Bond and Anchorage

Debonding of EB FRP at the FRP-concrete interface has been observed since early experimental studies and has been shown as a dominant failure mode in bonded EB FRP (Tanarslan and Altin 2010). In addition to concrete crushing and FRP rupture, debonding at the ends due to shear and debonding due to intermediate flexural cracks (IFC) have been observed to cause pre-mature failure (see Figure 1.2 in Section 1.2.2 for failure modes).

Current North American codes do not explicitly account for debonding in resistance models, instead, prescribed limit on the usable strain is placed by these standards to ensure that debonding will not occur (CSA S806:17; CSA S6:19; and ACI440.2R:17). These limits do not appear to be reliability-based and appear to be experimentally driven due to lack of research. As is stated in the in ACI440 standard (ACI 440.2R:17), these strain limits on the ultimate tensile strain of the EB

FRP are calibrated using measured values of FRP strain during pre-mature debonding failure meaning the limit is experimentally based.

A study in 2015 helped address the lack of knowledge around debonding by examining several models for calculating effective strain for a database of over 200 beams through MCS-FORM (Shi et al. 2015). The models by Said and Wu (Said and Wu 2008) and Wu and Niu (Wu and Niu 2007) were found to yield the lowest COV. Furthermore, as the variation in the random variables of FRP modulus, E_{frp}, yield strength of internal steel, f_y, and depth to height ratio of the concrete section, d/h, increased, the calculated reliability index decreased. This indicates that these parameters, in addition to the model error, are the most significant contributors to decreasing the reliability of strengthened members.

Another experimental debonding study looked at the strength of CFRP-concrete bond to provide valuable insight into the behavior of the bond long-term performance (Liang et al. 2018). Specifically, the fracture energy, G_f, of the bond under the dual action of wet-dry cycle and sustained loading was studied. Results showed that G_f is found to be lognormally distributed under each action individually and when acting together. It is worth noting that the reliability of the bond (or fracture energy) was found to follow an exponential decay stochastic process as the number of wet-dry cycles increases.

In more recent times some researchers have studied both anchored and non-anchored strengthening systems (Huang et al. 2020; Kalfat et al. 2018; Tanarslan and Altin 2010) and some have also started to assume proper anchorage will be provided and do not consider end debonding as a failure mode (Bigaud and Ali 2014). Consideration should be given to the failure mode of the member when anchorage is added as the failure mode can potentially switch to FRP rupture. It was

observed that when anchorage is present, other parameters like laminate thickness have a larger effect on reliability and may not be able to be taken as deterministic (Ali et al. 2012).

Another study in 2018 has tried to quantify the effectiveness of the anchorage systems for EB FRP, by the use of the efficiency factor (k_{eff}) proposed in the ACI440.2R (Kalfat et al. 2018). This study noted that there exists still a large variation in the experimental data and more work needs to be conducted to quantify the short- and long-term effects of adding anchorage to EB FRP strengthening systems.

2.5.5 Extreme Loads

Extreme loads can be loads such as seismic or blast and are rare in occurrence but can cause severe damage. The majority of the research publicly available has been done into the use of EB FRP for seismic retrofit. Only one reliability-related study on the blast loading is available (Hao et al. 2016). There have been a limited number of studies examining the seismic response of FRP strengthened structures from a reliability approach (Ali et al. 2018; Bagheri et al. 2019; Mahdavipour et al. 2020; Zou et al. 2018). The use of EB FRP in seismic retrofit is limited due to the brittle behavior of FRP since the ductility of structural components is a key parameter in seismic design (Oudah and El-Hacha 2014).

The use of EB-FPR in seismic retrofit is focused on controlling the formation of plastic hinges. In seismic applications it has been shown that FRP can be added to the joint column connections wrapped at the column ends to help with controlling the formation of the plastic hinge, and/or, on the face of the beams to improve capacity (Ali et al. 2018). Seismic analysis is known to come with high uncertainty of loading and added complexity due to system reliability needed to quantify the action of the structure locally and globally. These added complexities create a need for more

adaptive methods to compute the reliability than historically used. The complex nature of the limit state function and high computational cost associate with executing system reliability analysis combined with FE analysis is a further limitation to seismic applications.

There has been some seismic studies that have looked at minimizing the amount of FRP material (cost) used for retrofitting while meeting a pre-determined target reliability index (Ali et al. 2018; Zou et al. 2018). Another study focused on seismic reinforcing of columns within a frame and the analysis framework considered capturing the uncertainty in seismic loads through statistical inputs of the inter-story drift associated with ground movement (Zou et al. 2018). Inter-storey drift was taken to be the only random variable in the reliability analysis. Optimal strengthening schemes were established by minimizing cost-reliability curves (i.e., amount of FRP vs. reliability index). An advantage to this framework is that it can probabilistically account for the uncertainty of earthquake loading while minimizing the amount of FRP needed to meet a pre-defined target reliability index, though the study did not account for variability in material strength or geometry.

A study in 2018 used non-linear FE analysis to assess the reliability of an RC building, looking at inter-storey drift ratios (Ali et al. 2018). This analysis used MCS instead of first-order methods to better account for the uncertainty, including both material strength and geometry. It was found that concrete strength, dead load, live load, and model error affected reliability the most.

A 2019 study assessed the system performance of an RC for three far field earthquakes using a non-linear FE analysis (Bagheri et al. 2019). The RC building was subjected to select ground accelerations while varying the length of the GFRP wrap on the columns. FORM was employed to calculate reliability values for each scenario, optimized for the amount of FRP needed. Both studies (Bagheri et al. 2019; Zou et al. 2018) found that increasing the amount of FRP material does not significantly increase reliability once confinement is achieved. Moreover, the reliability

will decrease once the optimal length of wrap is exceeded. This is due in part to the effect the FRP has on the formation of the plastic hinge during ground motion.

A study examined the optimization problem of lowering the cost of FRP strengthening in seismic applications using reliability (Mahdavipour et al. 2020). Reliability analysis based on Latin hypercube sampling (LHS) and FE pushover analysis were employed. Various configurations and combinations of FRP wrapping were considered to compare the failure modes and capacity. A key added parameter included in this study that had not yet been investigated by others is the addition of configurations that use end straps as additional anchorage to avoid premature debonding. Some studies (Bagheri et al. 2019; Mahdavipour et al. 2020) have seen that flange-bonding is more effective for increasing the capacity of the frame, whereas column wrapping is shown to be more effective for increasing ductility during ground motion.

2.6 RESEARCH GAPS

The following is a summary of identified gaps and future work from the review of current literature completed in the discussion of reliability-based research section:

Reliability Statistical Parameters: Review of Tables 2.2 to 2.4 shows no agreeance on a set of uniform statistics for analysis. Some researchers use statistics used in code calibration of load and resistance factors, conducting their own bench scale testing to propose certain statistics, assuming values, or take them to be deterministic. Additional work is needed to propose a uniform scheme of calibrating FRP material resistance or member reduction factors for concrete sections strengthened using FRP, based on a universal set of input statistical parameters categorized based on the application type (i.e., building applications, bridge applications, industrial applications etc.).

Reliability-Based Calibration of FRP Strain Limits in CSA standards: The CSA standard (CSA S806:17 and CSA S6:19) specify fixed tensile strain limits for the design of EB FRP strengthened members (0.007 and 0.004 in flexure and shear, respectively, in CSA S806:17; and 0.006 and 0.004 in flexure and shear, respectively, in CSA S6:19). These limits appear to be experimentally based. Research indicates that these imposed strain limits yield high variation and over-conservative designs in some cases. Reliability-based assessment is needed to validate the safety associated with the specified strain limits or propose optimum limits based on research, to meet code target safety.

Reliability-Based Evaluation of Anchorage Type for Code Application: It is suggested to formulate a reliability-based criterion for proposing code-compliant anchorage systems. For example, if an anchorage system is proven to meet a predefined target reliability index, it can be deemed code compliant. To achieve this, research is needed to (1) propose optimum target reliability indexes for evaluating compliance of anchorage with the respective design code; and (2) conduct a comprehensive reliability-based comparative analysis of existing anchorage systems to evaluate their compliance with the proposed target limit. System-based reliability can be used to propose the optimum target reliability index since it accounts for the consequence of anchorage failure. Kalfat et al. (2013) provides a single point of reference for experimental databases that could be used to help calculate the input statistics needed to calibrate the resistance models of different anchorage systems. In their work, anchorage efficiency factors have also been proposed to provide qualitative performance benchmarks.

Reliability-Based Calibration of FRP Material Resistance Factors in CSA Standards: Current research on strengthened columns confined with EB FRP has focused on the member strength reduction LFRD format, with limited studies on the material resistance factor format adopted by

CSA standards. More research is needed to incorporate current experimental databases (Huang et al. 2016, 2019, 2020; Lima and Barros, 2011; Smith and Teng 2003; Nasrollahzadeh and Aghamohammadi 2018; Okeil et al. 2013; Shi et al. 2013; Kalfat et al 2018; Alabdulhady and Sneed 2019) to calibrate the North American FRP design standards to suggest updated and centralized FRP material resistance factors. These databases contain experimental tests of axial, flexural, shear, and torsional members which include anchored and non-anchored tests.

Reliability-Based Sensitivity Analysis of Shear and Torsion ULS: Size effect, number of internal stirrups, and shear span have been shown to impact the reliability of EB FRP shear and torsion strengthened members. More experimental work conducted on full scale sections will ensure that the statistics used in the calibration of design standards and research capture the effect of size noted in several studies. Furthermore, additional work is needed to evaluate the reliability of EB FRP strengthened for torsion. Review of the different analytical, FE, and numerical models proposed to predict the capacity show that a large bias and variance currently exists between nominal and experimental results. To reduce the large uncertainty in the reliability analysis, more reliability-based work incorporating results from the growing number of experimental studies is needed to refine the resistance models used to represent the limit state.

Time-Variant (TV) Reliability-Based Analysis of EB FRP Strengthened RC Members Subjected to Stationary and non-Stationary Processes: Time-variant reliability analysis is an integral part of understanding the long-term effects of the use of FRP. Several reliability methods have been established in literature to conduct TV analysis, but few have been employed in EB FRP research. Processes involved in TV analysis can be stationary or non-stationary, which can relate to the variations in loads with time or variation of resistance with time. For example, live loads (in building and bridge applications) can be loosely considered stationary processes, while the

degradation in the resistance of an EB FRP strengthened member can be considered as a non-stationary process. Future research related to TV analysis should: (1) evaluate the applicability of current TV reliability techniques for evaluating the reliability of EB FRP members; (2) propose distribution types of the degradation processes related to RC members strengthened using EB FRP (Gaussian, non-Gaussian); and (3) evaluate the fatigue cumulative behavior of EB FRP strengthened RC members.

Reliability-Based Durability Limit State for Code Adaptation: Several studies looking at durability of strengthened members have put forth input statistics for time-variant (TV) reliability (summarized in Table 2.4). These statistics are based on limited number of experiments, mostly for bridge components, and more testing is needed to quantify these parameters. The variation of the existing concrete and steel were shown to impact reliability more negatively than the variation of the EB FRP design parameters. Future work should aim to investigate these effects. Fatigue has received only limited attention from a reliability perspective as the incorporation of it is usually deterministic. Research studies combining the study of durability and fatigue together probabilistically would ensure the long-term effects of strengthening are well understood.

Sensitivity of Member Reliability to the Reliability Method of Computation: Historical methods such as first order methods (FORM/FOSM) and MCS are still the standard reliability methods in EB FRP research. The first order methods can provide in-accurate reliability indexes should the EB FRP strengthened members limit state be non-linear limit and MCS can become costly to compute for low probabilities of failure. Novel methods using advanced techniques like adaptive reliability and machine learning are increasingly being employed to reduce the number of realizations needed to evaluate the performance functions (i.e., limit state functions) in civil applications like Adaptive Kriging techniques (Buckley et al. 2021). Future work should

investigate the feasibility of the use of these techniques in reliability-based analysis for EB FRP strengthening, to ensure accurate and efficient analysis.

Reliability-Based Optimization of EB FRP Design Based on Load History and Past Performance: Limited research has examined the impact of load type and history on the reliability of existing members. Consideration of load history parameters can allow the updating of the reliability of the member based on the loads it has seen to date. This is due to the truncation of the probability distribution function (PDF) of the load variables. Future research needs to include these load parameters in the reliability analysis of EB FRP strengthened RC members to better account for the existing conditions of the structure prior to strengthening, allowing an optimization of the design of upgrades for structures with satisfactory past performance. Care must be given when including load history parameters as the truncation of the PDF of any random variable can cause the limit state to become more non-linear. It is recommended that a robust method such as MCS be chosen for computation of reliability index to ensure that this non-linearity is captured.

Reliability-Based Analysis of EB FRP RC Members to the Spatial Variation in Material Properties and Degradation Processes: The additional consideration of random fields in reliability analysis can be a powerful tool for accounting for the randomness in the spatial distribution of certain random variables. Additional research is needed to account for the impact of considering the spatial distribution of the random variables on the structural reliability of EB FRP strengthened members in flexure, shear, and torsion. Accounting for this randomness is key to capturing the non-uniform distribution of physical parameters of each material. For example, random fields can be used to model the spatial variability in concrete compressive strength or bond strength at the FRP-concrete interface.

2.7 SUMMARY AND CONCLUSION

The present chapter summarized the research done to date on the reliability-based methods used to evaluate, calibrate, and optimize EB FRP strengthened concrete members. The reviewed works have covered a wide range of research categories around the use of EB FRP, covering many strengthening applications using a variety of reliability techniques. Reliability analysis requires input statistics of the random variables involved in analysis and the use of representative values is key for proper calibration of design standards. Multiple experimental databases have been collected in literature by researchers testing EB FRP strengthened members, with a range of full- and small-scale tests that contain both anchored and unanchored members. Such databases synthesized into a unified set of descriptive statistics for EB FRP could provide more accurate calibration and help reduce the variation in safety prescribed by each code for the same target reliability index. This work attempts to bridge this gap by providing a single point-of-reference for researchers and code committee members involved in calibration of design standards by providing summary tables of input statistics used in literature for conducting reliability analysis.

The continued revision and updating of design standards around the world to provide safe and economical retrofit designs with EB FRP is helping push FRP into a more competitive place when compared against conventional reinforcing materials like steel, used for strengthening. The overall goal should be to continually move toward having refined, optimized design standards that prescribe safe and economical designs using EB FRP. Reliability-based assessment procedures better integrated into design standards will give practicing engineers confidence when choosing FRP for retrofit as these standards can be continually updated each code cycle.

CHAPTER 3 STOCHASTIC FE MONTE CARLO SIMULATION RELIABILITY BASED ANALYSIS OF EB FRP STRENGTHENED RC BEAMS

3.1 EXECUTIVE SUMMARY

An identified research gap in Chapter 2 related to the design of EB FRP strengthening of existing members is the lack of research accounting for the existing conditions of a RC member prior to strengthening. Specifically, in accounting for the existing condition of the concrete substrate prior to strengthening and its effect on the FRP-concrete bond. To investigate this effect on the reliability of the strengthened beam, an experimentally tested beam with intermediate flexural crack (IFC) debonding failure mode has been chosen for assessment (Zhang et al. 2006). A validated FE model has been developed in LS DYNA of this beam. A novel framework has been developed for conducting automated SFE reliability analysis of EB FRP flexural strengthening of existing beams, considering the spatial variability of the concrete through random fields. The analysis has been completed for beams designed to CSA S806:17, CSA S6:19, and ACI 440.2R:17 standards, on a set of four strengthened sample beams. A total of 3,000 stochastic FE models have been generated and evaluated at ultimate conditions to establish the resistance statistics for the various analysis performed. To investigate the effect of spatial variability of the concrete strength on the beam's strengthened reliability, the coefficient of variation of the existing concrete strength ($COV_{f_c'}$) used to generate the random field has been varied. Comparison of the safety of both compression- and tension-controlled beams, between the three design standards, is presented herein. Parametric analysis on the effect of the tensile strain limit on the reliability of the strengthened tension-controlled members is also presented. Results show that the bias of the resistance models for the three codes are high, providing designs that are above the target index value. Effect of increased

strain limit was found to be minimal, showing that another source of conservatism is present in the design.

3.2 INTRODUCTION

Debonding failure of EB FRP strengthened RC beams that have been externally strengthened in flexure occurs when flexural cracks in the concrete reach the FRP-concrete bond surface. This phenomenon has been reported in literature during pre-mature failure of strengthened members during experimental tests (Smith and Teng 2002a; b). Section 1.2 explains the different failure modes of an EB FRP strengthened beam, including debonding. The failure mode of IFC debonding, typically occurs when a dominant flexural crack in the concrete substrate reaches the tension face, initiating debonding from inside the shear span towards the end of decreasing moment (Shi et al. 2015). As RC members are in-service, the concrete will degrade over time and may have a higher variation spatially. This variation could affect the reliability of the strengthened member and the member could be more likely to debond. Design standards such as CSA S806 prescribe that the concrete substrate be adequate to provide a full bond for strengthening purposes (CSA S806:17). The standard does not give further guidance on evaluating the amount of degradation in an existing member's concrete substrate prior to application of FRP. Similarly, the CSA S6 bridge code, in chapter 16, does not give guidance on how to assess the existing concrete substrate prior to strengthening (CSA S6:19). Instead, conservative limits are set by these standards on the usable strain that can be developed in the EB FRP to mitigate debonding (ACI 440.2R:17; CSA S806:17; CSA S6:19). ACI 440.2R:17 takes a similar approach by setting a maximum effective strain to mitigate debonding based on the work of Teng et al. (2003) and Teng et al. (2004). Proper consideration of the condition of the existing concrete substrate and calibration of the strain limit can be achieved with the incorporation of a reliability-based framework to assess the safety.

A prior study has investigated the effect of existing conditions on the reliability of FRP-based repair by varying the COV of the design variables (Wieghaus and Atadero 2011). The variation and amount of remaining area of steel prior to strengthening played a more significant role in negatively affecting the strengthened beam reliability than the variation in FRP. Other reliability studies have investigated EB FRP strengthened beams in flexure including debonding failure modes (Huang et al. 2019, 2020; Okeil et al. 2002; Petrie and Oudah 2021; Wang et al. 2010; Wang and Ellingwood 2015), but none have included the effects of accounting for the variation spatially of the concrete strength.

A method of accounting for the spatial variation in a member is through the use of stochastic FE (SFE), using random fields. An SFE model is an extension of deterministic FE modeling techniques, which are limited to using mean values to represent the material and load parameters. Prior research in civil engineering has investigated the use of SFE reliability to examine the safety of mono and group piles (El Haj and Soubra 2020; Khorramian et al. 2022; Li et al. 2020; Xiao-ling et al. 2021), and one work has applied SFE to assess the reliability of an internally reinforced GFRP RC beam (Oudah and Alhashmi 2022). Three proposed reliability frameworks exist in literature to conduct SFE analysis using random fields (Stefanou 2009): i) monte carlo simulation (SFE-MCS), ii) spectral stochastic finite element method (SSFEM), and iii) perturbation approach. These methods are general and can be applied to any FE software if the SFE model can be formulated.

The objectives of this works are two-fold: 1) develop a framework of analysis for assessing the safety of RC concrete beams strengthened using EB FRP using SFE analysis and MCS; and 2) apply the developed framework of analysis to assess the effect of the concrete spatial variability on the reliability of the EB FRP strengthened beams designed as per CSA S806:17, CSA S6:19,

and ACI 440.2R:17. The non-linear FE software LS DYNA has been chosen for developing the SFE models. An LSDYNA-Python-MATLAB interface has been developed to link and automate the generation of the random fields, discretization of the FE model to include stochastic element mesh (SEM), run SFE-MCS simulations in parallel, and conduct the reliability analysis to assess the safety.

3.3 BACKGROUND

3.3.1 Stochastic FE Modeling

Three-dimensional (3D) non-linear finite element (FE) analysis can be used to approximate the response of structural components (i.e., beams, columns) without extensive experimental testing. A Stochastic FE (SFE) model can be an additional powerful tool for the assessment of a structural component, as they allow the modeling of certain parameters as random fields. Random fields mathematically account for a parameter as a stochastic process, through the generation of a correlated field of random realizations.

In the example case of a reinforced concrete (RC) beam, the concrete is a heterogeneous material, and it is expected that the ultimate compressive strength, f_c', will vary throughout the volume. The variation can also be time-dependent if the concrete element is exposed to a time-dependent degradation process such as freeze-thaw damage. Figure 3.1 shows a representation of the spatial variability of f_c' along the longitudinal axes of the beam presented as a one-dimensional field. Typical engineering practice is to model this beam deterministically with mean values. Moreover, FE modeling software typically only allow the use of mean values to represent the strength and modulus throughout the section. Meaning this variability in the concrete is not

captured. As the beam remains in service, the concrete can degrade furthering the variation spatially throughout the concrete volume.

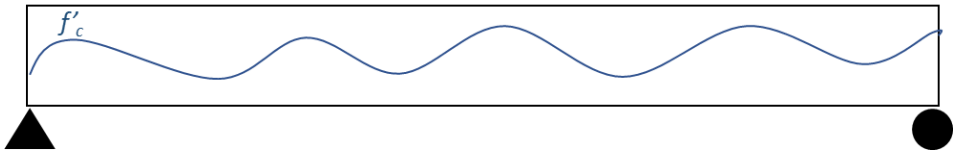

Figure 3.1. Representation of the spatial variation of concrete strength through an RC beam (an example of one-dimensional random field)

Each SFE model must have two sets of meshes: i) the FE model element mesh (EM) and ii) the stochastic element mesh (SEM) as schematically presented in Figure 3.2. The EM is the mesh generated by discretizing the beam geometry in the FE software, while the SFM is the mesh generated by discretizing the EM. It should be noted that each mesh is generated independently of each other. Both the EM and SEM can vary in density and do not need to be the same density. When the EM is a subset of the SEM, a mesh size ratio, *SEM/EM*, can be established. This ratio denotes the size of the SEM compared to the EM mesh of the SFE model and will be used for comparison of results in the mesh sensitivity analysis in section 3.6.1.

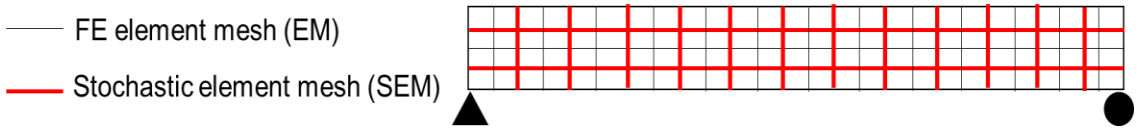

Figure 3.2. Schematic illustration of the FE element mesh (EM) and the stochastic element mesh (SEM) concepts.

Several methods of discretizing the SEM and generating the correlated random field have been proposed in literature and details of the methods can be found here (Li and Der-Kiureghian 1993; Sudret and Der-Kiureghian 2000). These techniques include methods to discretize the field based on point discretization techniques, such as the midpoint (MP), the shape function (SF), and optimal linear estimator (OLE) methods; based on average discretization techniques, such as the spatial

average (SA) and weighted integral methods; or based on series expansion techniques, such as the Karhunen-Louve expansion, and the expanded optimal linear expansion (EOLE) method. The EOLE method is a spectral presentation of the OLE method and has been shown to have low error with fewer terms in the truncation when generating the field (Li and Der-Kiureghian 1993). The EOLE method was used for discretization in this study and is explained in detail Section 3.2.2.

3.3.2 Random Fields – EOLE Method

This section covers the generation of a random field using the EOLE method. The present work uses a lognormally distributed 3D random field using the EOLE method, with Nataf transformation to convert the guassian field to a lognormal field (Nataf 1964; Li and Der Kiureghian 1993; Sudret and Der-Kiureghian 2000).

The first step in discretization of the SEM is the selection of a stochastic mesh density for representng the geometry of the member as a 3D mesh. Let $\boldsymbol{M_{SEM}}$ represent an array containing all $\boldsymbol{SEM}$ vectors at a given mesh density, $\boldsymbol{M_{SEM}} = \{\boldsymbol{SEM^{(1)}}, \boldsymbol{SEM^{(2)}}, \boldsymbol{SEM^{(3)}}, \dots, \boldsymbol{SEM^{(N_{mesh})}}\}$, where N_{mesh} is the number of discretized stochastic elements, and $\boldsymbol{SEM^{(i)}}$ is the ith element in $\boldsymbol{M_{SEM}}$ and is represented by its 3D corrdinates in space, $\boldsymbol{SEM^{(i)}} = (X_{SEM,i}, Y_{SEM,i}, Z_{SEM,i})$. The first two moments (i.e., the mean and standard deviation) are found for each point in the mesh. To do this, the mean value of the lognormal field is evaluated at the centroid of each SEM, the standard deviation of each SEM is evaluated as the mean multiplied by the coefficient of variation of the field. Next, the lognormal covariance matrix must be established using a chosen correlation function. The equation for the covariance matrix, $\boldsymbol{C_{YY'}}$ is given in Eq.[3.1]. A squared exponential correlation function, ρ, was utilized as expressed in Eq.[3.2].

$$\boldsymbol{C_{YY'}} = C_{Y^iY^j}(i,j) = \sigma_i\sigma_j\rho_{ij} \qquad [3.1]$$

$$\boldsymbol{\rho_{ij}} = \prod_{k=1}^{n} \exp\left(-\frac{\left\|Y_k^{(i)} - Y_k^{(j)}\right\|^2}{a_k^2}\right) \quad [3.2]$$

where, σ_i and σ_j are the standard deviation of ith and jth point considered (for a monolithic concrete medium $\sigma_i = \sigma_j$), and ρ_{ij} is the correlation function between the set of two points.

The term $Y_k^{(i)}$ represents the ith point in the field for the kth iteration and similarly $Y_k^{(j)}$ represents the jth point for the kth iteration. The term a represents the autocorrelation length (also referred to as the correlation length). It is a measure of how correlated two points are in any given direction. Expanding Eq.[3.2] for a 3D problem will give Eq.[3.3] where each of the two points considered is represented by a 3D vector of coordinates. A Nataf transformation can be applied to the lognormal covariance matrix to convert it to be in Gaussian space using Eq.[3.4] (Nataf, 1964).

$$\rho_{ij} = \rho_{YY'}(i,j) = \prod_{k=1}^{n} \exp\left(-\frac{\left(Y_x^{(i)} - Y_x^{(j)}\right)^2}{a_x^2} - \frac{\left(Y_y^{(i)} - Y_y^{(j)}\right)^2}{a_y^2} - \frac{\left(Y_z^{(i)} - Y_z^{(j)}\right)^2}{a_z^2}\right) \quad [3.3]$$

$$\rho'_{ij} = s\rho_{ij} = \frac{\ln\left(1 + \rho_{ij} v_i v_j\right)}{\rho_{ij}\sqrt{\ln\left(1+v_i^2\right)\ln\left(1+v_j^2\right)}} \quad [3.4]$$

where, ρ'_{ij} is the correlation for the standard normal field between two points $Y^{(i)}$ and $Y^{(j)}$, and s is a conversion factor converting the lognormal field. The terms v_i and v_j are the coefficient of variation of the mesh points $Y^{(i)}$ and $Y^{(j)}$, respectively.

Once in standard normal space, eigenvalues and eigenvectors can be obtained and ranked so that the r largest ($r\ out\ of\ N_{mesh}$) participating eigenmodes can be retained for field generation. Realizations of the gaussian field can be calculated using Eq.[3.5] by generating r randomly generated standard normal variables, $\xi(\theta)$.

$$\widehat{H}(Y,\theta) = \mu_{lny} + \sigma_{lny} \sum_{i=1}^{r} \frac{\xi_i(\theta)}{\sqrt{a_i}} \boldsymbol{\psi}_i^T \boldsymbol{C}_{Y,Y_i} \quad [3.5]$$

Where,

$$\sigma_{lny} = \sqrt{\ln\left(1 + \frac{\sigma_y^2}{\mu_y^2}\right)} \quad [3.6]$$

$$\mu_{lny} = \ln(\mu_y) - \frac{1}{2}\sigma_{lny}^2 \quad [3.7]$$

$\widehat{H}(Y,\theta)$ is the Gaussian field, made of two parts: i) the points within the discretized mesh, Y, and ii) the random component of generated standard normal random variables, θ; where σ_{lny} is the lognormal standard deviation of H, calculated using Eq.[3.6] and μ_{lny} is the lognormal mean of H, calculated using Eq.[3.7]. The ith standard normal random variable is represented by $\xi_i(\theta)$. The variable λi is the ith eigenvalue, while ψ_i^T is the ith eigenvector matrix. Finally, C_{YY_i} is the ith vector of the correlation matrix. The generated field values from Eq.[3.5] can be converted to be lognormal through Eq.[3.8].

$$\widehat{H_{ln}}(Y,\theta) = \exp\{\widehat{H}(Y,\theta)\} \quad [3.8]$$

A measure of the representation quality of the generated field needs to be assessed based on the truncation value, r. Two measures in literature have been used; one based on the variance of the field (Li and Der Kiureghian, 1993), shown in Eq.[3.9], and another based on the participation of retained eigenmodes used in field generation (Most and Bucher, 2006), expressed in in Eq.[3.10], where $H(Y)$ and $\widehat{H}(Y)$ are the exact and randomly realized value, respectively, of the stochastic field realization for point $\boldsymbol{Y}$. Note the terms in Eq.[3.9] are the same as Eq.[3.5] above. The term Q in Eq.[3.10] is named the representation quality, where the sum of the eigenvalues divided by the trace of the covariance matrix.

$$Var\left[H(Y) - \widehat{H}(Y)\right] = \sigma_{lny}^2\left[1 - \sum_{i=1}^{r}\frac{1}{a_i}\left(\psi_i^T\, C_{Y,Y_i}\right)^2\right] \quad [3.9]$$

$$Q = \frac{\sum_{i=1}^{r} \boldsymbol{C}_{Y,Y_i}}{tr(\boldsymbol{C}_{YY})} \quad [3.10]$$

It should be noted for both equations the value of r (i.e., the number of eigenvalues and eigenvectors included in field generation) will need to be increased with decreasing correlation length to maintain adequate representation quality using either measure.

3.4 METHODOLOGY

The methodology for delivering on the research objectives described in the introduction section consists of the following sequential phases:

1) *Development and Validation of a Base FE Model in LS DYNA.* Develop and validate a base 3D FE model of an experimentally tested EB FRP strengthened RC beam in LS-DYNA.
2) *Development of the SFE model***.** Describe the methods of discretization and generation of stochastic FE models in LS-DYNA using random fields. Describe the steps followed to generate SFE models.
3) *Conduct the reliability analysis***.** Develop a framework of reliability analysis using MCS and an automated computer code that was developed to perform the reliability analysis through an LSDYNA-Python-MATLAB interface to link the discretized SFE model and generated random field. Investigate the sensitivity of analysis results to the input stochastic parameters. Assess the effect of the concrete spatial variability on the safety of steel RC beams strengthened using EB FRP and designed using CSA S806:17, CSA S6:19, and ACI 440.2R:17.

3.5 DEVELOPMENT AND VALIDATION OF THE BASE FE MODEL

The following section describes the development of the base FE model to be used in the generation of the SFE model within the non-linear FE software LS DYNA. The beam chosen for analysis is an experimentally tested steel RC beam that has been strengthened externally with FRP. The beam description, model parameters, and validation with experimental results are presented in the

following subsections. The FE models are run using implicit displacement-controlled analysis in LS DYNA SMP single-precision solver.

3.5.1 Beam Description

A RC beam has been chosen from the experimental work of Zhang et al. (2006) for validation. The strengthened beam chosen from the study is beam A20. The geometry and location of reinforcement (internal and external) is shown in Figure 3.3. The concrete beam is reinforced internally with steel rebars and strengthened using CFRP laminate bonded externally to the tension face.

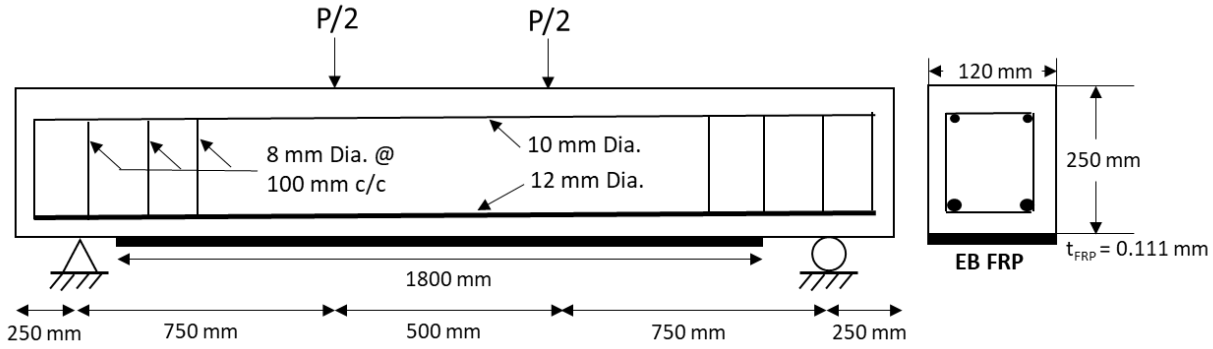

Figure 3.3. Overview of strengthened Beam A20 (Zhang et al., 2006)

The RC beam has a length, L, width, b, height, h, and depth to tensile rebar, d, equal to 2500 mm, 120 mm, 250 mm, and 225 mm, respectively, and f'_c equal to 23MPa. The internal tensile rebar consists of two 12 mm diameter bars and two 10 mm diameter bars in compression. The stirrups are 8 mm diameter bars spaced at 100 mm center on center. All steel has a yield strength. f_y, equal to 335 MPa and a modulus of elasticity, E_s, equal to 200 GPa. The EB FRP used for strengthening is a CFRP laminate that with a single layer thickness, t_{frp}, equal to 0.111 mm, with two layers used for a total thickness of 0.222 mm. The cross sectional width of the FRP, w_{frp}, equal to 120 mm, and has been attached to the tension face of the concrete with a length, L_{frp},

equal to 1800 mm. The CFRP has a tensile strength, f_{frpu}, equal to 3350 MPa and a modulus of elasticity, E_{frp}, equal to 235 GPa. Table 3.1 summarizes the sectional parameters of the strengthened beam.

Beam A20 was tested as a simply supported beam with no pre-load, in four point bending. Testing shows the failure mode of the strengthened section as debonding due to intermediate flexural cracks (IFC-debonding) after the internal steel had yielded. The ultimate load, P_u, at failure, was found to equal to 75.8 kN, with a deflection at ultimate load, Δ_u, equal to 27.0 mm. The ultimate tensile strain in the EB CFRP was also measured. At failure, the strain in the CFRP was measured to be equal to 11,000 $\mu\varepsilon$.

Table 3.1. Sectional properties of strengthened Beam A20 (Zhang et al., 2006).

Variable	Mean Value	Units
	Concrete	
b	120	mm
h	250	mm
d'	25	mm
d	225	mm
L	2500	mm
f_c'	23	MPa
	Steel	
f_y	335	MPa
$A_s\ (T)$	260	mm^2
$A_s'\ (C)$	142	mm^2
A_v	100	mm^2
E_s	200	GPa
	FRP	
f_{frp_u}	3350	MPa
E_{frp}	235	GPa
t_{frp}	0.222	mm
w_{frp}	120	mm
A_{frp}	26.6	mm^2
L_{frp}	1800	mm

b = beam width; h = beam height; d = depth to extreme tensile rebar; d' = depth to extreme compression rebar; L = length of beam; $f'c$ = concrete strength; f_y = steel yield strength; $A_{s,v}$ = Area of steel rebar; E_s = modulus of elasticity of steel; f_{frp_u} = FRP ultimate tensile strength; E_{frp} = FRP modulus; t_{frp} = FRP thickness; w_{frp} = FRP width; A_{frp} = Area of FRP; L_{frp} = Length of bonded FRP.

3.5.2 Mesh Density, Boundary Conditions, Loading, and Contact Definition

3.5.2.1 Mesh Density

A 3D non-linear FE model has been developed in LS DYNA to represent the chosen sample beam described in Section 3.5.1. A full model of the beam made has been created and validated against experimental results. Figure 3.4 shows an overview of the developed model, showing the various locations of the concrete and reinforcement, location of loading, and boundary conditions. The mesh of the shell and solid elements that make up the EB FRP and concrete, respectively, is shown.

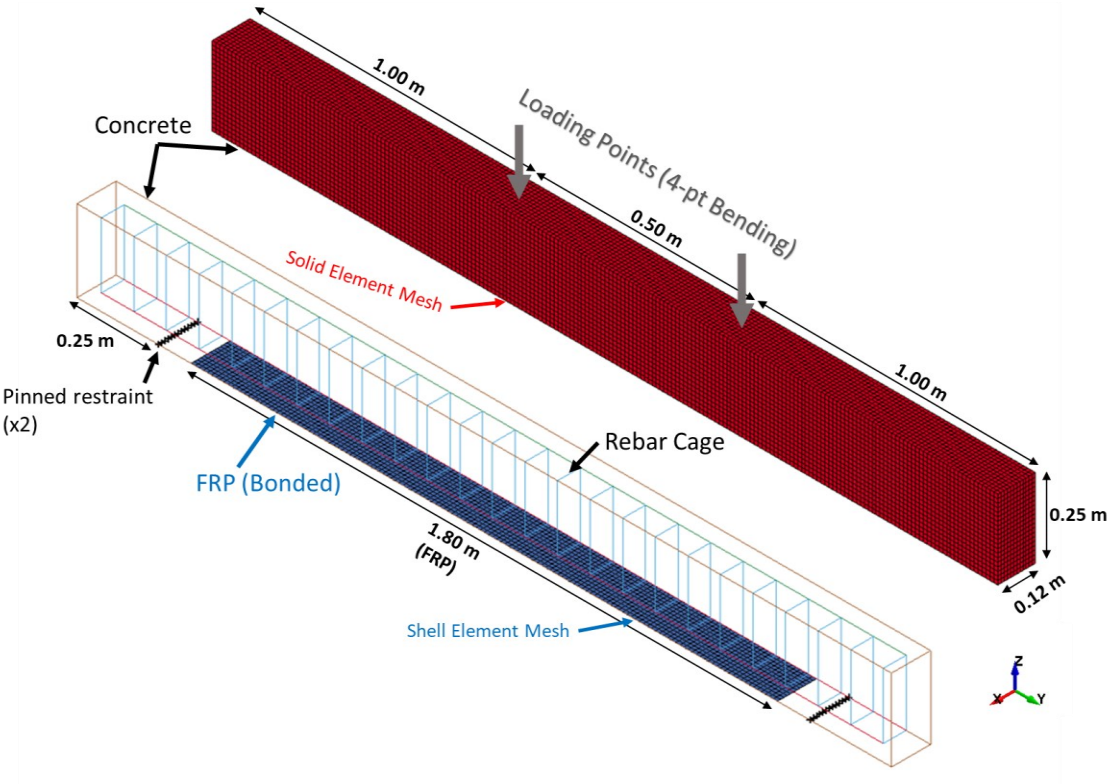

Figure 3.4. Overview of FE model of Beam A20 (LS DYNA)

3.5.2.2 Boundary Conditions

Boundary conditions need to be assigned to the full model to idealize the sample beam selected as shown in Figure 3.3. At the two support locations, 250 mm away from the ends of the beam, a pin restraint and a roller restrain were added to each side, respectively. This restricted translational movement in the z-directions. Figure 3.4 shows the locations of both boundaries (shown as a line of black 'x', labeled "pinned restraint").

3.5.2.3 Contact

Rebar-concrete Bond: Constrained Lagrange in Solid

A Lagrange constraint (*CONSTRAINT) type keyword was used to model a perfect bond between the steel rebar and the concrete volume in LS DYNA. This constraint works by bonding the two materials together using central nodes and solving for the contact forces. This constraint definition requires a slave and a master part to be defined. For this application, the steel was chosen as the salve and the concrete as the master. For the steel and concrete to be defined in the constraint, a part set (*SET_PART) was defined for each.

FRP-concrete Bond Contact: Automatic_Surface_To_Surface_Tiebreak

A tiebreak contact definition has been chosen to simulate the FRP-concrete bond in LS DYNA. Specifically, the 'automatic surface to surface' tiebreak definition was used. This is a penalty-based contact that, depending on the option of formulation selected, will tie the master and slave surfaces together and assign a failure criterion for debonding. Segment (*SET_SEGMENT) definitions were employed. Segment definitions ensure the bonding of surfaces are localized so the program does not tie any extra surfaces.

Several options exist in LS DYNA for how elements that are initially in contact are treated. Option 2 – tie all surfaces initially in contact until failure is reached – was selected, as it ties all nodes of the FRP and concrete segments that are in contact with each other at the onset of analysis. This will then allow the concrete and FRP to be "stuck" together until the failure criteria is met and debonding occurs at that location.

The failure criterion used in this model is based on the failure normal and shear surface stresses of the contact interface, given by inputs $NFLS$ and $SFLS$, respectively (Chen and Teng 2001; Lu et al. 2005). The failure criterion follows Eq.[3.11] taken from the LS DYNA theory manual:

$$\left(\frac{|\sigma_n|}{NFLS}\right)^2 + \left(\frac{|\sigma_s|}{SFLS}\right)^2 \geq 1.0 \qquad [3.11]$$

The numerators of Eq.[3.11] are the normal and shear stresses, calculated by the FE software, at the bond interface nodes. The denominators are the user defined failure limit stresses, $NFLS$ and $SFLS$. These parameters are key to defining when the FRP will debond from the concrete. Several empirical formulas have been proposed to calculate these inputs for various materials. For externally bonded FRP, the work by Neale et al. (2005) was used to estimate the stress limits using Eq.[3.12] and Eq.[3.13]. Other studies on EB FRP strengthened beams have also used these equations to establish a debonding failure criteria (Almusallam et al. 2015; Elsanadedy et al. 2013). These equations work by estimating the bond failure stress limits based on the concrete strength and several scale factors, as shown.

$$NFLS = 0.62\sqrt{f_c'} \quad [3.12]$$

$$SFLS = 1.5\beta_w NFLS \quad [3.13]$$

$$\beta_w = \sqrt{\frac{2.25-\frac{b_f}{b_c}}{1.25+\frac{b_f}{b_c}}} \quad [3.14]$$

The term β_w in Eq.[3.14] is a scale term based on the ratio of the width of the FRP (b_f) and the width of the concrete section (b_c). Using the inputs of beam A20 from Table 3.1, the $NFLS$ and $SFLS$ stresses were found to be 2.97 MPa and 3.32 MPa, respectively. All other parameters on the contact card are set to default.

3.5.2.4 Loading Protocol

Monotonic loading using displacement control was considered in this study. Displacement control allows investigation into the both the ultimate and post-peak response of the beam during failure. The model is set up to have 4-pt bending to conform with the experimentally tested beam. The shear span of the experimental beam was reported to be 750 mm, with 500 mm of space between loading points (Zhang et al. 2006). Figure 3.4 shows the location of loading points for 4-pt bending.

A load protocol is implemented in LS DYNA to simulate flexural bending. Definition of the load curve is key, so that an appropriate rate can be found so that no dynamic force is introduced into the system. To accomplish this, a displacement-controlled load curve was defined with 1:1 slope. The range of the curve is set from 0s to 10s in 0.01s intervals. The choice of range is so that the simulation terminates at a maximum of 10s.

3.5.3 Material Models and Element Type

3.5.3.1 Steel Reinforcement

Plastic-kinematic material (*MAT_003) was chosen to idealize the internal steel reinforcement. The reinforcement used in the experimental study had a yield strength of 335 MPa. The density (RO) and modulus of elasticity (E) of the steel was taken to be 7700 kg/m^3 and 200 GPa, respectively. A Poisson's ratio of 0.3 was used. The tangential modulus ($ETAN$) is also needed to be define in this model. Based on the estimations in Almusallam et al. (2014), $ETAN$ was taken as 468 MPa. Figure 3.4 shows the reinforcement (rebar) cage inside the concrete volume. The reinforcement was modeled using a beam element (*SECTION_BEAM) with a truss element formulation.

3.5.3.2 Concrete

The concrete damage model (*MAT_72R73) was selected to idealize the concrete volume. This concrete model is robust as it generates the other parameters needed based on the concrete compressive strength ($A0$), density (RO), and Poisson's ratio (PR) provided. Figure 3.4 shows the concrete volume in LS DYNA for a given mesh density. The compressive strength and density were taken to be 35 MPa and 2400 kg/m^3, respectively. A Poisson's ratio of 0.2 was used.

The concrete volume was modeled using solid elements. A solid element (*SECTION_SOLID) was selected to be used to represent the solid element of the concrete. An element formulation and mesh density must be chosen. Several element formulations and mesh densities are investigated as part of a sensitivity analysis. The following element formulations are investigated in the model validation in Section 3.5.5:

- EQ. 1: constant stress solid element (default).
- EQ. 2: fully integrated S/R solid.
- EQ. -1: fully integrated S/R solid for poor aspect ratio elements, efficient formulation.
- EQ. -2: fully integrated S/R solid for poor aspect ratio elements, accurate formulation.

3.5.3.3 EB FRP Reinforcement

An enhanced composite material (*MAT_54) was chosen to idealize the EB CFRP as a shell element. The use of this material in LS DYNA is useful for simulating FRP as it provides input for all laminate properties, along with added failure criteria for the laminate. Figure 3.4 shows the EB FRP (shown in blue) bonded at the tension face to the reinforced concrete volume shown in brown. The CFRP was idealized as an orthotropic material.. An isotropic material definition has been used other works investigating the debonding of FRP laminate from RC sections as pre-mature debonding is the focus of investigation (Almusallam et al. 2015). This assumption allows the properties of the FRP in the tensile direction to be used in all directions but may not be representative.

The parameters of the EB CFRP given in Section 3.5.1 were used to calibrate the material model in LS DYNA. The density (RO) and modulus of elasticity ($EA\ and\ EB$) are taken to be 1740 kg/m^3 and 235 GPa, respectively. The ultimate failure strength (XT/YT) for the CFRP was given to be 3500 MPa.

Additional parameters of shear strength (SC) and shear modulus ($GAB/GCB/GCA$) were needed for material input for the CFRP in LS DYNA. The parameters were estimated based on laminate theory and were found to be 60.7 MPa and 13.1 GPa, respectively. It was recommended that the shear modulus be set to the same in all directions (Elsanadedy et al. 2013). All other parameters in the card are set to default.

The external FRP reinforcement was modeled using a 4-node shell element in LS DYNA. The section *SECTION_SHELL was selected, and the following shell element formulations were considered in the sensitivity analysis in Section 3.5.5:

- EQ. 16: Fully integrated shell element (very fast).
- EQ. -16: Fully integrated shell element modified for higher accuracy.

3.5.4 Model Limitations

With any FE model, limitations to the model are always present. The following limitations should be considered for the present work:

- FRP is idealized as an isotropic material.
- Perfect Bond assumed between internal steel reinforcement and concrete when defining constraint.
- Stirrups have been drawn at the centroid of the longitudinal reinforcement.
- Additional parameters of shear strength and modulus were not available and were estimated based on laminate theory.
- Separate models for examining crack propagation and debonding were used. Both actions should be considered together when considering IFC-debonding.

3.5.5 Base FE Model Validation

The validation of the proposed FE model in Section 3.5.3 is presented in this section for the experimentally tested beam shown in Section 3.5.1. The EB FRP strengthened RC beam model for beam A20 shown in Section 3.5.1 will be referred to as the "strengthened beam model" from herein. Sensitivity of the strengthened beam model to two varying FE element mesh (EM) densities, two shell formulations, and four solid formulations is conducted to investigate the optimal configuration of FE model to run the reliability analysis. Refer to Section 3.5.2 for explanation of the various element formulations. Table 3.2 lists the range of parameters varied in LS DYNA for the sensitivity analysis.

Table 3.2. FE parameters included in the sensitivity analysis (Beam A20)

Parameter	Range			
EM Density (mm)	25x25x25		12.5x12.5x10	
Shell Formulation	16		-16	
Solid Formulation	1	-1	2	-2

Table 3.3 shows the performance of the 16 different configurations of the FE model compared to experimental results. Comparison of the FE results to the experimental results is conducted to find the optimal configuration for the FE analysis. Table 3.3 gives the ratio of experimental to FE (EXP/FE), to show how each strengthened beam model configuration performs. A satisfactory performance is one that agrees with experiment and provides an EXP/FE ratio close to unity. Failure mode and tensile strain in the EB FRP at failure of each beam is reported in the table. With Y-IC representing yielding of the internal rebar followed by IFC debonding, and Y-Cr representing yielding of the internal rebar followed by crushing of the concrete.

Table 3.3. Results of the FE sensitivity analysis.

Trial	LS DYNA	Element Formulation			Output Parameters					
#	FE Mesh Density (mm)	Shell (FRP)	Solid (Concrete)	Results	P_u (kN)	P_y (kN)	Δ_u (mm)	Δ_y (mm)	ε_{frpu} (mm/mm)	Failure Mode
0	---------- *Experimental Results* ----------			EXP	75.8	--	27.0	--	11,000	Y-IC
1	25x25x20	16	1	FE	66.2	59.1	7.89	5.38	3,745	Y-IC
				EXP/FE	1.15	--	3.42	--	2.94	
2			-1	FE	64	62.2	5.52	5.39	2,679	Y-IC
				EXP/FE	1.18	--	4.89	--	4.11	
3			2	FE	N/A	N/A	N/A	N/A	N/A	Y-IC
				EXP/FE	--	--	--	--	--	
4			-2	FE	65.8	61.6	7.33	5.02	4,080	Y-IC
				EXP/FE	1.15	--	3.68	--	2.70	
5	25x25x20	-16	1	FE	65.5	59.1	8.7	5.1	4,483	Y-IC
				EXP/FE	1.16	--	3.10	--	2.45	
6			-1	FE	65.1	53.4	6.87	4.3	3616	Y-IC
				EXP/FE	1.16	--	3.93	--	3.04	
7			2	FE	66.9	5.2	7.3	4.6	3,879	Y-Cr
				EXP/FE	1.13	--	3.70	--	2.84	
8			-2	FE	64	55.2	5.72	4.4	2,550	Y-IC
				EXP/FE	1.18	--	4.72	--	4.31	
9	12.5x12.5x10	16	1	FE	76.9	58.9	24.7	5.3	7,750	Y-IC
				EXP/FE	0.99	--	1.09	--	1.42	
10			-1	FE	84.1	60.5	27.8	5.4	10600	Y-IC
				EXP/FE	0.90	--	0.97	--	1.04	
11			2	FE	83.3	61.8	27.7	5.3	10660	Y-IC
				EXP/FE	0.91	--	0.97	--	1.03	
12			-2	FE	84.6	60.6	28.9	5.3	10640	Y-IC
				EXP/FE	0.90	--	0.93	--	1.03	
13	12.5x12.5x10	-16	1	FE	78.6	59	22.9	5.4	9,210	Y-IC
				EXP/FE	0.96	--	1.18	--	1.19	
14			-1	FE	84.4	60.4	27.6	5.3	10,200	Y-IC
				EXP/FE	0.90	--	0.98	--	1.08	
15			2	FE	82.7	60.6	27.5	5.5	10,170	Y-IC
				EXP/FE	0.92	--	0.98	--	1.08	
16			-2	FE	80.3	60.1	27.5	5.4	10,600	Y-IC
				EXP/FE	0.94	--	0.98	--	1.04	

P_u = Ultimate Load at Debonding; P_y =Yield Load; Δ_u = Deflection at Ultimate Load; Δ_y = Deflection at on set of yielding of internal steel rebar; ε_{frpu} = Ultimate Tensile Strain in EB FRP; N/A = no results obtained for sample.

From Table 3.3, the finer EM (12.5x12.5x10 mm), trials 9 to 16, perform best at predicting the ultimate response of the strengthened beam as compared to experimental tests than the coarser EM (25x25x20 mm), trials 1 to 8. This may be due to the finer mesh allowing the cracking pattern to better be propagated through the section to allow the initiation of debonding. It was found the best performing configuration of all trials is trial #16. Trial #16 is an FE configuration using the finer

EM mesh with a shell formulation of 'fully integrated shell, accurate formulation' (EQ.-16), combined with the solid formulation of 'fully integrated solid, accurate formulation' (EQ.-2). This configuration of mesh density and shell / solid formulation will be used moving forward to generate all SFE models. Results of this configuration against experimental are shown in Table 3.4 and the FE model at ultimate is shown in Figure 3.5. The top image in Figure 3.5 is an elevation view of the beam showing the cracking of the beam at ultimate, while the bottom image is a plan view of the bond surface showing the nodes of the FRP-concrete bond that have debonded (shown in red). As can be seen, the flexural cracking that has reached the tension face has caused the FRP to debond from the center outward.

Table 3.4. Validation results for EB FRP strengthened RC beam.

Beam A20	P_y (kN)	P_u (kN)	Δ_y (mm)	Δ_u (mm)	ε_{frpu} (mm/mm)
*EXP	--	75.8	--	27.0	11,000
FE	60.1	80.3	5.4	27.5	10,600
EXP/FE	--	0.95	--	0.98	1.03

*(Zhang et al., 2006)

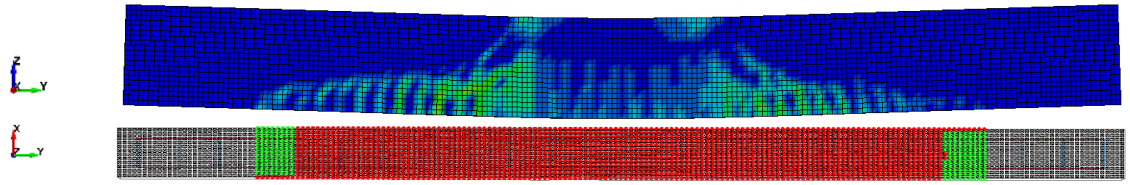

Figure 3.5. FE Model of Beam A20 at Ultimate: IFC Debonding Failure (LS DYNA)

3.6 DEVELOPMENT OF THE SFE MODEL

To consider the effect of the spatial variation in the material properties, 3D random fields representing the concrete strength are generated and applied to the strengthened beam model developed in Section 3.5. A fully correlated 2D random field for the normal and shear stress limit

parameters of the FRP-concrete bond are also generated based on the equations for bond stress limits presented. The spatial discretization of the concrete and bond strength, based on the existing condition of the concrete, allows the effects of spatial variation in the concrete strength parameters on the IFC debonding failure mode to be captured.

An automated MATLAB code has been developed to generate the random fields using the EOLE method to model the variation in material strength. An automated script in Python has also been developed to discretize the SFE model to have two meshes (EM and SEM) and link the generated random field (MATLAB) to the SFE model (LS DYNA). Section 3.6.1 covers the discretization of the SFE model. Section 3.6.2 covers the framework for the generation of the random field and construction of the SFE model. A flow chart of the code showing the general process is presented in the following subsections.

3.6.1 Discretization of SFE Model in LS DYNA

For simplicity of application, it is typical that the SEM be a subset of the EM (Sudret and Der-Kiureghian 2000). This is to ease the burden of discretization the SEM mesh in the FE software. EM elements can be grouped together through special definition of groups within the FE software (see Section 3.3.1). In LS DYNA, the SEM can be included through the assignments of numerous parts (*PART) to represent each element of the discretized random field, which can be assigned the unique value. The discretization of the SEM through assignment of unique parts (*PART) in LS DYNA is tedious and needs to be done for each new SEM density.

Cfiles (.Cfile) is used to automate the SEM discretization process. A Cfile is a command file read by LS DYNA that can execute a series of commands within the program to build or modify an FE model. An automated computer code has been developed in MATLAB to take the base FE model generated in Section 3.5 and discretize the model to include a secondary stochastic element

mesh using Cfile assignment. The Cfile is generated based on the chosen density of SEM and will generate unique parts (*PART), materials (*MAT), segments (*SEGMENT), and contacts (*CONTACT) to represent each stochastic element in the SEM.

Figure 3.6 shows sample two images of the same generated 3D strengthened beam model in LS DYNA, showing both the EM (left) and SEM (right). Each 3D SEM made of 4 EM in each direction (x, y, z), making the dimensions of a single EM and SEM equal to 12.5x12.5x10 mm and 50x50x40 mm, respectively, and having mesh size ratio = 4x4x4 (SEM/EM). A different color is assigned to each SEM part in LS DYNA to show the density of the field.

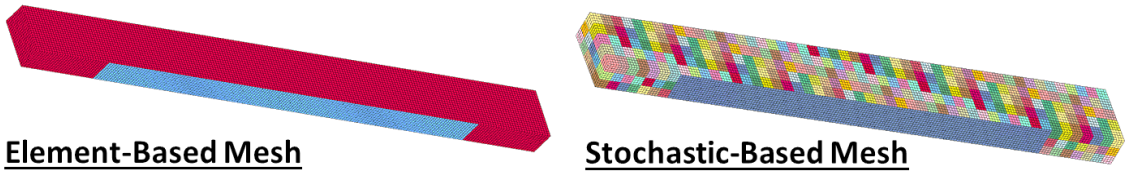

Figure 3.6. Representation of the spatial variation of concrete strength through an RC beam.

3.6.2 Generation of SFE Model in LS DYNA

A 3D random field has been generated to represent the variation in concrete strength throughout the beam using the EOLE method presented in section 3.3.2. The validated FE model from Section 3.5 is discretized to include the stochastic mesh using a Cfile to discretize the concrete volume. A random field generates values at the centroid of each SEM to create the 3D random field representing the correlated concrete strength. A fully correlated 2D random field of bond strength parameters is generated based on the concrete strength at the contact location to simulate the effect of concrete variation on bond strength. To generate the 2D field, the FRP-concrete contact definition in LS DYNA has been discretized to have the same SEM density as the concrete volume SEM. This will allow a 2D random field to be calculated of the normal and shear failure limit stress

($NFLS\ and\ SFLS,$ respectively). These bond parameters make up the failure criteria for debonding (see Section 3.5.2).

Figure 3.7 shows the steps of the code developed to generate the random field values and discretization of the SFE models, using MATLAB and Python scripts. The main MATLAB script is to generate the random field using the EOLE method and discretize the SEM. A Python script is used to call and manipulate the SFE files in LS DYNA. An open-source Python code package was used to call and manipulate the input file (.k file) (Diez, 2018). This package was used as a base to develop a script in Python to be called by MATLAB to populate the SEM with the generated random field values.

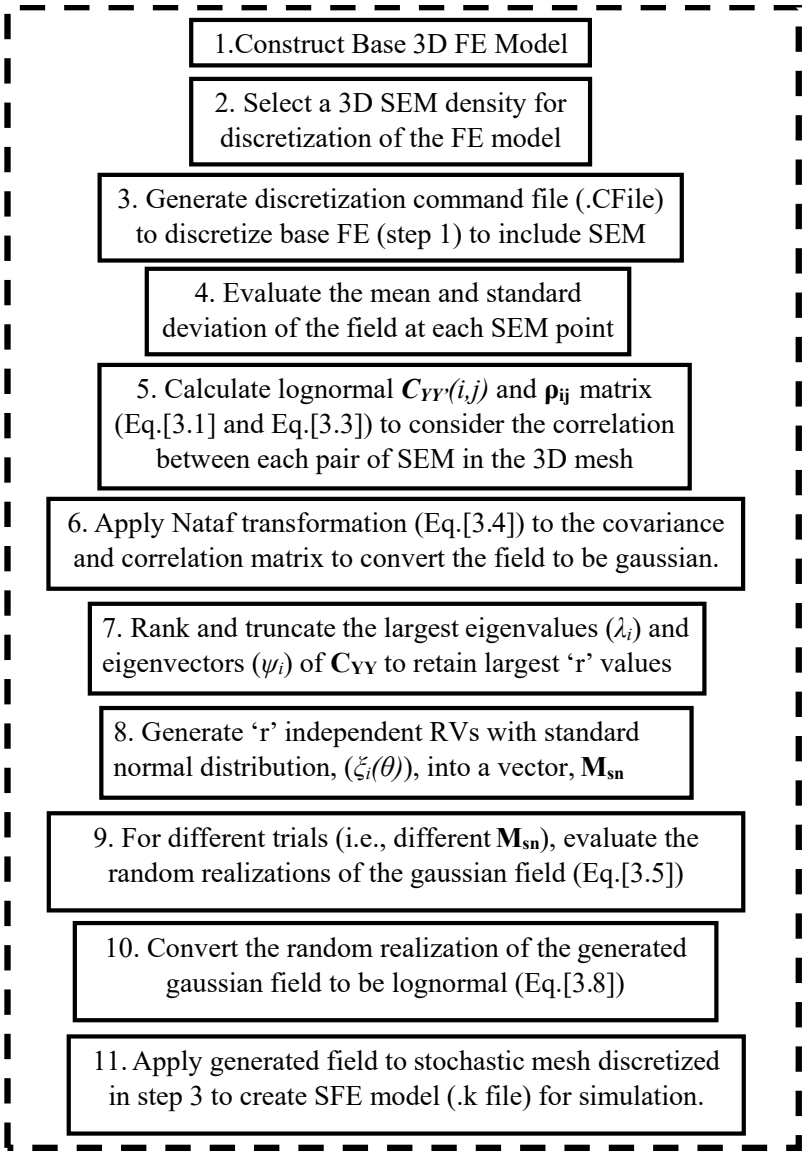

Figure 3.7. Steps of discretization / generation of SFE model using EOLE

3.7 RELIABILITY ANALYSIS USING MCS AND STOCHASTIC FE MODEL

Reliability analysis for a set of sample EB FRP strengthened FRP beams (both compression and tension controlled) is presented using the validated SFE model and Monte Carlo simulation (MCS). The framework of analysis and description of LSDYNA-Python-MATLAB computer interface is given in Section 3.7.1. A sensitivity analysis on the stochastic inputs of SEM density

and correlation length are presented in Section 3.7.2 and 3.7.3, respectively. SFE-MCS analysis is completed on the beams for varying concrete COV to simulate increased in the variability in the concrete strength spatially. Comparison of the codes and parametric analysis on the effect of the prescribed FRP tensile strain limit is presented in Section 3.7.4. Clause 16.8.2.2 of CSA S6:19 and Clause 8.2.2 of CSA S806:17 state that if the ULS design of the section is governed by FRP rupture, M_r shall be greater than 1.5 and 1.6 times, respectively, the value of M_f. These factors were not considered in the reliability analysis as the inclusion would increase the reliability index of the strengthened beams to be much greater than most target reliability index, as discussed in Section 3.7.4.

3.7.1 Framework of Analysis and Computer Code Description

An automated computer code has been developed to conduct the reliability analysis. An interface has been established to link the generated random field in MATLAB and the SFE model in LS DYNA, through the use of a Python script. Each program (MATALB, LS DYNA, Python) is designated by a color and a colored label withing the figures. When a script of one program calls another programs script (i.e., MATLAB, or Python, calling LS DYNA) this will be represented by having the called program labeled box nested within the primary program labeled box. Reliability analysis is complete in two steps: (i) pre-processing SFE-MCS analysis to establish resistance statistics (Figure 3.8); and (ii) post-processing SFE-MCS reliability analysis to assess the safety of the strengthened beam (Figure 3.9).

The pre-processing framework is used in establishing the resistance statistics using the steps in Figure 3.7 for discretization and generation of the random field using EOLE. To start, the inputs for the random variable statistics, beam geometry, material properties, and stochastic parameters

are taken by MATLAB. The inputs are passed to Python and MATLAB scripts. The MATLAB script generates the random values for the design random variables and generates the random fields for the concrete and bond. The Python script generates the discretization file and applies it to the base FE model. The generated random field values in MATLAB are linked to LS DYNA through Python to create the SFE model. This process is repeated for 'N' number of times needed to complete the MCS analysis.

The running of SFE simulations in LS DYNA SMP solver has been automated through MATLAB and has been optimized to run several simulations in parallel. In this work a total of 9 simulations were run in parallel to improve computation time. All analysis were run on the structural assessment and retrofit (SAR) server: a windows-based server with dual Intel Xeon Gold 5220R 2.20GHz processors (48 cores), a NVIDIA Quadro P620 graphics card, and 128 Gb of available RAM.

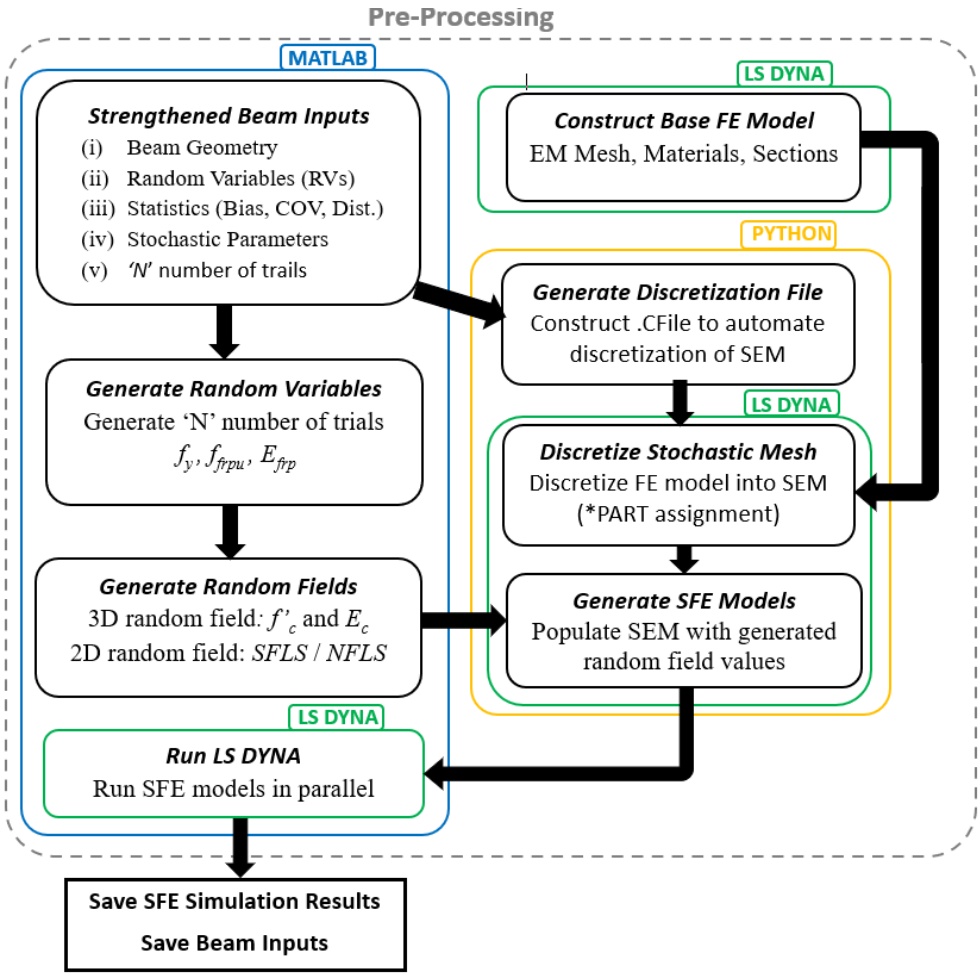

Figure. 3.8. Flow chart of SFE model generation: Pre-processing

The post-processing framework shown in Figure 3.9 is used to conduct the reliability assessment of the strengthened beams by MCS. An automated python script has been used to extract the ultimate moment from the saved simulation data and calculate the resistance statistics (mean and standard deviation) for each sample population of beams generated in the pre-processing SFE-MCS. Then, using the resistance statistics calculated, a model error term for the SFE model, and the load statistics of the various codes, MCS is conducted considering these variables as random inputs in the performance function (Section 3.8.2). Evaluation of the probability of failure and reliability index can be completed by Eq.[1.3].

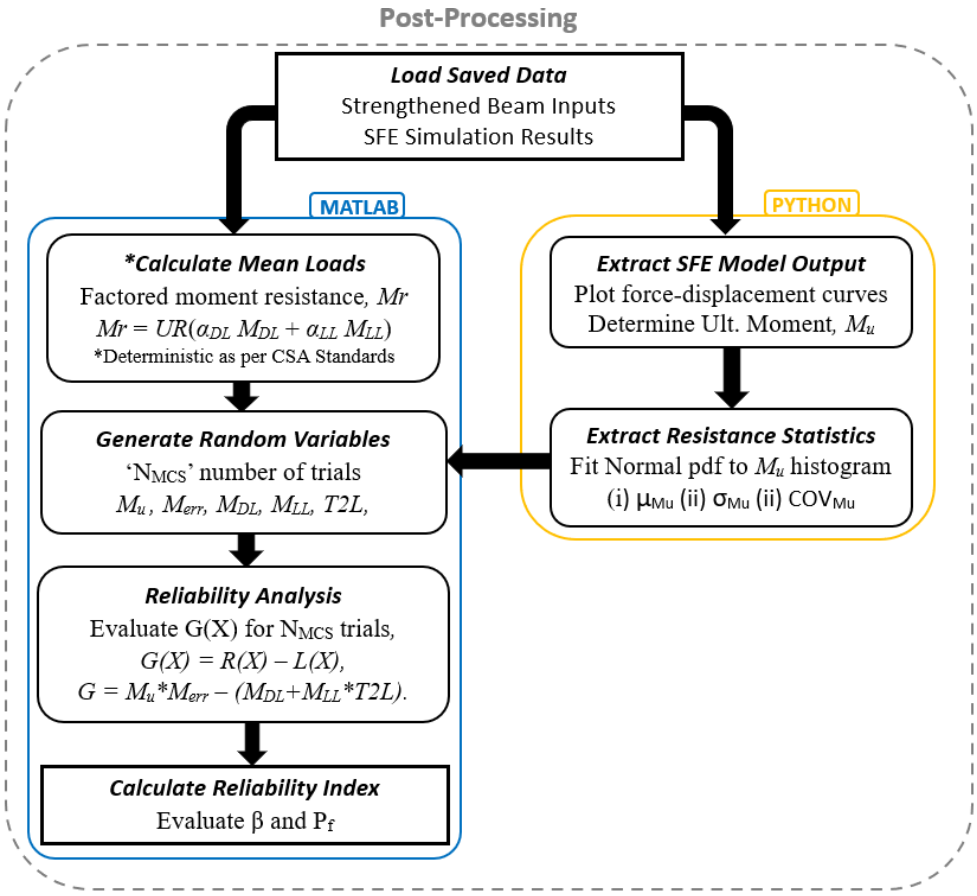

Figure. 3.9. Flow chart of SFE reliability analysis: Post-processing

3.7.2 Sensitivity of Stochastic Model Parameters

A parametric analysis on the effect of two stochastic input parameters that relate to the stochastic field generation is investigated for the chosen beam, Beam A20. The input parameters for the beam are given in Table 3.1 with the concrete strength taken as, $f'_c = 25\,MPa$ and a $COV_{f'_c} = 0.1$. The density of the SEM and the value of the correlation length have been investigated.

A total of 200 SFE simulations have been run for each configuration in two sequential analyses. In Analysis 1, the SEM mesh density has been varied for three different densities. In Analysis 2, the correlation lengths in the 3-dimensions (a_x, a_y, a_z) needed in the EOLE method when

generating the random field are varied based on the optimal mesh density found in Analysis 1. Note the number of terms kept in the truncation, r, in generating the field has been varied for each configuration so that the representation quality, Q, is at least 0.80.

The analysis results are evaluated based on the *efficiency* and *quality* of the configurations on estimating the ultimate response and capturing the debonding failure mode. *Efficiency* relates to the cost of computation and the effort needed to compute a result. *Efficiency* matters as it can be costly to compute multiple SFE to conduct reliability analysis such as MCS when a small probability of failure is expected. *Quality* relates to the number of terms needed to be included in the generation of the field to ensure a refined accurate field representation. Each term kept in the truncated series is a random variable that needs to be considered in the analysis. The configuration chosen should be able to consistently capture the response of the member while including the effects of the stochastic field in an accurate matter. An optimal configuration of SFE will be one that balances quality, consistency, and efficiency.

3.7.2.1 Stochastic Element Mesh (SEM) Density

The *mesh size ratio* (SEM/EM) is varied of the SFE model to investigate the effect on the performance of the SFE models. Three mesh size ratios were examined. Table 3.5 summarizes the SEM densities considered. It provides the total number of elements in the discretized SEM, the size of each SEM, and the mesh size ratio. The steps in Figure 3.7 were used to generate and run 200 SFE models of each beam configuration. Performance of each mesh density is investigated based on efficiency and to show the effect of different mesh densities on the distribution of the ultimate response (moment resistance, M_u, at ULS) of the SFE models. The EM mesh of the model was kept constant with a size of 10x12.5x12.5 mm (x, y, z) based on the validation done in Section

3.5. Figure 3.10 shows isometric view of the three SFE models with each cross section shown below it, showing the different SEM density.

Table 3.5. SEM parametric analysis: Considered configurations of SME density.

Config ID	MESH60	MESH40	MESH20
Total SEM	320	750	6000
SEM (mm)	60x62.5x62.5	40x50x50	25x25x20
SEM/EM (x, y, z)	6x5x5	4x4x4	2x2x2

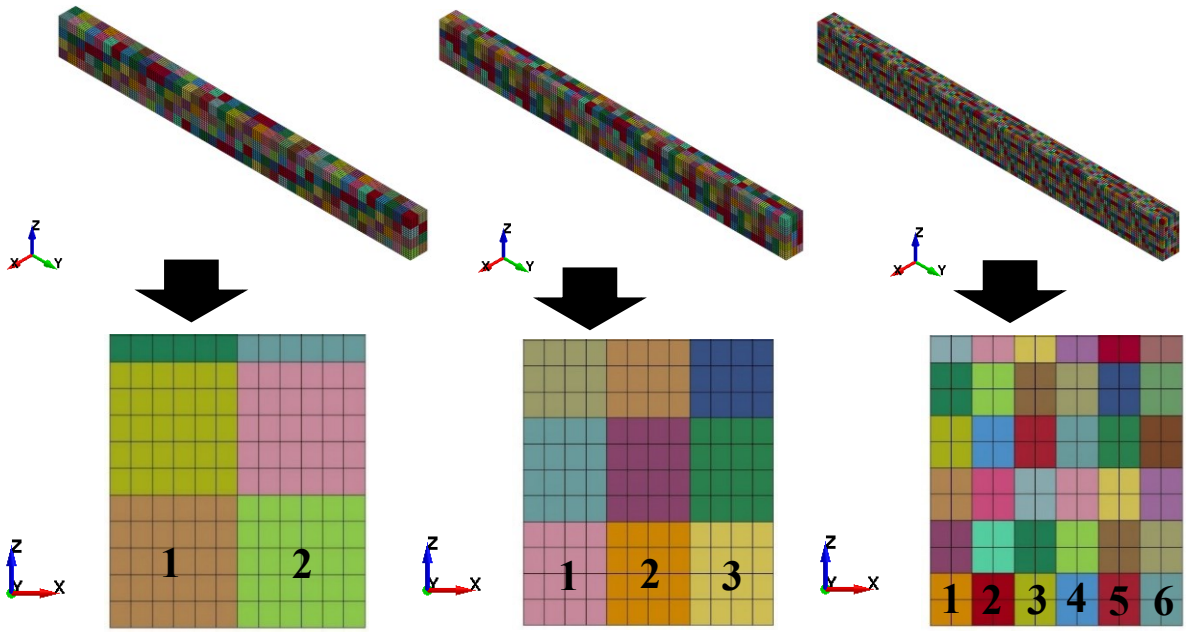

(a) MESH60 (b) MESH40 (c) MESH20

Figure 3.10. SEM parametric analysis: SFE Mesh for Different SEM/EM ratio.

Figure 3.10(a) shows a MESH60 SFE model with a mesh size ratio of 6x5x5 (*SEM/EM)* that consists of 2, 4, and 40 SEM across the $x-$, $y-$, and $z-$axis, respectively (refer to Section 3.6.1 for sample calculation of SEM/EM). Figure 3.10(b) shows a MESH40 SFE model with a 4x4x4 mesh that consists of 3, 5, and 50 SEM across the $x-$, $y-$, and $z-$axis, respectively. Figure 3.10(c) shows a MESH20 SFE model with a 2x2x2 mesh that consists of 6, 10, and 100 SEM across the $x-$, $y-$, and $z-$axis, respectively. The choice of the SEM/EM ratio directly affects

the number of elements that make up the 3D stochastic mesh representing the concrete volume, and also the number of elements that make the 2D bond of the FRP-concrete contact definition in LS DYNA. The concrete SEM that in contact with the FRP have been numbered (in black) in the figure to show how the increase in concrete SEM density allows more random elements to be included in simulating the bond. Figures 3.11 to 3.13 show plots of the generated field realizations for the 3D concrete volume (left) and 2D bond surface (right) for the different SEM/EM models. Each line in the plot representing a vector of generated field values running the length of the cross section (i.e., each line shown in Figure 3.11 is for an row of SEM along the length of the beam in the cross section of the MESH60 density). Each point on a line represents a realization of the random field along the length of the beam. For the bond plots, the number of normal and shear lines shown corresponds to the number of discretized elements across the bond surface. As stated above, the number of SEM elements that make up the bond increases with increased mesh density.

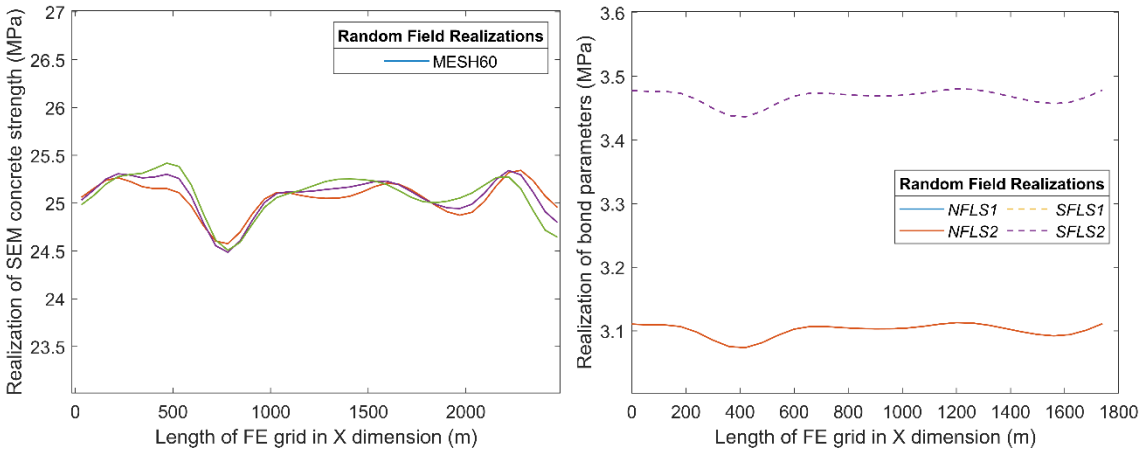

Figure 3.11. SEM parametric analysis: Random field realizations of the SFE model (MESH60).

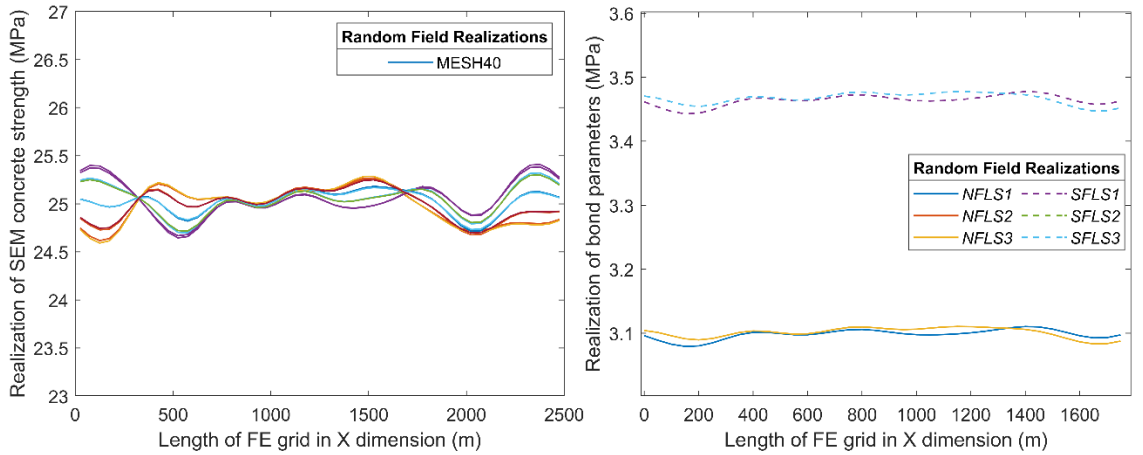

Figure 3.12. SEM parametric analysis: Random field realizations of the SFE model (MESH40).

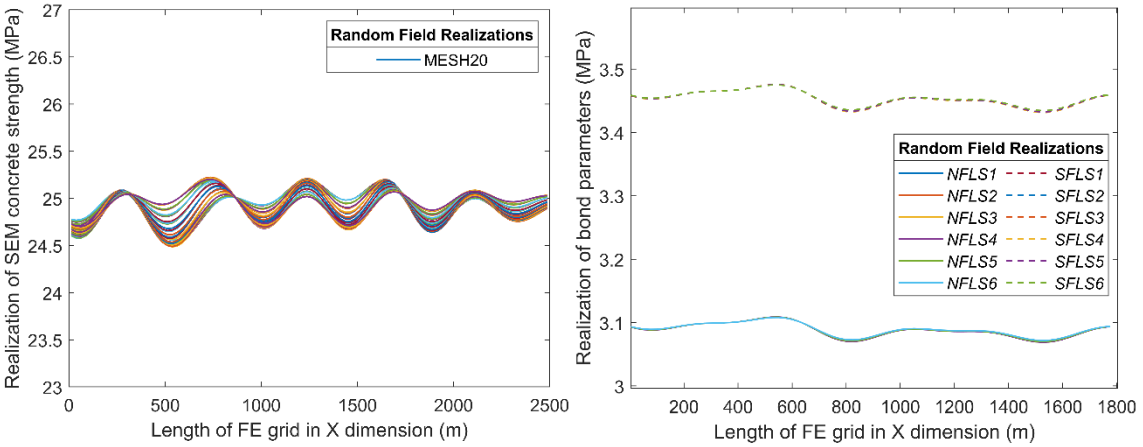

Figure 3.13. SEM parametric analysis: Random field realizations of the SFE model (MESH20).

Table 3.6 shows the average times to compute one analysis of the 200 SFE runs, for the different mesh densities. Results of running the 600 (3x200) SFE models with different SEM density showed that the SFE models are costly to compute. The increase in the number of SEM decreases the efficiency to compute the same strengthened beam model. Despite taking the longest to compute, the MESH20 (2x2x2 SEM/EM) was able to achieve the debonding failure mode more consistently than the courser meshes, showing debonding of the FRP in almost all cases (please refer to Appendix C for select snapshots of the debonding failure for MESH20 models), whereas the other mesh densities showed a variation in debonding failure and early termination (termination without showing any failure mode). A high number of early terminations of a mesh configuration speaks to its consistency in prediction. Early termination can occur when running non-linear analysis due to poor convergence of the model, meaning the chosen configuration may not be optimal. All simulations ran were checked for early termination and removed from the analysis if no failure mode has occurred after termination of the solver.

Table 3.6. SEM parametric analysis: Average run time of a single SFE model by SEM density.

Config. ID	SEM/EM	Average Run time (hr)*
MESH60	6x5x5	1.02
MESH40	4x4x4	1.40
MESH20	2x2x2	1.57

* Average time of 200 SFE models per configuration

Table 3.7 summarizes the statistics of fitting a normal probability density function (pdf) on the data. Figure 3.14 shows the histograms of the 3 configurations, showing the distribution of the moment resistances at ULS. The moment resistance was found by plotting the force-displacement curves of the 600 SFE models (3 configurations x 200 SFE models per configuration), extracting the peak force, and calculating the applied moment given the moment arm.

Table 3.7. SEM parametric analysis: Statistics of normal fit of beam resistance .

Beam ID	Failure Mode	μ_{Mu}	σ_{Mu}	COV_{Mu}
MESH60	Y-IFC	33.48	0.858	0.0256
MESH40	Y-IFC	33.81	0.987	0.0292
MESH20	Y-IFC	33.98	1.007	0.0296

μ_{Mu} = Mean of M_u; σ_{Mu} = Standard Deviation of M_u; COV_{Mu} = coefficient of variation of M_u

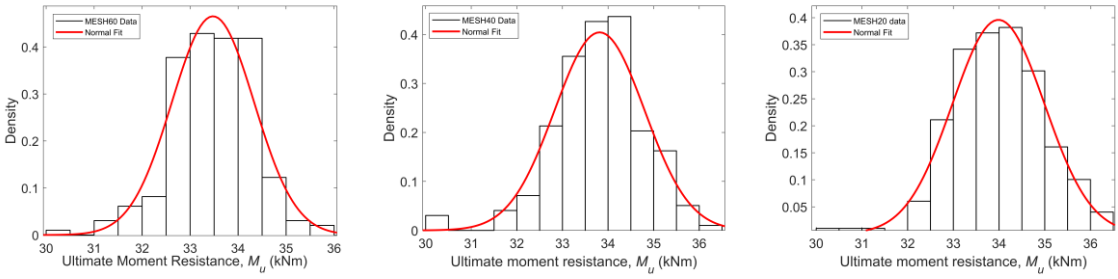

(a) MESH60 (b) MESH40 (c) MESH20

Figure 3.14. SEM parametric analysis: Histograms of M_u with fitted normal pdf.

The representation quality of the random field was also calculated to see the effect of the choice of SEM density on the quality of the generated field. Table 3.8 summarizes the results. It can be seen that the SEM density does not significantly affect the quality of the field, though 26 terms were needed to be kept in the truncation to achieve the desired quality ($Q > 0.8$).

Table 3.8. SEM parametric analysis: Random field truncation order / representation quality.

Variable	Strengthened Beam ID		
	MESH60	MESH40	MESH20
Correlation length, a		150 mm	
Coefficient of variation, $COV_{f_c'}$		0.1	
Truncation order, r	26	26	26
Representation quality, Q	0.822	0.817	0.801

3.7.2.2 Correlation Length (a_X, a_Y, a_Z)

The effect of correlation length on the performance of the SFE models is also investigated. The SEM/EM ratio used in this analysis corresponds to MESH20 configuration (2x2x2 SEM/EM

model) based on the performance found in Section 3.7.2.1. When considering a 3D random field, three correlation lengths exist for each axis $a_x, a_y, and\ a_z$ (Eq. [3.3]). The ratio of stochastic field length to correlation length, L_{SEM}/a, is used to determine the size of the discretization based on correlation length. A range of $L_{SEM} = a/5$ to $L_{SEM} = a/10$ is recommended to ensure a sufficiently refined mesh (Sudret and Der-Kiureghian 2000). In this work a range of L_{SEM}/a = 1/2 to 1/13 is chosen, with L_{SEM} taken as the average of the field length in the three directions. The number of terms needed to be kept in the truncation of the expansion, r, when generating the field has been varied in each trial to meet the recommended representation quality limit greater than 80%. A total of 4 configurations of correlation length are investigated by generating 200 SFE models using the steps of Figure 3.7 to generate the random field. Config CL75, CL150, and CL600 use the same correlation length value in all directions (x, y, z), while CLVar varies the three values based on the relative lengths of the field in each axis. Table 3.9 summarizes the correlation lengths considered in the sensitivity analysis.

Table 3.9. CL parametric analysis: Considered configurations of correlation length.

Config. ID	CL75	CL150	CL600	CLVar
$* L_{SEM}/a$	1/13	1/6	1/2	1/4
a_x	75	150	600	75
a_y	75	150	600	600
a_z	75	150	600	150

$*Average\ in\ x, y, z$

Figures 3.15 to 3.18 show plots of the generated fields values for the 3D concrete volume (right) and 2D bond surface (left). Similarly, to the plots in Section 3.6.1, each line plotted represents a vector from the cross section of the beam that contains values of the generated field values running the length of the member. For the concrete plot, 60 vectors are plotted for the 60 SEM elements in the cross section. For the bond parameter plot, the bond is surface is split into 6 SEM elements for a MESH20 configuration, with 6 lines plotted for the normal and shear stress limits ($NFLS/SFLS$).

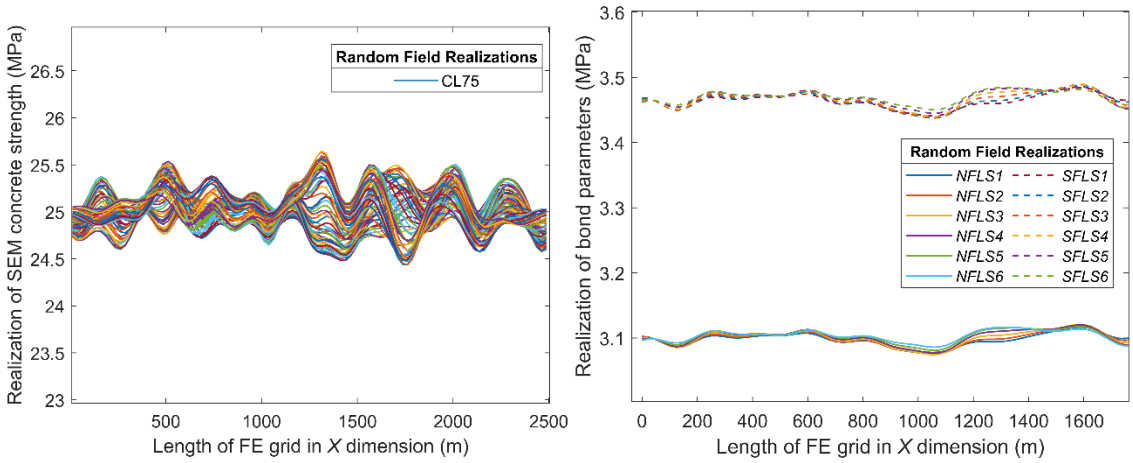

Figure 3.15. CL parametric analysis: Realizations of RF along the length of beam (CL75).

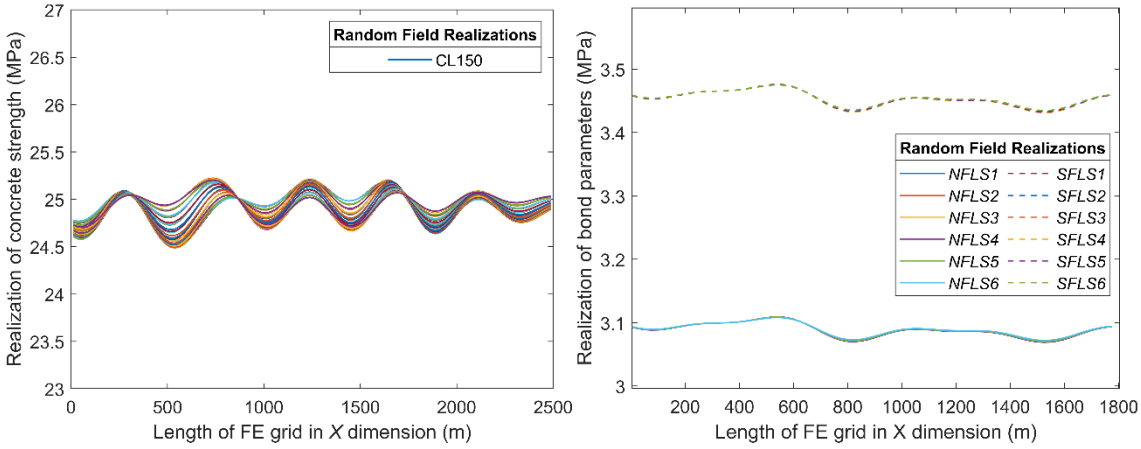

Figure 3.16. CL parametric analysis: Realizations of RF along the length of beam (CL150).

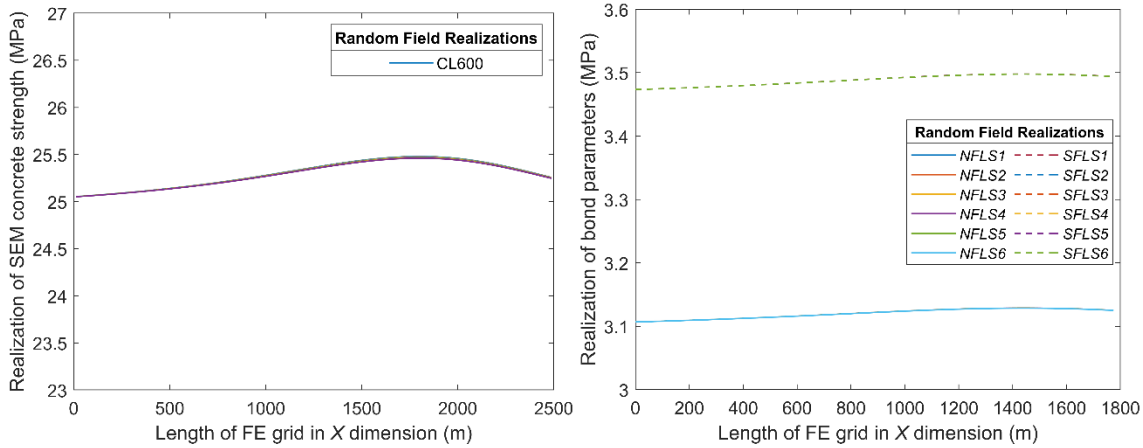

Figure 3.17. CL parametric analysis: Realizations of RF along the length of beam (CL600).

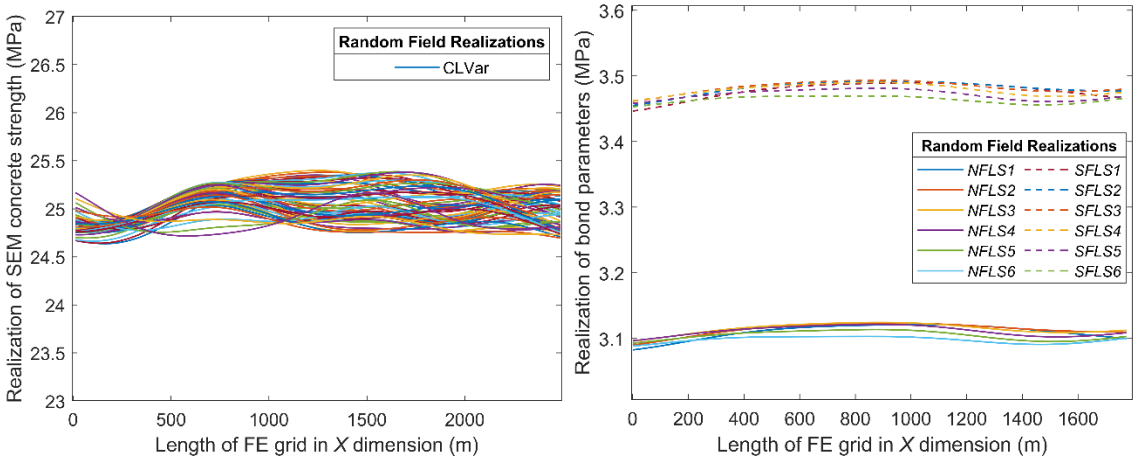

Figure 3.18. CL parametric analysis: Realizations of RF along the length of beam (CLVar).

It can be seen that as the correlation length decreases (i.e., decreased correlation between points), the variation in the field realizations increases as shown by the larger scatter of the curves over a larger range of values. The decrease in the correlation length will decrease the correlation of the points in the mesh, increasing the variation of the field realizations. As shown, the CL75 configuration gives the most variation in the field around the mean value, for the same strengthened beam. Conversely, the CL600 shows the field with the least variation around the mean. When the correlation lengths are set to be the same direction, the realizations follow a general trend across the length of the beam (Figure 3.15-17), and when they correlation lengths differ, the field will disperse more unevenly from the mean value when the length is varied based on the dimension of the concrete volume being discretized (Figure 3.18).

Table 3.10 gives the mean and standard deviation of the normal pdf of the four configurations, along with the failure mode observed in the beams. Figure 3.19 shows the histogram of the ultimate moment resistance found by the SFE models, showing the fitted normal distribution to the moment resistances at ULS. Table 3.11 summarizes the representation quality and number of terms kept in the truncation based on correlation length chosen. Results show that the mean of the fitted normal pdf is similar in all cases. The difference in results can be seen in the variation (COV) at the ultimate

response. Increased COV_{Mu} is reported for the sample data when the correlation length is decreased. It should be noted that no significant difference in computational time was reported between the 4 different configurations.

Table 3.10. CL parametric analysis: Statistics of normal fit of beam resistance, M_u.

Strengthened Beam ID	Failure Mode	μ_{Mu}	σ_{Mu}	COV_{Mu}
CL75	Y-IFC	33.85	1.202	0.0355
CL150	Y-IFC	33.87	1.070	0.0316
CL600	Y-IFC	33.90	1.041	0.0307
CLVar	Y-IFC	38.89	1.087	0.0321

μ_{Mu} = Mean of M_u; σ_{Mu} = Standard Deviation of M_u; COV_{Mu} = coefficient of variation of M_u

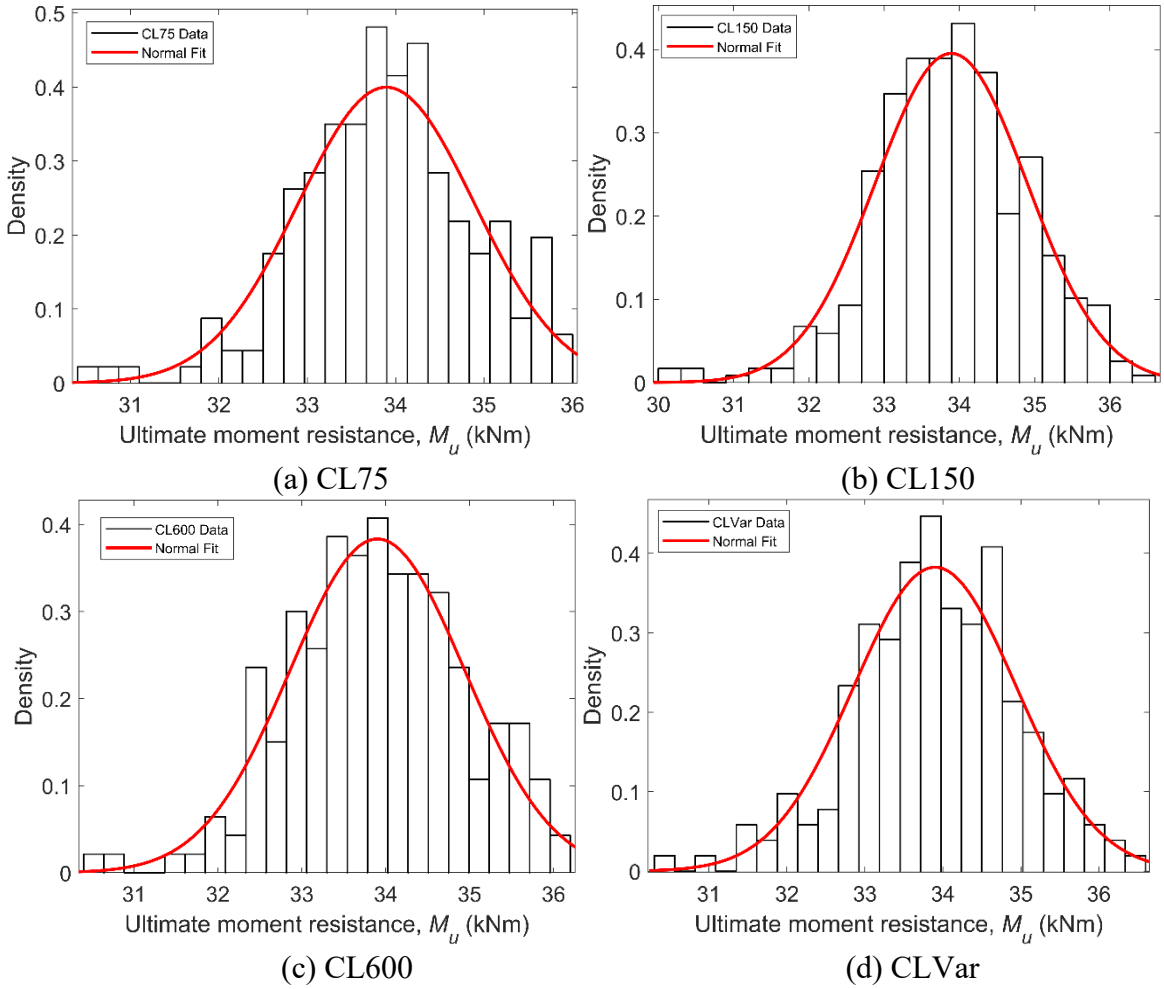

Figure 3.19. CL parametric analysis: Histograms of M_u with fitted normal pdf.

Table 3.11. CL parametric analysis: Random field truncation / representation quality.

Variable	Strengthened Beam ID			
	CL75	CL150	CL600	CLVar
a_x *(mm)*	75	150	600	75
a_y *(mm)*	75	150	600	600
a_z *(mm)*	75	150	600	150
$COV_{f_c'}$	0.1	0.1	0.1	0.1
r	3	26	150	22
Q	0.821	0.817	0.827	0.819

3.7.3 Parametric Reliability Analysis

The framework described in Section 3.7.1 has been used to conduct the SFE reliability analysis using the validated FE model from Section 3.5. The configuration chosen for SEM density and

correlation length is the MES20 and CL150, respectively, to generate all SFE models in the analysis. A two-step reliability analysis is conducted to assess the safety of eight sample EB FRP flexural strengthened RC beams for the CSA and ACI FRP design standards (CSA S806:17; CSA S6:19; ACI440.2R:17). In Step 1, a SFE-MCS analysis is conducted to establish the resistance statistics (bias and COV) of the ultimate moment resistance of the beam. A total of 200 SFE models with unique random fields are generated for each beam configuration, running 9 simulations in parallel to reduce the computational burden of SFE analysis. Load-displacement curves are plotted for each beam and the ultimate response is extracted to calculate the moment resistance. A normal distribution is fit to the ultimate moment data and the resistance statistics are established for the strengthened beam. Step 2, is to calculate the strengthened beam reliability using MCS, with 1e8 trials, using the established resistance statistics, and the load statistics for each design standard. A variable for the model error of using the SFE to calculate the ultimate response, M_{err}, is also introduced (Castaldo et al. 2019). The mean and COV for M_{err} is equal to 1.10 and 0.12, respectively.

Eight configurations of strengthened beams have been chosen to investigate the effect of increased spatial variability in the concrete strength on the strengthened beam reliability. The beam configurations chosen are included in Table 3.12, while an overview of the beam geometry is shown in Figure 3.20. Both compression and tension-controlled members have been chosen, with varying concrete strength, f'_c, and coefficient of variation of concrete strength, $COV_{f_c'}$. The difference between the tension- and compression-controlled section is the size of the tensile reinforcement. The larger diameter bar is associated with the compression-controlled section. The varying $COV_{f_c'}$ will simulate increasing variability in the concrete due to several effects, such as degradation or heterogeneity in the volume. Each strengthened beam has a unique ID label to

denote it, where the first letter denoted the failure modes of tension (T) and compression (C). The second letter and following two-character number denote the concrete strength of the beam (i.e., F25 denotes f'_c = 25 MPa). The last letter-numeric combination gives the $COV_{f'_c}$ value (i.e., C01 denotes $COV_{f'_c}$ = 0.1). The other section and material parameters of the concrete, steel, and EB CFRP are given in Table 3.13. The CFRP chosen for strengthening has an ultimate tensile strength of 3350 MPa, and a modulus of 235 GPa. Two layers of laminate have been used to have a thickness of FRP of 0.222 mm and a width of 120 mm.

Table 3.12. Parametric reliability analysis: Summary of strengthened beam configurations.

Strengthened Beam ID	Design Failure Mode	A_b (mm^2)	f'_c (MPa)	$COV_{f'_c}$
TF25C01	Tension	130	25	0.1
TF25C03	Tension	130	25	0.3
TF45C01	Tension	130	45	0.1
TF45C03	Tension	130	45	0.3
CF25C01	Compression	520	25	0.1
CF25C03	Compression	520	25	0.3
CF45C01	Compression	520	45	0.1
CF45C03	Compression	520	45	0.3

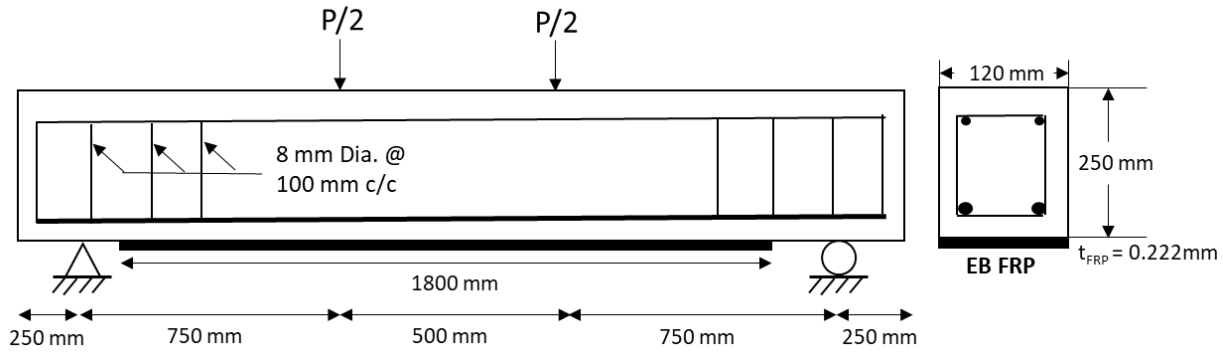

Figure 3.20. Parametric relaiability analysis: Overview of strengthened beam geomtry.

Table 3.13. Parametric reliability analysis: Sectional properties of strengthened beam.

Variable	Mean Value	Units
	Concrete	
b	120	mm
h	250	mm
d	225	mm
L	2500	mm
f'_c	*Varies	MPa
	Steel	
f_y	335	MPa
$A_b\ (T)$	*Varies	mm^2
$A'_b\ (C)$	80	mm^2
A_v	100	mm^2
E_s	200	GPa
	FRP	
f_{frpu}	3350	MPa
E_{frp}	235	GPa
t_{frp}	0.222	mm
w_{frp}	120	mm
A_{frp}	26.6	mm^2
L_{frp}	1800	mm

b = beam width; h = beam height; d = depth to extreme tensile rebar; L = length of beam; f'_c = concrete strength; f_y = steel yield strength; A_v = Area of shear rebar; E_s = modulus of elasticity of steel; f_{frpu} = FRP ultimate tensile strength; E_{frp} = FRP modulus; t_{frp} = FRP thickness; w_{frp} = FRP width; A_{frp} = Area of FRP; L_{frp} = Length of bonded FRP

3.7.3.1 Input Parameters

Table 3.14 summarizes the statistics of the design random variables used in establishing the resistance statistics in Step 1 of the analysis. The mean concrete strength used to generate the random field is taken as the value given in Table 3.12 and the bias is set to 1.0. The change in $COV_{f'_c}$ from 0.1 to 0.3 simulates various levels of concrete quality. The statistics for the FRP random variables are taken from the work of Huang et al. (2019) in which a bench-scale testing regiment of more than 500 concrete cylinders and 50 FRP tensile tests have been conducted to establish the values.

Table 3.14. Parametric reliability analysis: Input statistics of the design random variables.

	FRP		Concrete	Steel
Variable	f_{frpu}	E_{frp}	f'_c	f_y
Units	MPa	GPa	MPa	MPa
Dist. Type	Lognormal	Normal	Random Field	Normal
Mean, μ	3,350	235	[25, 45]	335
Bias, λ	1.15	1.0	1.0	1.145
COV	0.1	0.04	[0.1, 0.3]	0.05
Ref.	(Huang et al. 2019)	(Huang et al. 2019)	(This study)	(Nowak and Szerszen 2003)

Summary of the parameters used in generating the random field of the concrete strength are shown in Table 3.15. Tables 3.16 and 3.17 summarizes the load, and resistance statistics, respectively, used in the MCS reliability analysis in Step 2 (post-processing). The choice of the load statistics is those used in calibration of the different design codes to align with the calibration process taken by each. The load statistics are listed by code and provide the governing load combination used. Note for the CSA codes, a transformation to load effect variable, $T2L$, is implemented and is multiplied by the live load, LL. The analysis in Step 2 is to assess the reliability of the various strengthened beams when designed using the three standards using the statistics for calibration.

Table 3.15. Parametric reliability analysis: Stochastic inputs used in generating the random field.

Input Parameter	Value
Random Field Type	Lognormal
Correlation Function	Squared Exponential (see Eq.[3.3])
3D EM Density (mm)	12.5x12.5x10
3D SEM Density (mm)	25x25x20
SEM/EM	2x2x2
Correlation Length (mm)	150

Table 3.16. Parametric reliability analysis: Statistics of load random variables, per code.

	CSA S806:17			CSA S6:19			ACI 440.2R:17		
Combin.	$1.25DL + 1.5LL * T2L$			$1.2DL + 1.7LL * T2L$			$1.2DL + 1.6LL * T2L$		
Variable	DL	LL	$T2L$	DL	LL	$T2L$	DL	LL	$T2L$
Dist.	Normal	Gumbel	Normal	Normal	Normal	Normal	Normal	Normal	N/A
Bias	1.050	0.900	1.000	1.040	1.168	1.020	1.050	1.000	--
COV	0.100	0.170	0.206	0.036	0.069	0.090	0.100	0.180	--
(Ref.)	(Bartlett et al., 2003a,b)			(Commentary CSA S6:19)			(Nowak and Szerszen 2003)		

Table 3.17. Parametric reliability analysis: Statistics of resistance random variables.

Variable	Moment Resistance, R	Model Error, $Merr$
Dist.	Normal	Normal
μ_{M_u}	Table 3.18	1.00
λ	Tables 3.19 to 3.22	1.10
COV_{M_u}	Table 3.18	0.12
(Ref.)	(This Study)	(Castaldo et al., 2019)

3.7.3.2 Performance Function

The performance function, $G(X)$, must be defined for the ULS (see Section 2.2). The performance function defined in Eq. [2.1] as the difference between the resistance, $R(X)$, and the loads, $L(X)$, for a given set up random inputs, X. A member is considered failing under when the performance is below zero. In the case of the ULS of EB FRP strengthened beam, *G(X)* is defined by Eq.[3.15] as the difference in unfactored resistance, $R(X)$, multiplied by a model error term, M_{Err}, and the unfactored combined loads, $L(X)$, multiplied by the utilization, UR. The term $L(X)$ is made up of three load random variables representing the dead load, DL, live load, LL, and transformation to load effect, $T2L$, calculated using Eq.[3.16]. The vector X contains the values of the random variables and RFs that represent the uncertainty in the loads, resistance, and FE model.

$$G(X) = R(X) * Merr - L(x) \quad [3.15]$$

$$L(X) = DL(X) + LL(X) * T2L(X) \quad [3.16]$$

The resistance term $R(X)$ consists of three random variables for the material properties of the FRP, and steel. The concrete strength is represented by a lognormal random field where the generation of r (truncation value) standard normal (SN) random variables is used. The loads are also represented by three random variables for dead, live, and transformation to load effect. Mean loads are calculated based on calculating the factored resistance of the member as per the given code and governing load equation.

3.7.3.3 Pre-processing: Establishing resistance statistics (SFE-MCS)

The results of establishing the resistance statistics based on an assumed normal distribution are presented in Table 3.18 for the 8 beam configurations chosen. Histograms of the ultimate moment data are shown for the beams in Figures 3.21 for the tension-controlled and Figure 3.22 for the compression-controlled members. The statistics found for the moment resistance will be used in the post-processing step to conduct MCS to assess the reliability of the beams. Failure mode of the beams are shown by ID. Failure mode Y-IFC stands for IFC debonding failure mode after yielding of the internal reinforcement, and Y-Crush stands for crushing of the concrete after yielding of the internal steel.

Table 3.18. Parametric reliability analysis: Strengthened beam resistance statistics.

Strengthened Beam ID	Failure Mode	μ_{Mu}	σ_{Mu}	COV_{Mu}
TF25C01	Y-IFC	33.87	1.07	0.0316
TF25C03	Y-IFC	33.59	1.07	0.0319
TF45C01	Y-IFC	38.59	0.91	0.0236
TF45C03	Y-IFC	38.47	0.99	0.0257
CF25C01	Y-Crush	65.95	0.47	0.0072
CF25C03	Y-Crush	65.43	2.07	0.0316
CF45C01	Y-Crush	83.18	2.46	0.0296
CF45C03	Y-Crush	82.90	2.84	0.0343

μ_{Mu} = Mean of M_u; σ_{Mu} = Standard Deviation of M_u; COV_{Mu} = coefficient of variation of M_u

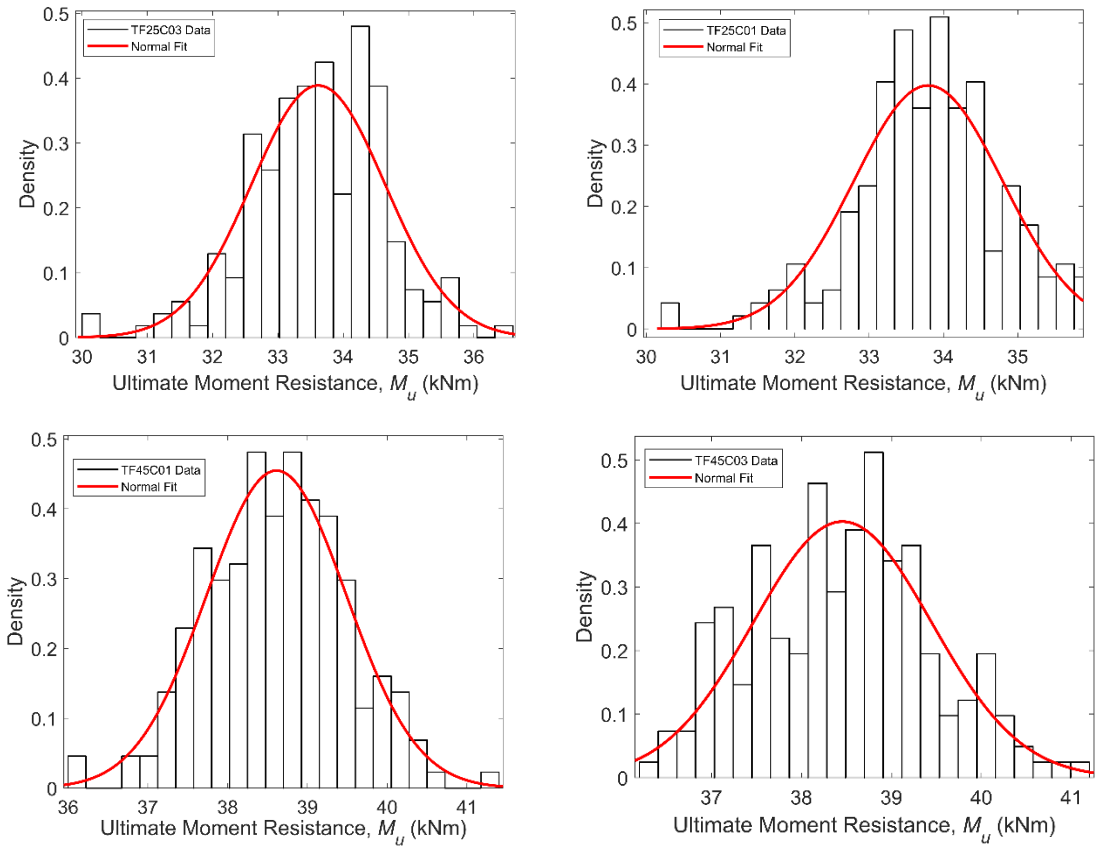

Figure 3.21. Parametric reliability analysis: Histograms of M_u with fitted normal pdf (Tension-Controlled).

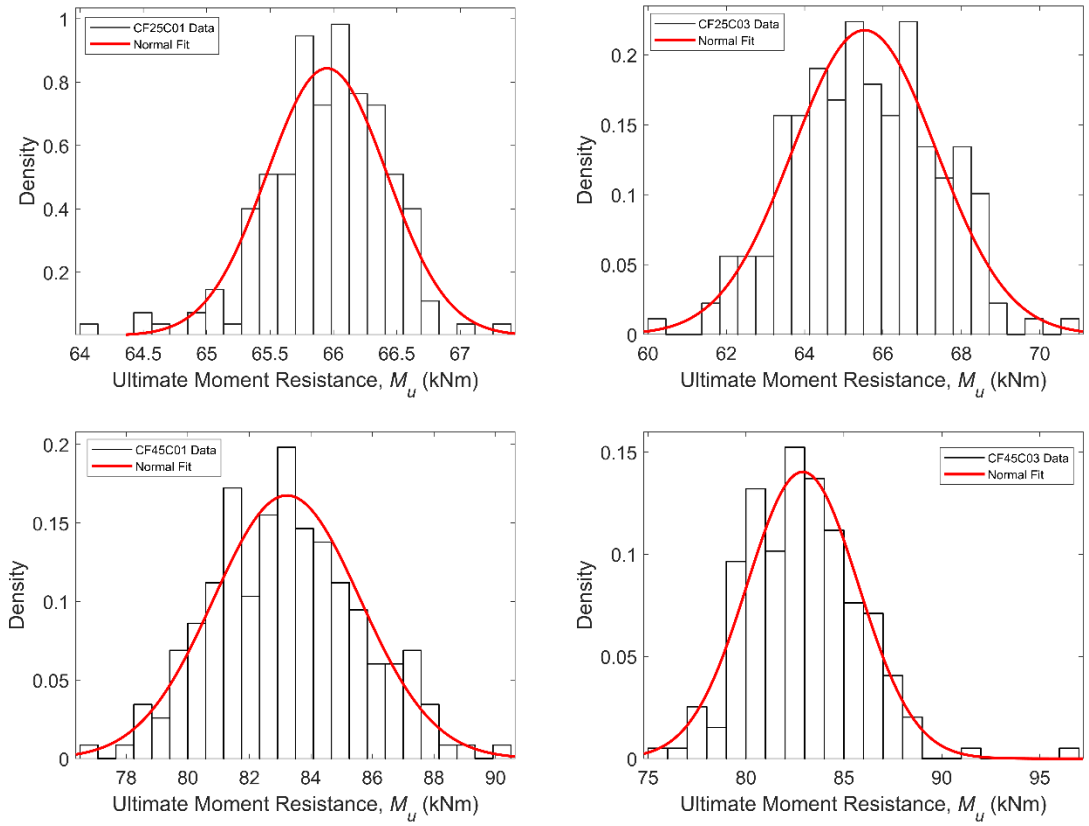

Figure 3.22. Parametric reliability analysis: Histograms of M_u with fitted normal pdf (Compression-Controlled).

To examine the effect of the EB FRP tensile strain limit imposed by the codes, a bias factor, λ, has been established, for each code, for all tension-controlled members considered. The term λ is defined as the experimental moment resistance given by the SFE model over the nominal moment code given resistance. The factored moment resistance, M_r, is given for the beams considered and is listed by code in Table 3.19. See Appendix B for sample calculations of M_r, for each code, for the TF25C01 beam. Tables 3.20 to 2.22 show the mean bias factors for the 200 SFE runs calculated using the code given resistance for the CSA S806:17, CSA S6:19, and ACI440.2R:17 codes, respectively. It can be seen that λ is large ($\lambda > 1.4$) for all codes, indicating that the code prescribed values are conservative irrespective of concrete strength and level of concrete

variability spatially. Moreover, the increase in strain limit does not appear to be the source of the conservativeness when it comes to the high bias factor reported.

Table 3.19. Parametric reliability analysis: Ultimate moment resistance of strengthened beams per code.

	Factored Moment Resistance, M_r [kNm]		
Strengthened Beam ID	CSA S806:17	CSA S6:19	ACI 440.2R:17
TF25C01/TF25C03	21.48	21.91	25.12
TF45C01/TF45C03	22.00	22.44	25.86
CF25C01/CF25C03	42.73	48.10	38.63
CF45C01/CF45C03	55.28	59.71	46.05

Table 3.20. Parametric reliability analysis: Bias of moment resistance (CSA S806:17).

(CSA S806:17)	Maximum allowable FRP tensile strain, ε_{frp} (mm/mm)				
	0.006	0.007	0.008	0.009	0.01
Beam ID	λ	λ	λ	λ	λ
TF25C01	1.500	1.495	1.492	1.489	1.488
TF25C03	1.500	1.496	1.492	1.490	1.488
TF45C01	1.675	1.670	1.666	1.663	1.660
TF45C03	1.670	1.665	1.661	1.658	1.656

Table 3.21. Parametric reliability analysis: Bias of moment resistance (CSA S6:19).

(CSA S6:19)	Maximum allowable FRP tensile strain, ε_{frp} (mm/mm)				
	0.006	0.007	0.008	0.009	0.01
Beam ID	λ	λ	λ	λ	λ
TF25C01	1.530	1.526	1.522	1.520	1.518
TF25C03	1.531	1.526	1.523	1.520	1.518
TF45C01	1.710	1.705	1.701	1.698	1.695
TF45C03	1.706	1.700	1.696	1.693	1.690

Table 3.22. Parametric reliability analysis: Bias of moment resistance (ACI440.2R:17).

(CSA S6:19)	Maximum allowable FRP tensile strain, ε_{frp} (mm/mm)				
	0.006	0.007	0.008	0.009	0.01
Beam ID	λ	λ	λ	λ	λ
TF25C01	1.344	1.340	1.337	1.335	1.333
TF25C03	1.344	1.340	1.337	1.335	1.333
TF45C01	1.501	1.496	1.493	1.490	1.487
TF45C03	1.497	1.492	1.488	1.485	1.483

The failure mode of the beam is reported to be IFC debonding, which is initiated by flexural cracks reaching the tension face. This can be visually seen in LS DYNA through the principal strains in the concrete volume. Figure 3.23 contains select images of the cracking pattern of the SFE models failing in IFC debonding, for various beam configurations, and shows plots of the generated random fields for comparison. The image in the center is of the SFE beam showing the 1st principal strain of the concrete volume to show the crack pattern, at failure. The top plot in Figure 3.23 contains the random field values of the concrete strength, f'_c, and the bottom plot shows the random field of the bond parameters, $NFLS$ and $SFLS$, at the location of the bond surface. The plots are scaled to line up with the dimensions of the SFE beam (i.e., the bond random field only runs along the length of the beam that the FRP makes contact with).

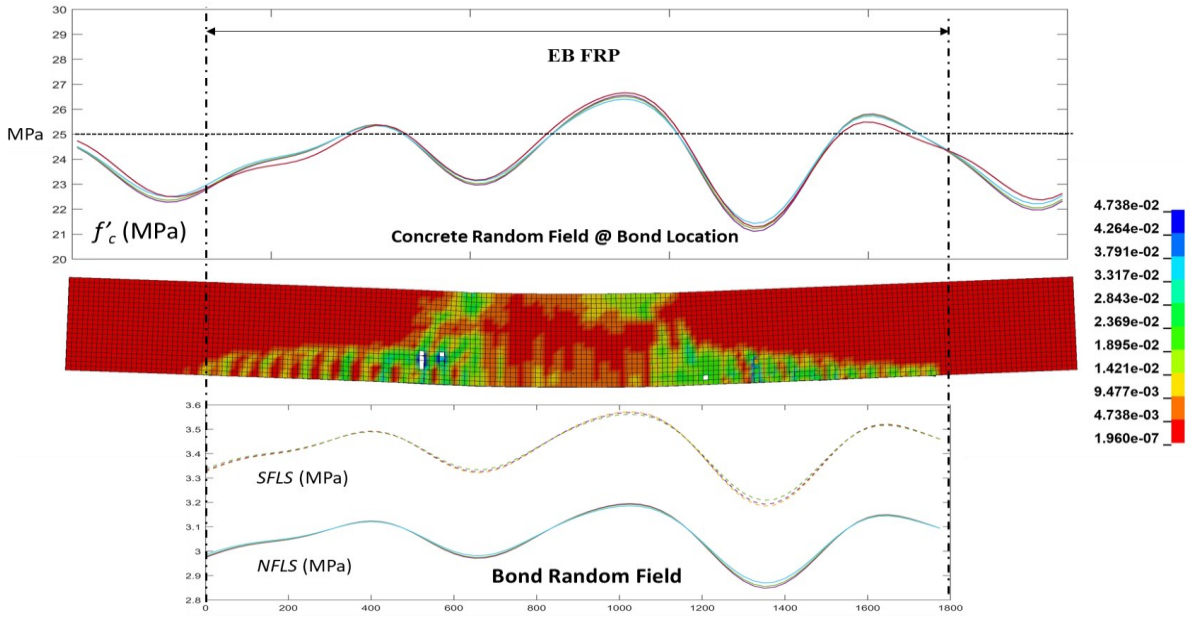

(a) Beam TF25C01

Figure 3.23a. Parametric relibaility analysis: Beam TF25C01 cracking pattern at ultimate versus random field realizations

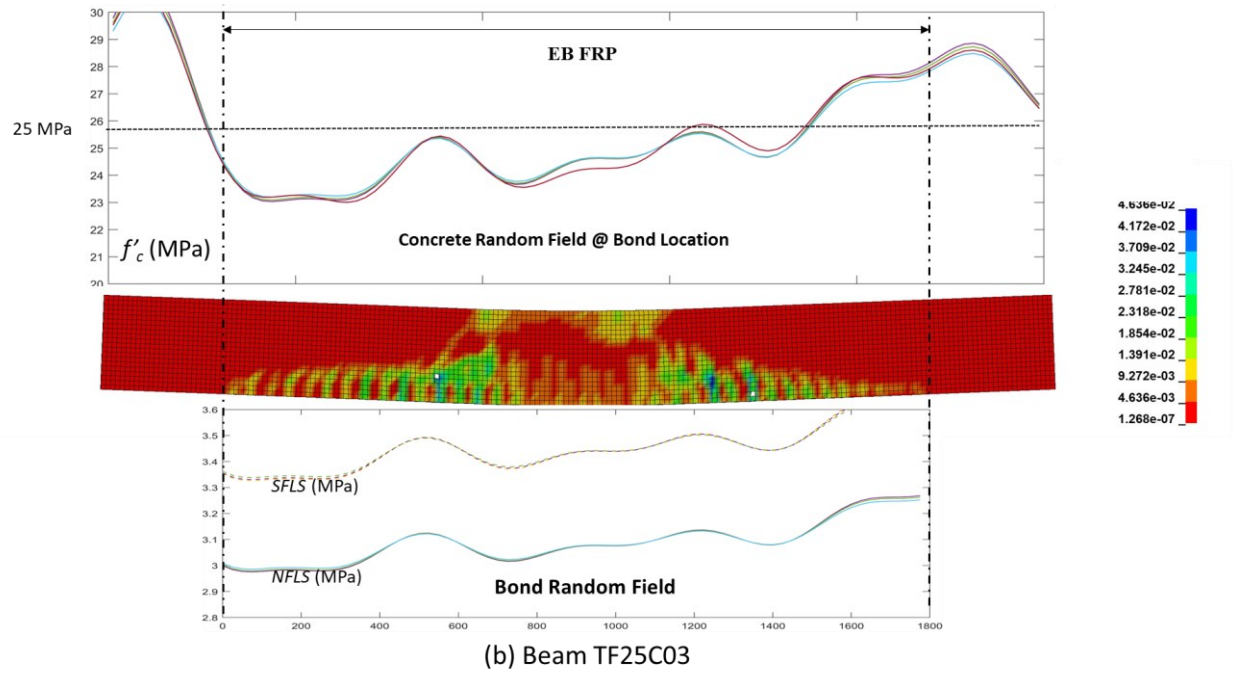

(b) Beam TF25C03

Figure 3.23b. Parametric relibaility analysis: Beam TF25C03 cracking pattern at ultimate versus random field realizations

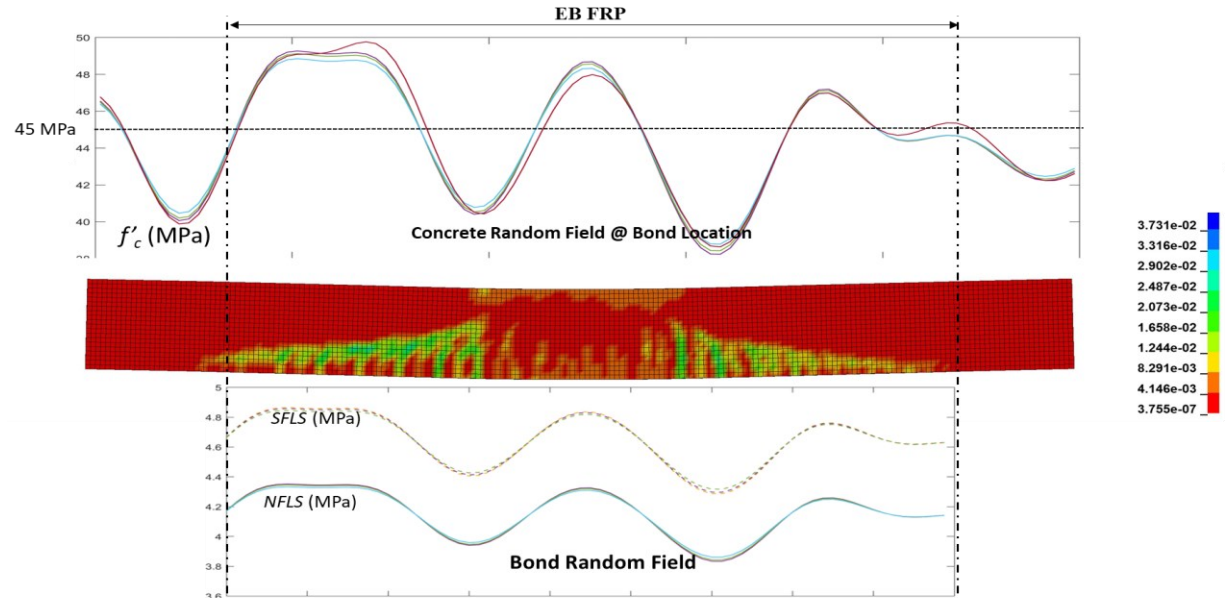

(c) Beam TF45C03

Figure 3.23c. Parametric relibaility analysis: Beam TF45C03 cracking pattern at ultimate versus random field realizations

3.7.3.4 Post-processing: Reliability of strengthened beams (MCS)

Results of running 1e8 MCS trials for each beam configuration is summarized in Figure 3.24, for the three design standards considered. Reliability index values of each code is plotted in one figure to show the difference in the code prescribed reliability for the same set of beams. Each beam shows a large variation of reliability index between codes for both compression and tension-controlled members.

The effect of increased spatial variation of the concrete showed less of an effect on the reliability of the strengthened member than the choice of code. Compression-controlled members had a larger change in reliability than tension-controlled members when increasing the concrete variability (i.e., increased $COV_{f_c'}$). Looking at beams TF25C01 and TF25C03, the increase in $COV_{f_c'}$ from 0.1 to 0.3 produces a slight decrease in reliability index. The same trend is seen with the compression-controlled beam with a concrete strength of 25 MPa. Generally, the CSA codes see a decreasing trend or no change in the reliability index for increased $COV_{f_c'}$. Conversely, for the ACI 440.2R guideline, the reliability index stayed about the same for tension-controlled members and the reliability increased by the largest margin for compression controlled members, when $COV_{f_c'}$ is increased.

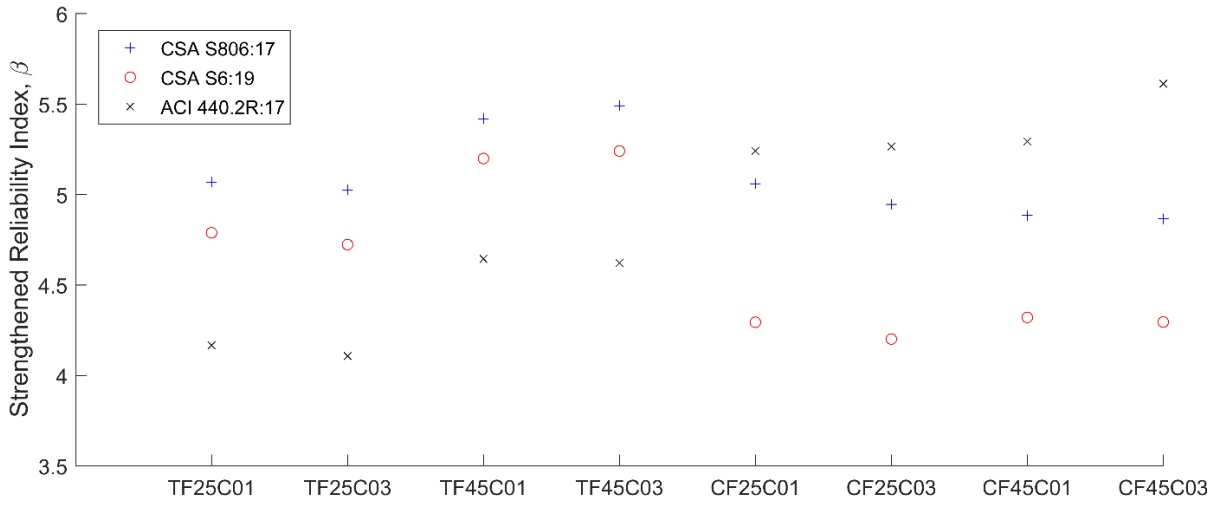

Figure 3.24. Reliability based code comparision for the considered EB FRP strengthened beams using SFE-MCS

Figures 3.25 and 3.26 show plots of strengthened beam reliability against utilization ratio (i.e., demand-to-capacity ratio) for the CSA standards and ACI guideline, respectively. The results show that the CSA S806:17 having the least sensitivity to input parameters of the strengthened beam. The other two codes show a sensitivity to both the change in f_c' and the failure mode chosen to control design. For all codes, a decreasing linear trend in reliability index is seen as the beam becomes increasingly deficient (i.e., increase in utilization ratio above unity). This is to be expected, though the initial reliability of the beams starts much higher than a target reliability index for new design of 3.0 to 4.5. The reliability for most beams does not decrease below 3.0 for utilization up to $UR = 1.3$.

The same range of target reliability index is not typically used for existing construction of in service members and is regarded as a high target to achieve. Large cost associated with upgrading existing building members to modern design standards, to meet target reliability index values set for new construction, typically warrant the choice of lower targets for assessment and upgrades. Target reliability index values are set on the basis of being able to verify the existing structures

based on current code recommendations, minimum total expected cost, and socio-economical criteria (ISO 13822:2010). For example, in the ISO 13822 specification for the bases of assessment of existing structures, recommendations are made for target reliability values of existing buildings, for a given limit state. It recommended that for an existing structure at ultimate limit state, which has a low probability of failure that the target reliability is equal to 2.0 and for components that cannot be inspected a target beta equal to 2.3. This means that the reported strengthened reliability values are quite high for existing construction and could produce costly and over-conservative designs for all codes. This observation is also consistent with the target reliability indexes using in the calibration of NBCC and ACI 318 which range from 3.0 to 4.5.

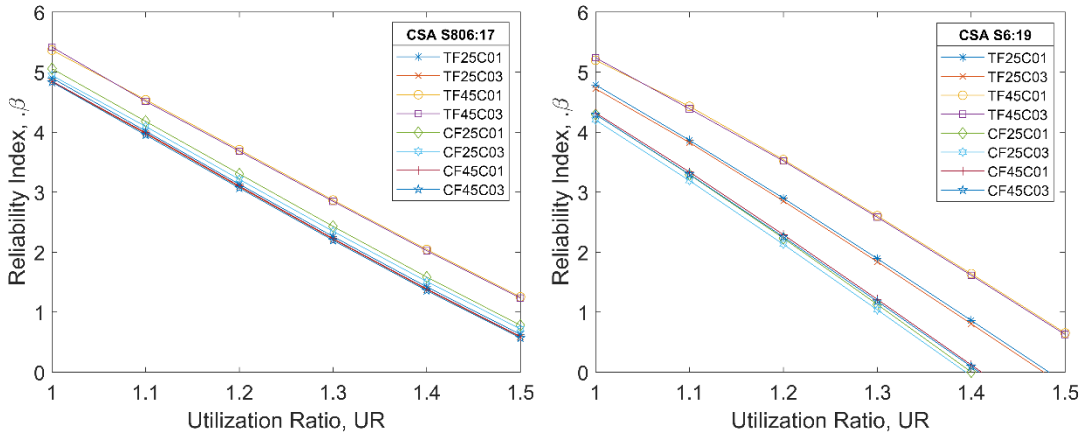

(a) CSA S806:17 (b) CSA S6:19

Figure 3.25. Strengthened beam relibaility versus utilization for the CSA Standards.

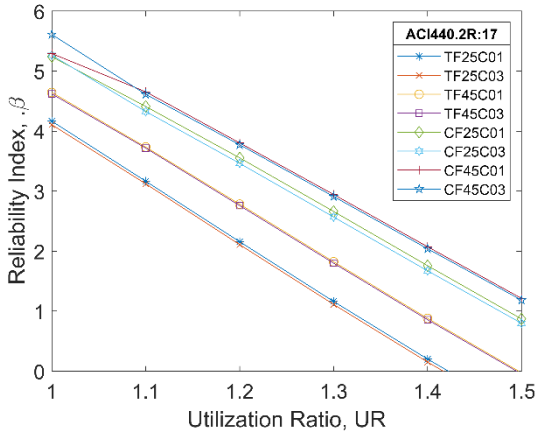

(c) ACI 440.2R:17

Figure 3.26. Strengthened beam relibaility versus utilization for ACI440.2R:17.

A parametric reliability analysis on the tensile strain limit of the FRP set be codes has been conducted using the bias factors established in Section 3.7.3.3. MCS with 1e8 trials was conducted for each tension-controlled beam, designed to each of the three codes considered. The value of the EB FRP tensile strain limit, ε_{frpu} has been varied for a range of ε_{frpu} = [0.006, 0.007, 0.008, 0.009, 0.010], to examine the effect of increasing ε_{frpu} on the reliability of the strengthened beam, β. The performance function given in Section 3.7.3.2 has been used with the input statistics from Section 3.7.3.1. The bias factors established in Tables 3.20 to 3.22 have been used to multiply the

code given factored moment resistance to give the mean resistance for analysis. Reliability index values for the strengthened beams are given, per code, in Tables 3.22 to 3.24.

Table 3.23. Parametric reliability analysis: Beam reliability at ultimate strain (CSA S806:17).

(CSA S806:17)	Reliability Index of Strengthened Beam, β				
Beam ID	Maximum allowable FRP tensile strain, ε_{frp} (mm/mm)				
	0.006	0.007	0.008	0.009	0.010
TF25C01	4.88	4.87	4.89	4.86	4.81
TF25C03	4.86	4.87	4.83	4.89	4.82
TF45C01	5.33	5.15	5.27	5.20	5.37
TF45C03	5.33	5.49	5.29	5.24	5.29

Table 3.24. Parametric reliability analysis: Beam reliability at ultimate strain (CSA S6:19).

(CSA S6:19)	Reliability Index of Strengthened Beam, β				
Beam ID	Maximum allowable FRP tensile strain, ε_{frp} (mm/mm)				
	0.006	0.007	0.008	0.009	0.010
TF25C01	4.74	4.74	4.73	4.73	4.71
TF25C03	4.75	4.74	4.72	4.75	4.73
TF45C01	5.33	5.37	5.22	5.29	5.24
TF45C03	5.33	5.22	5.22	5.20	5.24

Table 3.25. Parametric reliability analysis: Beam reliability at ultimate strain (ACI440.2R:17)

(ACI 440.2R:17)	Reliability Index of Strengthened Beam, β				
Beam ID	Maximum allowable FRP tensile strain, ε_{frp} (mm/mm)				
	0.006	0.007	0.008	0.009	0.010
TF25C01	4.15	4.15	4.13	4.12	4.11
TF25C03	4.15	4.14	4.14	4.11	4.11
TF45C01	4.68	4.67	4.68	4.66	4.67
TF45C03	4.68	4.62	4.65	4.61	4.64

3.7.4 Discussion of Results

The reliability analysis results are discussed in terms of the effect of random field density, random field correlation, increased concrete spatial variability, and strain limit on the beam reliability as follows.

Random Field SEM Density: Two major considerations, efficiency, and accuracy, of the generation of the random field have been considered. To be an efficient and accurate solution the field representation quality, Q, must be sufficient while still maintaining the computational efficiency. The choice of SEM density did not affect the quality of the realization given that enough terms are kept in the truncation of the eigenvalues/eigenvectors. A total of 26 standard normal random variables were kept in the truncation of the eigen to achieve an acceptable representation quality of the random field for all configurations. The addition of the high number of standard normal variables to the design random variables of the resistance make 34 random variables within the limit state. This means that the limit state is more complex and can increase the computational burden to compute.

The choice of SEM/EM ratio is important and will play a role in crack propagation. Initial validation of the base FE model is needed to ensure that the materials, sections, and contact before application of the SFE model. An increase in the cost of computation for the finer SEM mesh was also observed. This is due to an increased size of SFE model to be solved due to the increased in the assignment of parts (*PART) in LS DYNA to include the stochastic element mesh. This increase in computational cost may be offset by the fact that the finer mesh allows a more representative propagation of cracks though the concrete to initiate debonding. See Appendix C for examples of debonding failure modes of the TF25C03 beams with a CL150 and MESH20 configuration. The crack patterns in the concrete show how the flexural cracks reach the tension face and initiate debonding. Strain profile of the tensile strain in the FRP at debonding is provided in each figure.

Random Field Correlation Length: Choice of correlation length is a critical consideration when producing the random field. The randomness in the field realizations increases as the points

become more highly correlated (i.e., smaller correlation length). For EB FRP strengthened beams, the higher variation in concrete strength and bond may translate to a higher variation in the ultimate response of the strengthened member, as shown by the increase in variation in ultimate moment response of the beams with increased spatial variation . Recommendations in literature on a suitable correlation length are typically given for 1D and 2D problems and may not give a suitable range for practical applications using 3D fields. Experimental work to calibrate and quantify these distances to ensure representative fields are generated would ensure the concrete heterogeneity is being captured.

Effect of random fields and increased concrete variability: The use of 3D random fields to capture the spatial variability of the concrete and calculate the bond random field was successfully used to conduct SFE-MCS analysis. For tension-controlled sections the effect of accounting for the variability in the concrete did not effect the reliability significantly, even when accounting for the bond strength variation. All codes reported a slight decrease in reliability with increased concrete variation. Tension-controlled are less sensitive to the spatial variations in the concrete compressive strength since the ultimate resistance is governed by debonding. The random field of the bond may be the reason for the slight decrease in reliability with increased concrete variability.

The effect of the random field is more significant on the compression-controlled members, as the failure is governed by crushing of the concrete. It is generally seen that the increase in variation in concrete and bond strength (increased $COV_{f_c'}$) yields a decreased in the strengthened beam reliability for the CSA S6:19 and CSA S806:17. This same trend is not reported for the ACI 440.2R:17, with an increase in reliability reported for all compression controlled members considered.

EB FRP Strengthened Beam Reliability: The reliability index of all beams considered were found to be high irrespective of considered design code. This is reflected in the bias factors calculated between the SFE moment resistance and code given moment of resistance being between 1.3 and 1.8. This indicates that the design equations in the codes yield conservative designs that give high reliability index values that exceed target values for new construction.

It is interesting to note that ACI 440.2R gives higher reliability index values for tension-controlled members over compression-controlled, whereas the CSA codes generally show the opposite trend. This may not actually be the case for the CSA codes as the stipulations of Clause 8.2.2 of CSA S806:17 is not considered in this analysis. This clause states that the factored moment resistance shall be a minimum of 1.6 times the factored moment demand. This factor will increase the conservatism of the design and increases the amount of FRP needed for strengthening even though the reliability index of these beams is already high as compared to the target value. The same will be true of the CSA S6:19 code given the 1.5 factor stipulated in Clause 16.2.5.

The CSA S6 code shows to yield a higher reliability for all beams over the CSA S806:17 code irrespective of the design failure mode. Moreover, the reliability of the beams designed to CSA S806:17 shows less sensitivity to input parameters and failure mode than the CSA S6:19 code. For a target reliability index of 3.0, most beams considered did not drop below this target value until a utilization ratio of 1.21 on average.

The results show ACI 440.2R:17 provides the largest variation in reliability index values between the different beam configurations considered. This is partly due to the changing strength reduction factor (ϕ) that is based on the strain of the internal tensile rebar, for both tension and compression failure modes (see Appendix B). The factor ϕ is to account for the change in ductility that may occur in the beam with the addition of the EB FRP (ACI 440.2R:17 Commentary). This

means that the ACI 440.2R:17 considers a higher factor for beams that allow the rebar to yield past a strain value of 0.005 before failure.

Looking at Figure 3.26, for a target reliability index of 3.0, most beams considered did not drop below this target value until a utilization ratio of 1.24 on average. Showing that, like the CSA S806 and S6, the ACI 440.2R:17 still yield over-conservative designs even with a varying ϕ factor based on ductility.

FRP Strain Limits for Tension Controlled Sections: Investigation into the effect of increased strain limit on strengthened beam reliability was conducted using the established SFE-MCS framework. Little change in reliability is reported with increasing the strain limit on the EB FRP tensile strain. This finding is surprising in that the high bias values reported for the codes is due to different factors than simply a conservative strain limit for strengthened section considered. This is shown by the relatively unchanged reliability index for the tension-controlled beams for all strain limits considered. Consider that the work done to calibrate the ACI 318:19 code reports a bias, λ, of 1.11 to 1.13 for RC members in flexure (Nowak et al. 2003), whereas this study reports λ to be 1.39 on average for a EB FRP strengthened beams in flexure based on the ACI440.2R:17 code. Bias is defined as the ratio of actual to nominal resistance, meaning the code prescribed moment resistance is low compared to the actual resistance when the bias is large. This high bias factors lead to beams designed to have much higher reliability than the target in most cases, for all codes considered.

As the strain limit does not play a significant role in impacting the reliability for the considered beams, other phenomena are at play that causes the strengthened sections to have such high bias when designed using the codes considered. The nominal prediction of the codes does not capture the interaction of the three materials in the strengthened section. A compounding effect in the

addition of the phi factor for FRP material may be pushing the bias of the FRP codes to be overly conservative. In that case, re-calibration of the EB FRP phi factors in the CSA standards to include these effects of the EB FRP may be beneficial. Likewise, re-calibration of the additional strength factor included in the ACI 440.2R:17 code may also be beneficial for the same reason. More research is needed to understand the source of the conservatism in the codes.

3.8 CONCLUSION

This thesis chapter has examined the effect of accounting for the spatial variability in an existing RC beam on the reliability of the strengthened member using a two step stochastic reliability analysis. An novel automated framework is presented for conducting stochastic FE (SFE) reliability analysis using an LSDYNA-Python-MATLAB interface developed. A numerical example investigated the reliability of 8 strengthened beams (compression and tension controlled) designed to the two CSA S6, S806 and ACI 440.2R design standards to compare the reliability is also presented. Results of the SFE analysis show that increased spatial variability in the beams does not significantly affect the reliability of tension-controlled members. A larger effect was reported on the compression-controlled members, for the range of concrete spatial variability considered. For all design standards, the reliability of each beam is high compared to the typical target index for existing construction. This speaks to the conservative nature of the FRP design standards for strengthened beams in flexure. Parametric analysis on the strain limits of the EB FRP set by the codes to mitigate debonding show that an increase in the limit does not affect the beams' reliability. Further research is needed to identify the factors leading the conservative nature of the FRP design standards is needed. Calibration can be done to proposed reliability-based values that account for existing conditions of the beam prior to strengthening.

The choice of stochastic parameters is critical to ensure proper performance of the SFE model. A larger parametric analysis on the stochastic parameters used to generate the random field is needed to calibrate the field before conducting SFE-based reliability analysis. This will ensure that the field generated represents the spatial variability in the concrete. The finer discretized SEM of the SFE model was found to show a more typical crack pattern at ultimate and showed the least early terminations of the LS DYNA solver. This is due to the SEM/EM ratio of the SFE model being suitable to allow crack propagation. Choice of correlation length has a significant effect on the realizations of the random field. Determination of calibrated values of these lengths is difficult in many practical applications and more work is needed to experimentally calibrate values for RC and EB FRP strengthened RC members.

The presented results are limited to the beam configuration studied only and should not be extrapolated to other configurations of EB FRP strengthened beam. A larger, more general study, including may different geometries, strengthening configurations, and stochastic inputs is needed to propose general calibrated strain limits. This includes further analysis into choice of discretization method, correlation function, SEM/EM ratio, and correlation length for the stochastic field parameters.

Due to the computational burden of SFE-based analysis a limited number of realizations have been used to establish the resistance statistics. This is a major challenge with SFE reliability analysis using techniques that require many realizations of the SFE model, such as MCS, and should be addressed so that a wider design space can be analyzed efficiently. Computation optimization techniques such as active learning kriging SFE-reliability (Khorramian et al. 2022), and SFE-reliability analysis combined with artificial intelligence (Oudah and Alhashmi 2022) are potential ways that are being investigated to address this challenge.

CHAPTER 4 STOCHASTIC FE ACTIVE LEARNING KRIGING MONTE CARLO SIMULATION RELIABILITY BASED ANALYSIS OF EB FRP STRENGTHENED RC BEAMS

4.1 EXECUTIVE SUMMARY

Findings of the previous chapter investigating the use of SFE-MCS to conduct reliability analysis on EB FRP strengthened RC flexural beams showed a high cost of computation when evaluating SFE models to establish the resistance statistics. In this chapter, a clustered active-learning kriging (AK) reliability analysis framework has been implemented to conduct AK-SFE-MCS analysis on the same set of beams investigated in Chapter 3. The LSDYNA-Python-MATLAB interface developed in Chapter 3 was updated to perform the clustered AK analysis. A linear regression, spline correlation, and U-learning function have been selected as the AK configuration for analysis. The clustering technique implemented is based on the learning function to provide multi-point enrichment to improve convergence of the stopping criteria. The AK-SFE-MCS is compared against the SFE-MCS method for both accuracy and efficiency. A total of 1,066 stochastic FE models have been generated and evaluated at ultimate conditions to establish the resistance statistics using the AK method. Results show that the addition of AK to the reliability framework does reduce the number of calls to the original SFE model when assessing the reliability of a strengthened beam. Clustering was shown to improve convergence through allowing parallel computation of the clustered SFE models. Parametric analysis on the stopping criteria shows that the Schobi stopping criteria with $k \geq 1$ was sufficient to achieve consistent accuracy of prediction, while the Schobi stopping criteria with $k \leq 2$ provided more efficient solution as compared with the U stopping criteria.

4.2 INTRODUCTION

When developing reliability-based computational framework to assess and optimize the reliability of structures, efficiency and accuracy are key components that need to be balanced. Active learning-kriging (AK) Monte Carlo simulation (MCS) is a reliability method that can reduce the computational cost of evaluating a performance function through the reduction in the computational time of analysis (Echard et al. 2011; Buckley et al. 2020). Kriging is a form of a surrogate metamodel used to predict the limit state of the performance function while still maintaining an adequate level of accuracy (Kaymaz, 2005).It is employed to assess the reliability of complex structural limit states (highly nonlinear or include a large number of random variables) such as limit states in which the resistance model is obtained using SFE. Prior work has used AK reliability analysis in combination with SFE simulation of the resistance model to assess the reliability of bridge girders and of a RC beam (Khorramian and Oudah 2022), other works have investigated the reliability of mono and group piles (El Haj and Soubra 2020; Khorramian et al. 2022), and a book chapter on the theory of AK reliability methods for structural engineering has also recently been published by the structural assessment and retrofit (SAR) research group at Dalhousie University (Khorramian and Oudah 2022). Survey of the preliminary works show improvements in the computational efficiency of stochastic FE reliability analysis but no work to date has investigated the use of AK for the assessment of EB FRP strengthened beams.

In this chapter, a novel framework is proposed that incorporates the AK reliability method presented in Khorramian and Oudah (Khorramian and Oudah 2022) with added clustered learning, into the SFE-MCS framework proposed in Chapter 3. For the Kriging predictor, DACE MATLAB Toolbox is used to form it in the AK analysis (Lophaven et al. 2002a and 2002b).

From the Chapter 3 reliability analysis, a TF25C01 strengthened beam with a MESH20 and CL600 configuration is chosen for analysis. To improve the efficiency of solution, a clustering method has been implemented with the U-learning function to include multi-point enrichment (Lelièvre et al., 2018). This multi-point enrichment has been shown to improve the efficiency of solution (El Haj and Soubra, 2022). This is due to parallelization of computation, as the number of added points does not reduce. A second stopping criteria proposed by Schobi (Schöbi et al. 2017) has been used for comparison against the U-learning function. Sensitivity analysis on the stopping criteria of the AK-SFE-MCS analysis is conducted and the results of the reliability analysis are compared to the SFE-MCS results in Chapter 3.

The following chapter structure is as follows: Section 4.3 breaks down the AK method including the theory of the Kriging method, learning function, stopping criteria, and clustering method used; Section 4.4 presents the framework of analysis for conducting the clustered AK-SFE-MCS analysis; Section 4.5 presents the reliability analysis including a sensitivity study on the stopping criteria; Section 4.6 provides a discussion of the results; and finally, Section 4.7 provides recommendations and concluding remarks.

4.3 ACTIVE-LEARNING KRIGING (AK) RELIABILITY

Active-learning kriging (AK) is a method in which a surrogate model is trained to predict the outcome of a given performance function, using a set of design sites, $S(X)$, and corresponding outputs, $Y(X)$, called together the design of experiment (DoE) (Khorramian and Oudah, 2022). The AK method uses a set of correlation, regression, and learning functions to first train, and then update, the predictor using the DoE. This method is ideal for evaluating performance functions in which it is costly to evaluate the performance function, such as a highly non-linear limit state or the need for SFE simulation to evaluate the resistance. The use of a learning function allows the

user to grow the size of the DoE in a stepwise manor to find the most efficient solution while maintaining a sufficient level of accuracy (Buckley et al 2020). This can potentially save the number of calls to the costly original performance function by only evaluating the number of trials needed to ensure a well trained predictor. This section outlines the structure of the framework and theory of the AK method used in analysis.

4.3.1 Kriging

Kriging, also called the "optimal estimator," is a non-linear stochastic regression method in which a surrogate metamodel (referred to as the kriging predictor herein) is composed of two components: a regression component, and a random process component. The kriging predictor, $\hat{G}(X)$, can be trained to evaluate the desired limit state using the two components to form it, as expressed in Eq.[4.1]:

$$\hat{G}(X) = \mathcal{F}(b, X) + z(X) \quad [4.1]$$

where, $\mathcal{F}(b, X)$ is the regression function with of the random inputs, X, and unknown coefficient b, and $z(X)$ is the stochastic process of the random inputs, X.

By setting the mean of the predictor to zero, and minimizing the mean squared error (MSE) or the variance of the squared error, Eq.[4.2] to Eq.[4.7] are used to estimate the mean and variance of the kriging predictor, respectively (Kaymaz 2005; Khorramian and Oudah 2022):

$$\mu_{\hat{G}}(X) = \hat{G}(X) = \boldsymbol{f}(\boldsymbol{X})^T \boldsymbol{b}^* + \boldsymbol{r}(\boldsymbol{X})^T \boldsymbol{\gamma}^* \quad [4.2]$$

$$\sigma^2_{\hat{G}}(X) = \sigma^2 . \left(1 + \boldsymbol{u}^T (\boldsymbol{F}^T \boldsymbol{R}^{-1} \boldsymbol{F})^{-1} \boldsymbol{u} - \boldsymbol{r}(X)^T \boldsymbol{R}^{-1} \boldsymbol{r}(X)\right) \quad [4.3]$$

$$\boldsymbol{b}^* = (\boldsymbol{F}^T \boldsymbol{R}^{-1} \boldsymbol{F})^{-1} \boldsymbol{F}^T \boldsymbol{R}^{-1} \boldsymbol{Y} \quad [4.4]$$

$$\boldsymbol{\gamma}^* = \boldsymbol{R}^{-1} (\boldsymbol{Y} - \boldsymbol{F} \boldsymbol{b}^*) \quad [4.5]$$

$$\sigma^2 = \frac{1}{m} (\boldsymbol{Y} - \boldsymbol{F} \boldsymbol{b}^*)^T \boldsymbol{R}^{-1} (\boldsymbol{Y} - \boldsymbol{F} \boldsymbol{b}^*) \quad [4.6]$$

$$\boldsymbol{u} = \boldsymbol{F}^T \boldsymbol{R}^{-1} \boldsymbol{r}(\boldsymbol{X}) - \boldsymbol{f}(\boldsymbol{x}) \quad [4.7]$$

Where, the mean value of the kriging predictor, $\mu_{\hat{G}}(X)$, is considered to be the estimate of the limit state, $\hat{G}(X)$, as shown in Eq.[4.2], and the standard deviation of the field, $\sigma^2_{\hat{G}}(X)$, also referred to as the mean square error (MSE), is given by Eq.[4.3]. The terms $\boldsymbol{F}$ and $\boldsymbol{f}(\boldsymbol{X})$ are the regression function, and the associated term $\boldsymbol{b}^*$ is the regression parameter for chosen regression function. The terms $\boldsymbol{u}$ is a vector that is formulated for computational ease as it appears in the solution several times.

The correlation function, $\boldsymbol{R}$, is given by Eq.[4.8], where the term $\boldsymbol{L}$ is the vector of autocorrelation length (called 'correlation length' herein). The terms X_i and X_j are the two points considered. In the case of $\boldsymbol{r}(\boldsymbol{X})$, the two points considered are the design point S_i and all other points X_j, whereas $\boldsymbol{R}(\boldsymbol{X})$ is the correlation between the design points S_i and S_j. The vector $\boldsymbol{L}$ is calculated by minimizing the term in Eq.[4.9] in an iterative process, where m is the number of design sites (i.e., $S = [S_1, \dots, S_m]$), and k represents the kth dimension (i.e., k = [1,2,3] in a 3D problem). Figure 4.1 shows a flow chart of the solution scheme for updating the kriging predictor given a set of DoE. Reference to the above equations is provided in the figure.

$$\boldsymbol{R}\left(L, X_i, X_j\right) = \prod_{k=1}^{n} R_k(l_k, a_k, b_k)\,;\ \boldsymbol{X_i} = [a_1 \dots a_n];\ \boldsymbol{X_j} = [b_1 \dots b_n]\,;\boldsymbol{L} = [l_1 \dots l_n] \quad [4.8]$$

$$L^* = \min_{L}\left\{|\boldsymbol{R}|^{\frac{1}{m}}\,\sigma_k^2\right\};\ k = 1, \dots, n \quad [4.9]$$

In this work a linear regression function and a spline correlation function have been chosen to be the AK configuration for analysis based on a preliminary analysis. Table 4.1 shows the equations for both functions. Note that for a linear regression function a minimum initial points in the DoE are recommended to be equal to $n + 1$, where n is the number of random variables in the problem (Khorramian and Oudah 2022). In the present work an initial DoE size of $n + 6$ is chosen.

Table 4.1. Active-learning kriging: Regression and correlation functions.

Function	Name	Equation
Regression	Linear	$f_1(x) = 1, f_2(x) = x_1, \dots, f_{n+1}(x) = x_n$
Correlation	Spline	$R_k = \begin{cases} 1 - 15\zeta_k^2 + 30\zeta_k^3 & if\ 0 \le \zeta_k \le 0.2 \\ 1.25(1-\zeta_k)^3 & if\ 0.2 \le \zeta_k \le 1 \\ 0 & if\ \zeta_k \ge 1 \end{cases}$

Where $\zeta_k = \left| x_{k_i} - x_{k_j} \right| / a_k$

Active-learning kriging (AK) can further enhance the kriging method through the use of a learning function to select the next candidates to enrich the DoE. This enrichment process allows the use of a small number of initial DoE to train an initial kriging predictor, allowing the learning function to evaluate the accuracy of the predictor. An improved kriging predictor is trained each iteration through added design sites that the learning function designates to be added to the DoE. Stopping criteria should be established so that termination of the learning process can occur when the accuracy is sufficient.

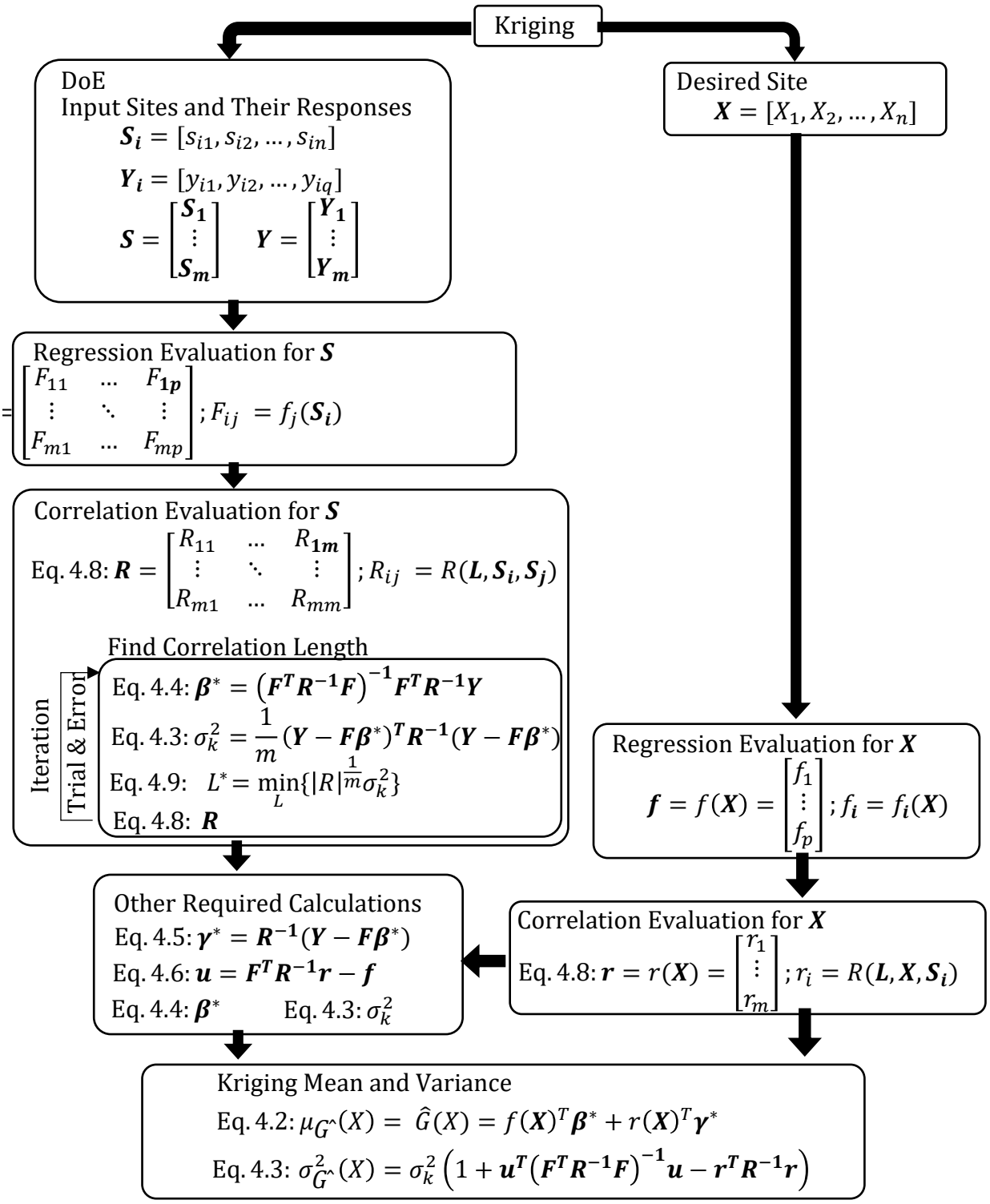

Figure 4.1. Summary of building Kriging predictor (Khorramian and Oudah, 2022).

4.3.2 U Learning Function

In structural reliability analysis using MCS, the performance function, $G(X)$, is set to zero to create the limit state, and the sign of the evaluated performance function will indicate if a trail has failed (i.e., $G(X) < 0$). This has led to a proposed learning function called the *U*-learning Learning Function (Echard et al. 2011). Shown in Eq.[4.10], the learning function works by calculating the reliability index of the prediction, $U(\boldsymbol{X})$, through definition of a linear equation that determines the number of standard deviations, $\sigma_{\hat{G}}(\boldsymbol{X})$, between the estimated kriging prediction value, $\hat{G}(\boldsymbol{X})$, and the limit state ($\hat{G}(\boldsymbol{X}) = 0$), for all design sites considered in the current DoE.

$$U(X) = \frac{\mu_{\hat{G}}(X)}{\sigma_{\hat{G}}(X)} \quad [4.10]$$

Once the kriging predictor has calculated the $\mu_{\hat{G}}(X)$ and $\sigma^2_{\hat{G}}(X)$ vectors of the MCS trials, Eq.[4.10] can be used to evaluate the U-value of each trial. The trial with the lowest U-value score is selected as the next candidate to update the kriging predictor and the original model is used to evaluate the design site to get the associated response site and add them to the updated DoE.

4.3.3 Stopping Criteria

A proposed stopping criteria based on the U-learning function in which the criteria are met when each realization of the kriging predictor has a U-learning score reach above 2.0 will be used in this work (Echard et al. 2011, Buckley et al. 2020; Khorramian and Oudah 2022).

The use of the U-learning stopping criteria has been shown by El Haj and Soubra (2020) to be conservative in the number of added points needed for enrichment of the kriging predictor. An alternative stopping criteria to the U-learning function stopping criteria (shown in Eq.[4.10]) has been implemented based on the work of Schobi (Schobi et al. 2016). The Schobi stopping criteria

uses the probability of failure as shown in Eq.[4.11], and calculates the difference between three probability of failures, P_f^0, P_f^+, P_f^-, given in Eq.[4.12] to Eq.[4.14], respectively:

$$\varepsilon_{P_f} = \frac{P_{f+}^k - P_{f-}^k}{P_f^0} \leq \varepsilon_{stop} \quad [4.11]$$

$$P_f^0 = P\left[\hat{G}(X) < 0\right] \quad [4.12]$$

$$P_{f+}^k = P\left[\left(\hat{G}(X) + k.\sigma_{\hat{G}}(x)\right) < 0\right] \quad [4.13]$$

$$P_{f-}^k = P\left[\left(\hat{G}(X) - k.\sigma_{\hat{G}}(x)\right) < 0\right] \quad [4.14]$$

Where ε_{P_f} is the calculated estimator error of the predator and ε_{stop} is the stopping criteria for ending enrichment of the kriging predictor using active-learning. The term P_f^0 is the probability of failure calculated using the kriging predictor to evaluate the limit state. The terms P_{f+}^k and P_{f-}^k are also the probability of failure, calculated using by taking the mean kriging predictor value, $\hat{G}(X)$, and adding or subtract, respectively, the MSE, $\sigma_{\hat{G}}(x)$, multiplied by a constant, k. Where k is the constant that represents the number of standard deviations away from the mean. The choice of k will determine how quickly the Schobi stopping criteria converges to the selected stopping value ε_{stop}. Table 4.2 summarizes the stopping criteria equations and stoppings values associated with the U-learning and Schobi stopping criteria used in this study.

Table 4.2. Active-learning kriging: Stopping criteria for kriging enrichment process.

Reference	Equation	Stopping Criteria
Echard et al., 2016	$U(X) = \frac{\mu_{\hat{G}}(X)}{\sigma_{\hat{G}}(X)}$	$Min\ [U(X_i)]\ >\ 2.0$
Schobi et al., 2016	$\varepsilon_{P_f} = \frac{P_{f+}^k - P_{f-}^k}{P_f^0} \leq \varepsilon_{stop}$	$\varepsilon_{stop} = 0.1$

4.3.4 U-Learning: K-w-means Clustering

A clustering method has been implemented to improve the efficiency of the AK method to meet the stopping criteria for learning, called k-w-means clustering (Lelièvre et al. 2018). When single-point enrichment is conducted, the trial with the lowest U-value identifies the next candidate to be added as a design site. By choosing the trial with the lowest U-value ensures that the design site with the most uncertainty can be evaluated by the original model. K-w-means clustering instead takes the set of trials with the lowest estimated U-value and breaks them to form several clusters. The number of clusters chosen will determine the number of added points per iteration of AK enrichment. The method makes use of the information gained by evaluating the U Leaning Function by calculating geometric mean of each cluster using the U-values of each trials as weights, to propose a set of enrichment points. The chosen enrichment points may not be the lowest U-value trials but are within the lowest and should be sufficient to yield convergence. By iterating through this procedure, an optimal set of design sites can be obtained.

A summary of the steps in the selection of the next cluster of design sites is presented below. These steps are incorporated into the MATLAB script to perform the AK-SFE-MCS analysis:

Step 1. Let the term K_{mean} be the number of clusters to be considered, and the term $N_{cluster}$ be the number of points included in each cluster.

Step 2. Calculate the U-values of the learning function based on the current kriging predictor using Eq.[4.10]. Sort the trials in a vector, $\boldsymbol{U_{Min}}$, in descending order of U-value.

Step 3. Select a total of P ($P = K_{mean}\, x\, N_{cluster}$) lowest ranked U-values from $\boldsymbol{U_{Min}}$ and randomly select K_{mean} of the P selected trials to be the initial cluster centroids $(c_1^{(1)}, c_2^{(1)}, \dots, c_{K_{mean}}^{(1)})$.

Step 4. Form a Voronoi diagram of the P number of trials selected by assigning all trials not designated as a centroid in step 3 to belong to the ith cluster centroid, $c_i^{(1)}$, that minimizes the Euclidean distance between them (Aurenhammer 1991).

Step 5. Determine a new set of centroids ($c_1^{(j+1)}, c_2^{(j+1)}, \dots, c_{K_{mean}}^{(j+1)}$) of each cluster using Eq.[4.15], which applies a weight based on the *U*-value of the given value of X.

$$c_i^{(j+1)} = \frac{\sum_{k=1}^{N_k}\left(\frac{1}{U_k}\right) X_k}{\sum_{k=1}^{N_k}\left(\frac{1}{U_k}\right)}; \quad i = [1, 2, \dots, K_{Mean}] \tag{4.15}$$

Where the terms j and N_k represent the iteration number and number of points within the *i*th cluster, respectively. The terms U_k represent the *U*-value of the *k*th trial, and X_k represents the vector of inputs for the kth trial.

Step 6. Calculate the error between the previous and current set of cluster centroids, $c_i^{(j)}$ and $c_i^{(j+1)}$, respectively, using Eq.[4.16]:

$$\Omega_{cluster} = \sum_{i=1}^{K_{mean}} \left(c_i^{(j)} - c_i^{(j+1)}\right)^2 \tag{4.16}$$

Step 7. Compare $\Omega_{cluster}$ found in step 6 to the stopping criteria, Ω_{stop}. If the stopping criteria is not met ($\Omega_{cluster} > \Omega_{stop}$), repeat steps 2 to 6 until criteria is met. If the stopping criteria is met ($\Omega_{cluster} \leq \Omega_{stop}$), move to step 8.

Step 8. Calculate the points that form the smallest Euclidean distance with each established centroid and select it for updating the kriging predictor DoE.

In this work, a k-w-means clustering algorithm considering 4 clusters with 5 points (i.e., $K_{mean} = 4$, and $N_{cluster} = 5$) is used. A stopping criteria is set as 2% for this study ($\Omega_{\text{stop}} = 0.02$). It should be noted that the algorithm will produce centroids that are not sample points in the design space. To overcome this, step 8 has been implemented.

4.3.5 AK Reliability Method

AK-MCS has been used in this work to assess the reliability of the strengthened beam using 500,000 trials in the MCS analysis. Using the constructed kriging predictor, the probability of failure, $P_{f_{\hat{G}}}$, and coefficient of variation, $COV_{P_{f_{\hat{G}}}}$, can be calculated using Eq.[4.17] and Eq.[4.18], respectively.

$$P_{f_{\hat{G}}} = \frac{1}{N_{mcs}} \sum_{j=1}^{N_{mcs}} I[\hat{G}(X)_j] \quad [4.17]$$

$$COV_{P_{f_{\hat{G}}}} = \sqrt{\frac{1-P_{f_{\hat{G}}}}{P_{f_{\hat{G}}} N_{mcs}}} \quad [4.18]$$

where, N_{mcs} is the number of trials included in the MCS, and $I[\hat{G}(X)_j]$ is the jth value of the indicator function denoting the sign of the kriging estimated performance function.

4.4 FRAMEWORK OF ANALYSIS AND COMPUTER CODE DESCRIPTION

An automated computer code has been developed to conduct the reliability analysis using the AK-MCS and stochastic FE model. The AK method requires the call of the original model to set up or update the DoE. The term original model refers to the calling of the SFE model to be generated and ran to extract the ultimate response of a strengthened beam. The flowchart of calling the original model to build or update the DoE is given in Figure 4.2. An LSDYNA-Python-MATLAB interface has been established generate the SFE models. This interface links the generated random field in MATLAB to the discretized FE model in LS DYNA, through the use of a Python script. Each program (MATALB, LS DYNA, Python) is designated by a color and a colored label withing the figures. When a script of one program calls another programs script (i.e., MATLAB, or Python,

calling LS DYNA) this will be represented by having the called program labeled box nested within the primary program labeled box.

The SFE models are generated using the interface by using the design sites given from the updated DoE and are run using the LS DYNA SMP solver. Load-displacement curves are plotted to extract the ultimate load at failure. Moment resistance of the beam is calculated and the performance function, $G(X)$, is evaluated to update the DoE. The running of SFE simulations in LS DYNA SMP solver has been automated through MATLAB and has been optimized to run several simulations in parallel. All analysis were run on a windows-based server with dual Intel Xeon Gold 5220R 2.20GHz processors (48 cores), a NVIDIA Quadro P620 graphics card, and 128 Gb of available RAM.

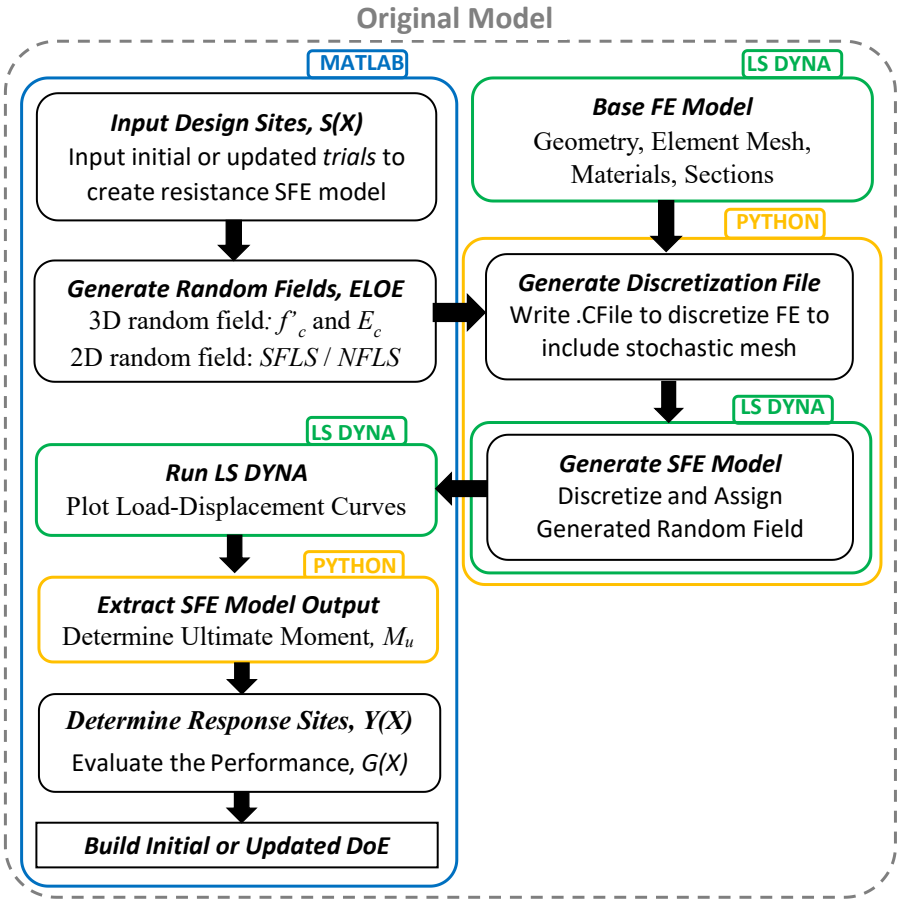

Figure 4.2. Flowchart of original model evaluation.

The flowchart outlining the general procedure to conduct AK-SFE-MCS analysis is given in Figure 4.3. This procedure uses the kriging framework presented in Figure 4.1 and the framework to call the original model presented in Figure 4.2. To begin, the MCS trials are randomly generated and from those trials N initial design sites are selected to be the initial points. The original model is called and SFE models are generated to extract the ultimate response. The performance function is evaluated, and the DoE updated. A surrogate kriging predictor is trained and is used to evaluate the performance function, $\hat{G}(X)$, and mean squared error, $\sigma_{\hat{G}}$, for all MCS trials. The kriging results are used to evaluate the U learning function using Eq.[4.10], to generate a vector of U-values for all trials and to calculate the probability of failures, P_{f0}, P_{f+}^{k}, P_{f-}^{k}, using Eq.[4.12] to Eq.[4.14], respectively. The stopping criteria is evaluated by identifying the minimum U-value and calculating the error, ε_{P_f}, using Eq.[4.11]. If the stopping criteria is not met, k-w-means clustering is used to select the next cluster of design sties for updating the DoE. Once the chosen stopping criteria is met the kriging predictor is adequately trained and can be used to calculate the probability of failure of the strengthened beam using Eq.[4.17].

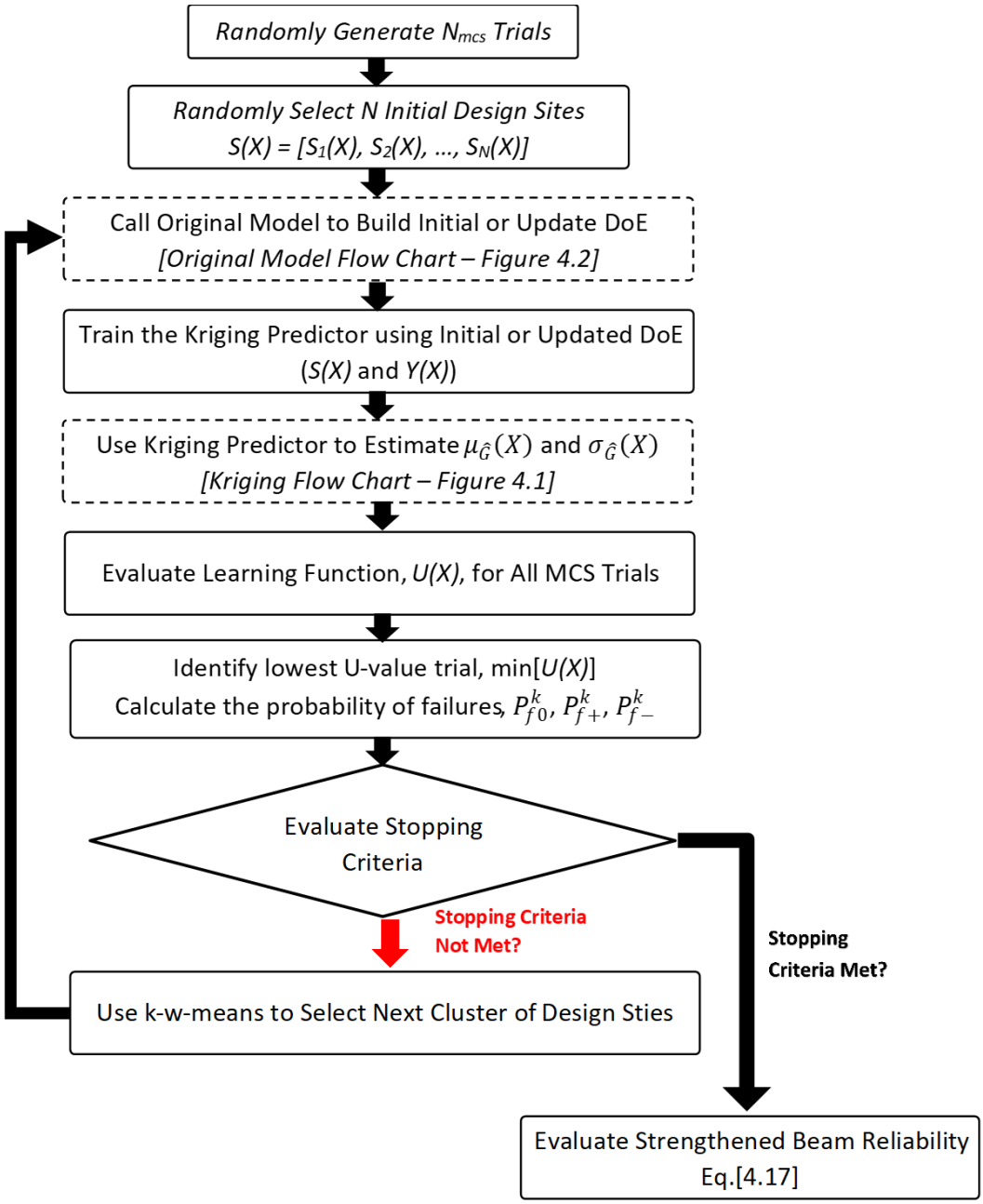

Figure 4.3. Flowchart of clustered AK-SFE-MCS Reliability Analysis.

4.5 RELIABILITY ANALYSIS USING AK-MCS AND STOCHASTIC FE MODEL

4.5.1 Input Parameters

The statistics of the random variables from Chapter 3 will be used in this analysis to compare results of both reliability methods. Table 4.3 and Table 4.4 summarize the random variable statistics for the resistance and load models, respectively, and Table 4.5 summarizes the stochastic inputs for the SFE model random fields. A SFE model with a element size of 12.5x12.5x10mm and a SEM/EM ratio equal to 2x2x2 was used (MESH20 configuration in Chapter 3). A correlation length of 600mm (CL600 configuration in Chapter 3) was used in all directions to reduce the number of standard normal variables while meeting an acceptable representation quality of the random field. A set of 4 standard normal variables was used to generate the 3D random field.

Table 4.3. Parametric reliability analysis: Input statistics of the resistance random variables.

	FRP		Concrete	Steel	Model Error
Units	MPa	GPa	MPa	MPa	(EXP/FE)
Variable	f_{frpu}	E_{frp}	f'_c	f_y	M_{err}
Dist. Type	Lognormal	Normal	*Rand. Fld.	Normal	Normal
Mean, μ	3,350	235	25	335	1.00
Bias, λ	1.15	1.0	1.0	1.145	1.10
COV	0.1	0.04	0.1	0.05	0.12
Ref.	*(a)	*(a)	(This study)	*(b)	*(c)

*(a) Huang et al., 2019; *(b) Nowak and Szerszen et al., 2003; *(c) Castaldo et al., 2019.

Table 4.4. Parametric reliability analysis: Input statistics of load random variables.

	CSA S806:17		
Combin.	$1.25DL + 1.5LL * T2L$		
Variable	DL	LL	$T2L$
Dist.	Normal	Gumbel	Normal
Bias	1.050	0.900	1.000
COV	0.100	0.170	0.206
(Ref.)		(Bartlett et al., 2003a,b)	

Table 4.5. Parametric reliability analysis: Stochastic inputs for generating random field.

Input Parameter	Value
Random Field Type	Lognormal
Correlation Function	Squared Exponential (Eq.[3.3])
3D EM Density (mm)	12.5x12.5x10
3D SEM Density (mm)	25x25x20
SEM/EM	2x2x2
Correlation Length (mm)	600
Truncation Value, r	4

4.5.2 Performance Function

The performance function used in the clustered AK-SFE-MCS analysis has been chosen to be the same performance function will be used in Chapter 3 (see Section 3.7.3.2). The performance function has been repeated here for convenience in Eq.[4.19] and Eq.[4.20]. The mean, bias, and COV of the resistance term, $R(X)$, has been taken from Table 3.18 for the TF25C01 strengthened beam ID. The other inputs for the design, load and model error variables used in the reliability analysis are listed in Section 4.5.1.

$$G(X) = R(X) * Merr - UR * L(x) \quad [4.19]$$

$$L(X) = DL(X) + LL(X) * T2L(X) \quad [4.20]$$

4.5.3 Parametric Reliability Analysis

The reliability analysis was conducted using both SFE-MCS and clustered AK-SFE-MCS. A TF25C01 strengthened beam with a MESH20 and CL600 configuration is selected for analysis. The reliability of the TF25C01 beam was found to be above 4.5 in the Chapter 3 analysis. To reduce this value for ease of computation, a utilization ratio, UR, equal to 1.3 is used when evaluating the limit state in Eq.[4.19]. A total of 1E8 MCS trials will be used to evaluate the probability of failure in both reliability analysis. For the two step SFE-MCS, a total of 400 SFE models are randomly generated to establish the resistance statistics. In the AK-SFE-MCS, 17 initial

trials were used in the DoE and the clustered learning proposes 4 new design sites for each iteration of enrichment.

A sensitivity analysis on the U-Learning and Schobi stopping criteria varying scale factors, k, was conducted. The efficiency of the reliability methods to reach a solution was evaluated. Efficiency in this case refers to the computational time to generate and evaluate the SFE models. A summary of the considered cases for the sensitivity analysis of the stopping criteria used in the AK-SFE-MCS analysis is included in Table 4.6.

Table 4.6. Parametric reliability analysis: Summary of stopping criteria considered.

Name	U	P_f^{05}	P_f^{10}	P_f^{20}
Constant, k	--	0.5	1.0	2.0
Stopping Criteria	$Min[U(X)] > 2$	$\varepsilon_{stop} = 0.1$	$\varepsilon_{stop} = 0.1$	$\varepsilon_{stop} = 0.1$
Equation	Eq.[4.10]	Eq.[4.11]	Eq.[4.11]	Eq.[4.11]
Reference	*(a)	*(b)	*(b)	*(b)

**(a) – Echard et al., 2011; *(b) – Schobi et al., 2016*

The clustered AK-SFE-MCS analysis conducted was run until all stopping criteria were met. Analysis results are summarised in Table 4.7, showing the number of added points for AK enrichment, the total number of calls to the original SFE model, and the calculated reliability index of the strengthened beam calculated once the stopping criteria is reached. Results from conducting the same analysis using SFE-MCS framework presented in Chapter 3 is also provided for comparison. The same number of initial points was used for all AK analysis, with the umber of added points needed for enrichment depending on how quickly the stopping criteria set is met. Results show that for the same number of MCS trials, the AK-SFE-MCS and SFE-MCS yield much different values of reliability index.

Table 4.7. Parametric reliability analysis: Results of different stopping criteria.

	SFE-MCS	AK-SFE-MCS			
Stopping Criteria	--	U	P_f^{05}	P_f^{10}	P_f^{20}
N_{mcs}	1e8	1e8			
Initial DoE	--	17			
Added Points	--	298	41	57	253
Total Calls of SFE	400	315	58	74	270
Reliability Index, β	2.28	3.68	3.72	3.66	3.67
Time (days)	2.2	4.1	0.75	1.2	2.4

As expected, the lower value of k in Eq.[4.13] and Eq.[4.14] allowed the stopping criteria to be met for the Schobi equation in fewer iterations of enrichment of the DoE. The number of added points slightly changed the calculated reliability of the strengthened beam, in the range of 3.6 to 3.8. Figure 4.4 shows a plot of the three probability of failures, P_{f0}, P_{f+}^k, P_{f-}^k for the various values of k considered. The solid line represents the kriging predictor probability of failure, P_{f0} and the dashed lines each represent a value of P_{f+}^k, P_{f-}^k. Figure 4.5 shows the progression of the U-learning stopping criteria through a scatter plot of all MCS trial U-values. A red line is provided on each plot showing the minimum U-value that all MCS trials must achieve to meet the stopping criteria. The figure shows the average U-value of the MCS trials increasing with each iteration of enrichment, having fewer points below the minimum value of 2.

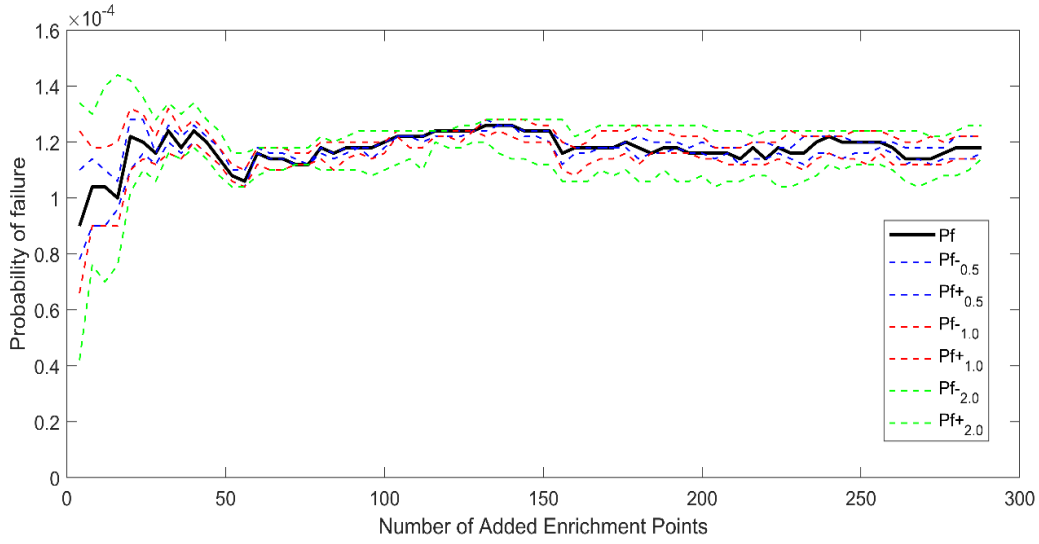

Figure 4.4. AK-MCS Relibaility analysis: Schobi stopping critera evaluation.

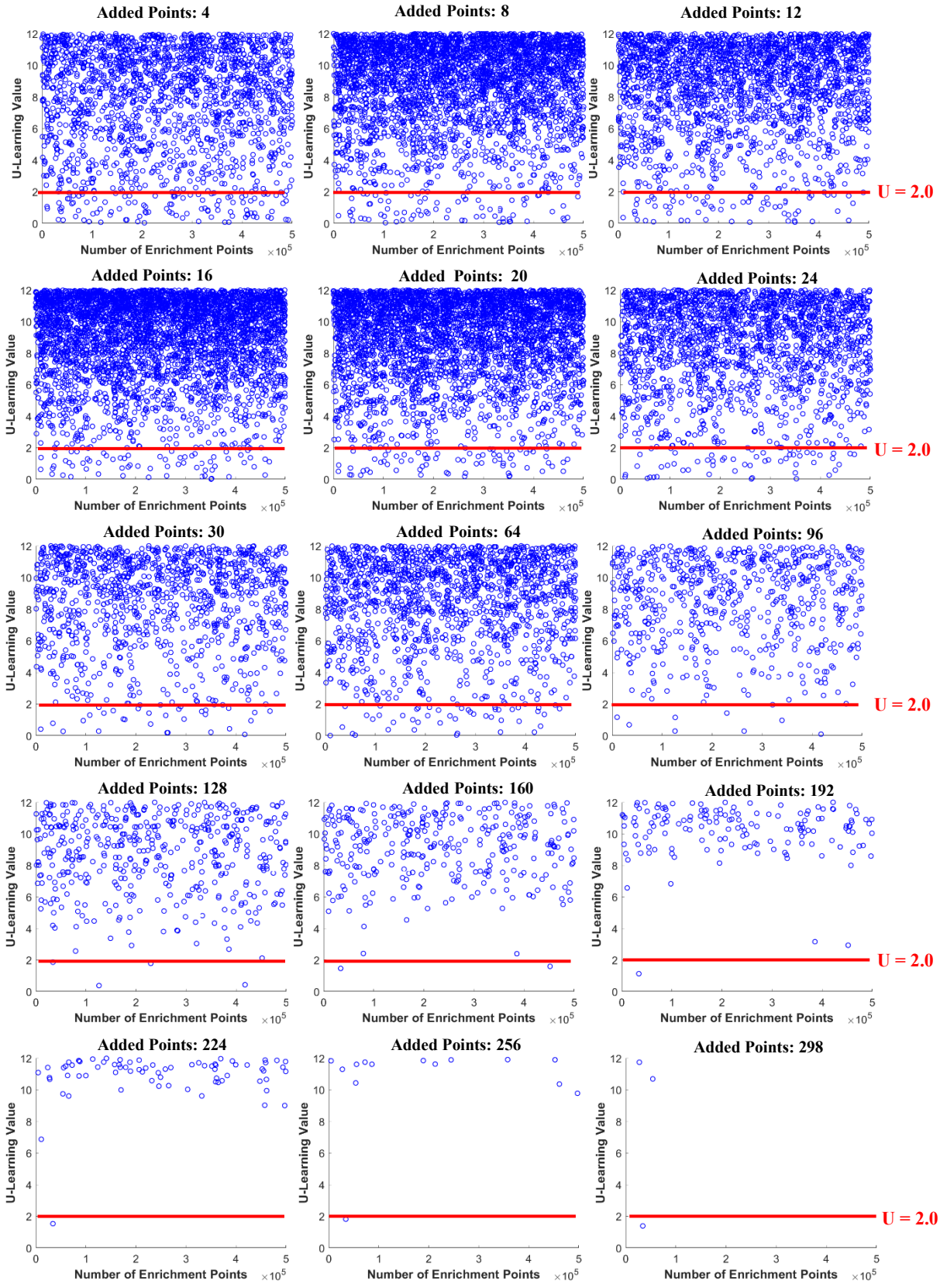

Figure 4.5. AK-MCS Reliability analysis: U-Learning function stopping Criteria Evaluation.

4.6 Discussion

4.6.1 Clustered AK Reliability for Strengthened Beam Assessment

A comparison of the SFE-MCS and AK-SFE-MCS method show a large discrepancy in the calculated reliability index for a similar number of calls to the original model. The AK configuration (Regression, Correlation, and Learning Function) chosen allowed for the convergence of all stopping criteria in fewer calls to the original model than SFE-MCS but yields higher reliability index values. It should be noted that for both methods, there is no 'exact' solution (i.e., an MCS with a high number of trials) that can be calculated due to the cost to compute the large number of SFE models needed. The low COV reported of the moment statistics in the SFE-MCS method indicate that an increase in the number of SFE models used to establish the resistance statistics (i.e., increased accuracy of the SFE-MCS) may not significantly affect the reliability index and will be used as the comparative case for the AK method. Using this line of thinking to take the SFE-MCS as the exact solution to compare the AK-SFE-MCS results, several reasons could cause the discrepancy in the calculated reliability index:

- The accuracy of the surrogate model is based on the quality of the training set provided and the AK configuration used to perform the kriging. Although both the U and Schobi ($k = 2$) stopping criteria are met after 300 points added, this may not ensure that the kriging predictor is accurately trained.
- The high number of random variables that make up the design site could also play a role. Most papers that have looked at AK-SFE-MCS (El Haj and Soubra, 2020; Khorramian et al. 2022) use a smaller number of random variables to act as the design sites. In this work, 11 random variables were considered made up of the load, resistance, and standard normal random variables.

- The kriging predictor is trained based on the design sites being made up of all random variables considered. This means that as the number of standard normal variables used to generate the random field is increased, so does the number of random variables in the design sites to be evaluated by the kriging predictor. The more random variables in the design sites (i.e., a larger value of m) may decrease the accuracy of the trained predictor. A balance between including enough standard normal variables for representation quality of the random field and keeping the number of variables in the design sites low must be achieved.
- The SFE-MCS reliability framework utilizes a two-step method to first establish the statistics of the resistance using the design variable statistics and SFE. Next, the resistance statistics are used with the load statistics to conduct MCS to calculate the reliability index of the strengthened beam. The AK method trains the kriging predictor directly without the establishment of resistance statistics by fitting a given distribution type (i.e., Gaussian distribution) that may not necessarily be representative of the resistance.

More research is needed to quantify the reason for this discrepancy through parametric analysis of the AK configurations, several random variables considered, and by allowing a higher number of added points for enrichment. It may be advantageous to use SFE-MCS with a higher number of SFE models used to establish the resistance statistics than to use AK-SFE-MCS, as more models can be run in parallel.

4.6.2 Stopping Criteria for AK Learning

A comparison of the Schobi and U Learning Function stopping criteria for the AK analysis shows a difference in the number of added points to meet convergence for the beam considered. The U Learning Function criteria took the most added points to converge while the Schobi stopping

criteria varied based on the constant k used in Eq.[4.11] (k is the number of standard deviations away from P_f that the upper and lower error bounds are calculated). Results show an agreeance between the U, P_f^{10}, and P_f^{20} stopping criteria, while the P_f^{05} showed a higher reliability index value.

4.6.3 Clustered U Learning

The k-w-means clustering technique allowed the parallelization of the enrichment of the DoE through the selection of multiple points for each iteration of training the kriging predictor. The added cluster of points in most cases did not coincide with the lowest U-value trial but still offer improved enrichment. This is due to having multiple points, and the fact that the cluster evaluates a set of trials that is still within the lowest ranked U-value of the trial that iteration.

Clustering improves the efficiency of the AK method most during the initial iterations and reduce the effectiveness in later iterations. This reduction in improvement in learning is due to the next candidates selected being of high certainty, meaning the improvement in the kriging predictor decrease after this point is reached. Looking at the results of the U Learning Function in Figure 4.5, as the number of added points reaches above 160 points, it can be seen that fewer than 5 trials have a U-value lower than 2. This increase in average U-value means that as the enrichment iterations increase to meet the U stopping criteria, the points taken into the clustering are of high U-value ($U >> 2$) and may not yield an improvement in the kriging predictor. It is recommended that the switch from multi-point clustered enrichment be switched to single-point enrichment of the lowest U-value trial once a certain threshold of average U-value is reached to ensure efficient convergence.

4.7 CONCLUSION

The use of the active-learning kriging (AK) reliability method, with clustered learning, for the application of augmenting SFE-MCS analysis was examined in this chapter on an RC beam strengthened with EB FRP in flexure. An AK framework has been developed and implemented to use an LSDYNA-Python-MATLAB interface to conduct AK-MCS using stochastic finite element (SFE) models with random fields. The use of AK-based reliability methods has been shown in other applications to reduce the number of calls to the original SFE model to improve efficiency while maintaining accuracy. An AK configuration of linear regression, spline correlation, and U-Learning function was selected to perform the analysis. Both clustered AK-SFE-MCS and SFE-MCS analyses were conducted on the same EB FRP strengthened beam to compare the efficiency of the solution scheme. A sensitivity study of the stopping criteria for active learning was also investigated.

Results showed that the clustered AK-SFE-MCS framework reduces the number of calls to the SFE models and allows some parallelization to computation. This reduced the number of SFE calls but yields conservative reliability values for the chosen AK configuration as compared to the SFE-MCS framework. The choice of stopping criteria directly affected the convergence of the stopping criteria. It was found that the Schobi stopping criteria with a constant, $k = 1.0$, is sufficient as a stopping criterion to allow efficient convergence while maintaining accuracy relative to a more stringent stopping criteria. More research is needed into the choice of AK configuration for the assessment of EB FRP strengthened beams to understand the source of the difference in results as compared to SFE-MCS. Further validation against crude MCS will allow investigation of the accuracy of the AK-SFE-MCS method as compared to SFE-MCS.

CHAPTER 5 RELIABILITY-BASED DESIGN CHARTS CONSIDERING LOAD TYPE / HISTORY FOR EB FRP STRENGTHENING OF EXISTING FLEXURAL MEMBERS AS PER CSA S806:17

5.1 EXECUTIVE SUMMARY

In this chapter, a novel approach to develop reliability-based framework to generate user friendly design aids is proposed, in the form of charts, to be used by engineers to evaluate the safety of existing concrete beams and optimize the repair scheme considering existing conditions. Based on the first identified research gap in the literature review in Chapter 2, the framework takes into account the load type and history of the existing beam prior to strengthening to update the unstrengthened beam's reliability index to assess for code deficiency.

An experimental database of tested beams based on current studies in literature has been formulated to obtain descriptive statistics (mean, bias, and COV) for strengthened RC beams. The statistics of unstrengthened beam and load are taken as the values used to calibrate the ACI 318 (ACI 319:19, 2019) and NBCC (NBCC, 2015) codes, respectively.

The design charts generated allow the user to find a strength multiplier, M_S/M_R, which represents the minimum amount of FRP needed to meet a target reliability, should the member be deficient. The reliability framework uses the principals of updated reliability, by taking into account the load type and history of the structure, using the principals of conditional probability. Load type refers to the type of load (dead, live, snow), while the load history refers to the magnitude of said load seen by the existing component to date. Design examples of strengthened flexural components using externally bonded CFRP laminates are provided to show the utility of the charts.

5.2 INTRODUCTION

The factors for load and resistance included in Canadian codes (NBCC 2015; CSA A23.3:19; CSA S806:17), were calibrated using reliability methods to meet predefined target safety limits for new construction. As stated by the NBCC 2015 in the Notes to Part 1 of Division A, practicing engineers should be careful in applying the code provisions when evaluating existing structures since these provisions may not necessarily reflect consistent safety levels when used in evaluating existing structures. Consequently, the use of reliability methods to optimize the evaluation and repair of existing structures taking into account load history is recommended (Hong 1998; Hong and Lind 1991). In this work, a reliability framework is proposed to account for the load history and load type of the existing beam prior to strengthening, to investigate the effect on the reliability of the strengthened beam.

To include load type and history in a reliability framework, two measurements of the loads experienced by the existing member are needed: i) the type of load, and ii) the maximum measured load experienced by the structure to date. This allows the removal of a part of the uncertainty that was present before construction through the structure experiencing a portion of the design loads without sustaining damage (Hong 1998). The structure has been service proven; thus, the failure surface can be truncated, and the structure will usually see an improvement in reliability.

The following sections describe the background, experimental databased of strengthened beams, methodology, and reliability analysis using FORM. Design charts that provide an optimized amount of FRP needed to meet target safety limits are proposed based on the results of the reliability analysis. These optimized designs are based on the utilization of the deficient beam and the load history of the beam prior to strengthening.

5.3 BACKGROUND

The principals of conditional probability will be used to accomplish this, using Eq.[5.1] for finding the updated probability of failure based on bayes theorem, where $P(B|A)$ is the likelihood of event A happening given B:

$$P(B|A) = \frac{P(A)\,P(A|B)}{P(B)} \quad [5.1]$$

The current study utilizes the work by Hong to calculate reliability based on service-proven dead loads and measured maximum live load experienced, S_T, based on satisfactory field inspection over a given period of time. All random variables in the limit state are lumped into two variables of load, L, and resistance above the dead load, R. Both variables are assumed to be independent and lognormally distributed. This method allows FORM to be utilized to find an updated reliability, β_{up}, by Eq.[5.2], based on the original reliability index, β_o, and update reliability index, β_s:

$$\beta_{up} = -\Phi^{-1}(P_{fup}) \quad [5.2]$$

$$P_{fup} = \Phi(\beta_o) + \frac{\int_0^{\rho} \Phi(-\beta_o, -\beta_s, r)\,dr}{\Phi(-\beta_s)} \quad [5.3]$$

$$\Phi(-\beta_o, -\beta_s, r) = \frac{1}{2\pi\sqrt{1-r^2}} \exp\left(\frac{-(\beta_o^2+\beta_s^2-2\beta_o\beta_s r)}{2(1-r^2)}\right) \quad [5.4]$$

$$\beta_o = \frac{m_{lnR} - m_{lnL}}{\sqrt{\sigma_{lnR}^2 + \sigma_{lnL}^2}} \quad [5.5]$$

$$\beta_s = \frac{m_{lnS_T} - m_{lnR}}{\sigma_{lnR}} \quad [5.6]$$

$$\rho = \frac{-\zeta}{\sqrt{\zeta^2+1}} \quad [5.7]$$

$$\zeta = \frac{V_{S_T}}{V_L} \quad [5.8]$$

Eq.[5.3] gives the updated probability of failure, P_{fup}, based on bayes theorem given by Eq.[5.1]. Eq.[5.4] represents the binormal probability density function, $\Phi(-\beta_o, -\beta_s, r)$, of the two reliability terms. The original reliability, β_o, and service proven reliability, β_s, are given by Eq.[5.5] and Eq.[5.6], respectively, by transforming the mean and standard deviation of $R, L,$ and S_T to be lognormal. Eq.[5.7] yields the integration limit rho, ρ, and is based on the ratio of the variation of resistance above the dead load to load, S_T. Finally, $\Phi(.)$ and $\Phi^{-1}(.)$ are the standard normal and inverse standard normal cumulative distribution functions, respectively.

5.4 EXPERIMENTAL DATABASE

Review of experimental studies from literature, which examine the use of EB FRP for strengthening RC beams in flexure was conducted. A database was obtained of rectangular RC beams, strengthened with EB FRP, that fail in either crushing of concrete or rupture of FRP (flexure). The strain limit imposed by the CSA S806:17 standard limits the allowable stress on the FRP, so that debonding is avoided. For this reason, beams that fail due to debonding were excluded from the present study.

The database consists of 41 experimentally tested beams, taken from studies done from 1998 to 2015. It consists of two sets of RC beam data: EB FRP strengthened beams and unstrengthened (control) beams. The following parameters are reported for every point in the database: beam geometry, concrete strength, steel yield strength, steel modulus of elasticity, area and location of internal reinforcement, nominal predicted strength based on the design provisions of CSA S806:17

and CSA A23.3:19 (strengthened and unstrengthened, respectively), actual resistance based on experimental tests (strengthened and unstrengthened), FRP ultimate strength, FRP modulus of elasticity, and area of FRP used for strengthening.

Descriptive statistics (bias, COV, distribution type) are found for every point of the database. The mean bias and COV for the strengthened beams were found to be 1.22 and 0.19, respectively, while the unstrengthened beams reported values of 1.19 and 0.089, respectively. The latter values for unstrengthened beams were taken as the values used in the calibration of ACI 318 code. The bias and COV for the loads used are 1.05 and 0.1, respectively, for dead load, and 0.9 and 0.17, respectively, for live load (Bartlett et al., 2003a; Bartlett et al., 2003b). Table 5.1 provides a summary of all input parameters used in the reliability analysis.

Table 5.1. Descriptive statistics of the random variables used in the reliability analysis.

Variable	Strengthened Moment Resistance (M_S)	Un-strengthened Moment Resistance (M_R)	Dead Load (DL)	Live Load (LL)
Bias	1.22	1.19	1.05	0.9
COV	0.19	0.089	0.1	0.17
(Ref.)	(This Study)	(ACI 318:19, 2019)	(Bartlett et al., 2003a,b)	(Bartlett et al., 2003a,b)

5.5 EQUIVALENT PHI FACTOR

Canadian codes use the concept of material resistance factors (ϕ_c, ϕ_s, ϕ_{frp}) applied to each component that makes up the member. Conversely, American codes use member strength reduction factors, applied to the action rather than each material to achieve the same reduction (ϕM_u). Both approaches can be calibrated to meet a pre-defined reliability index although the level of safety will be slightly different. To be able to use FORM to find the updated reliability, an equivalent phi factor, ϕ_e, must be introduced as an overall resistance reduction factor.

This factor will be equivalent to using the partial phi factors (ϕ_c, ϕ_s, ϕ_{frp}) from CSA S806:17 standard and is found by calculating the factored resistance, as per the code, and dividing this value by the nominal (unfactored) resistance as shown in Eq.[5.9]:

$$\phi_e = \frac{Factored\ moment\ resistance}{Nominal\ moment\ resistance} = \frac{M_r}{M_u} \quad [5.9]$$

A parametric analysis was completed in MATLAB using the database described in Section 5.4 consisting of rectangular RC beam samples. The results of applying Eq.[5.9] for every point in the database yielded a mean equivalent phi factor of 0.8368 with a coefficient of variation equal to 0.016. A value of ϕ_e = 0.84 is selected to be used in this study.

5.6 METHODOLOGY

The framework presented in the following section can be applied to flexural members (slabs and beams). The charts are based on the well-known parameter of utilization ratio, which is the factored demand over the factored resistance (Utilization, $UR = Demand/Capacity$). The steps in the following procedure were used to generate the user-friendly design charts per the S806:17:

- Step #1: Select the following input parameters: target reliability index, β_t, utilization ratio, UR (ratio of factored loads to factored resistance), ratio of maximum live load experienced over design live load, ψ_L, ratio of maximum dead load experienced over design dead load, ψ_D, ratio of dead-to-live load, D/L, and governing load combination ($1.25D + 1.5L$).
- Step #2: Calculate the members nominal flexural resistance, M_u, above and beyond the dead load based on parameters selected in step 1. Multiply M_u by the equivalent phi factor, ϕ_e, to obtain the factored resistance above dead load, M_R, as shown in Eq.[5.10].

$$M_r = \phi_e M_u \quad [5.10]$$

- Step #3: Calculate the updated reliability, β_{up}, for the unstrengthened member using equation (2), based on the statistics for unstrengthened beams presented in Table 5.1. The mean resistance and load values are found based on the beam's geometry and material properties and a utilization ratio of 1.0. These mean values are then multiplied by their given bias factors to produce the mean values for reliability analysis.

- Step #4: Compare the updated reliability index found in step 3 with the selected target reliability. If $\beta_{up} > \beta_t$, then the member is not deficient (terminate algorithm). If $\beta_{up} < \beta_t$, the member is deficient and repair is required, proceed to the next step.

- Step #5: A strength multiplier, M_S/M_R, is calculated to achieve the target reliability index selected. A new updated reliability based on the strengthened section, $\beta_{up,new}$, is calculated and iterated until $\beta_{up,new} = \beta_t$. This multiplier is optimized, based on the statistics presented earlier in this chapter for strengthened beams, to be the minimum value needed to achieve a suitable level of safety as defined by the CSA S806:17 standard.

- Step #6: For a given set of D/L and β_t values, user-friendly charts are generated to show how M_S/M_R changes with increasing utilization ratio, UR.

5.7 RELIABILITY ANALYSIS

The solution scheme of section 5.6 was programmed into MATLAB, to conduct a parametric study examining the sensitivity of the load parameters, on the needed amount of flexural strengthening. The parametric study included varying the following parameters for the given ranges: dead-to-live ratio, $D/L = [1, 2, 3, 4]$; target reliability index, $\beta_t = [3.0, 3.5, 4.0]$; ratio of experienced-to-design dead load, $\psi_D = [0.9, 1.0, 1.1]$; and ratio of experienced-to-design live load, $\psi_L = [0.5, 0.7, 0.9]$. Each design chart includes plots of utilization ratio versus strength multiplier for a multitude of target reliability indexes and dead-to-live load ratios. Each plot includes design lines for both the deterministic code and FORM-based values of the strength multiplier. Strict application of NBCC 2015 and CSA S806:17 (referred herein as the "code" or "codes") in determining the strength multiplier yields a linear relationship as shown, whereas reliability analysis from this study yield a non-linear curve that varies with inputs; sample analysis results are described herein.

The following charts show the effect of the load history and type on the amount of strengthening (strength multiplier, M_S/M_R) needed as utilization ratio increases. Results of using FORM to calculate the reliability index for a given range of $D/L = [1.0,\ 3.0]$, $\psi_D = [0.9,\ 1.0,\ 1.1]$, and $\psi_L = [0.5,\ 0.9]$ are plotted. The figures show a practical range of utilization ratio and the corresponding M_S/M_R. Figure 5.1 shows the values of M_S/M_R needed for a reliability index of β_t = 3.0; Figure 5.2 shows the values of M_S/M_R needed for a reliability index of β_t = 3.5; and Figure 5.3 shows a higher target reliability of β_t = 4.0, for the aforementioned range of load inputs.

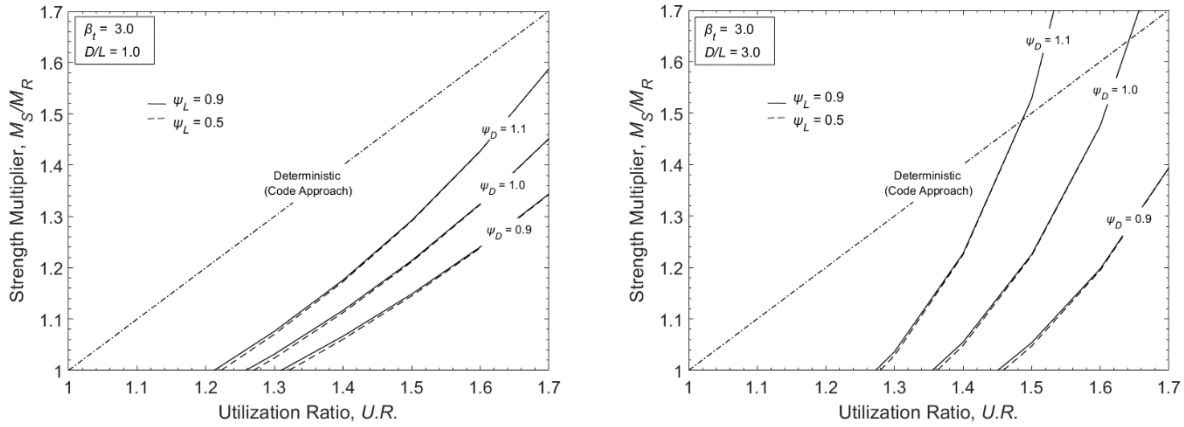

Figure 5.1. Generated sample plots of M_S/M_R versus UR for β_t= 3.0 for $D/L = [1.0, 3.0]$

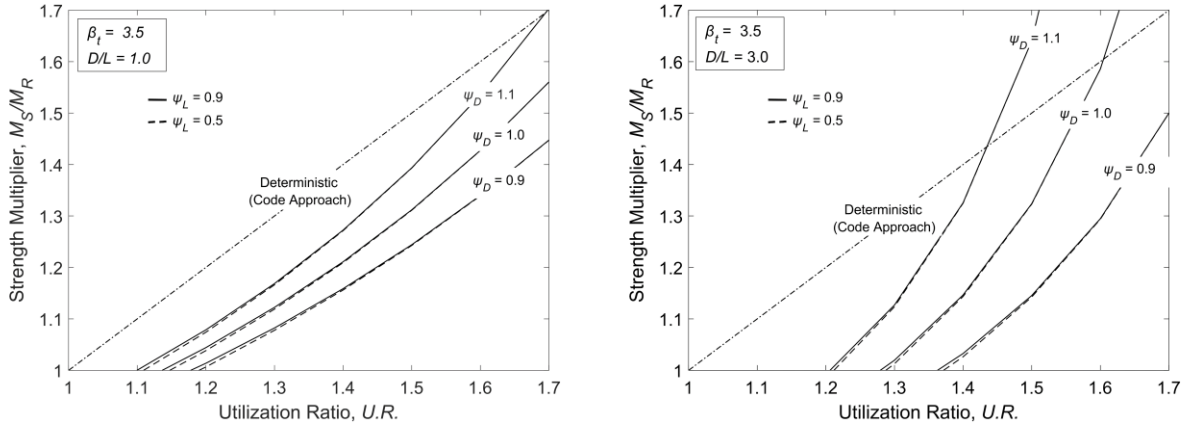

Figure 5.2. Generated sample plots of M_S/M_R versus UR for β_t= 3.5 for $D/L = [1.0, 3.0]$

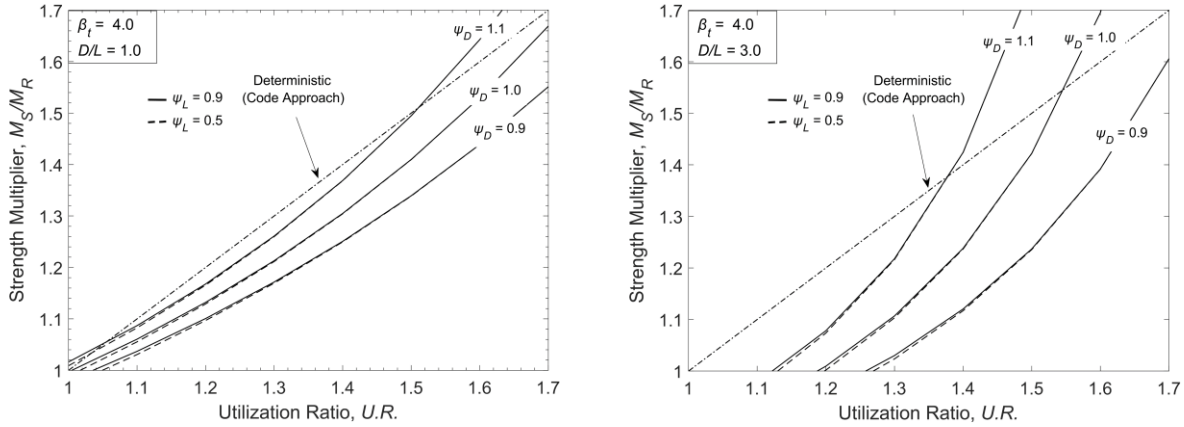

Figure 5.3. Generated sample plots of M_S/M_R versus UR for β_t = 4.0 for $D/L = [1.0, 3.0]$

5.8 DISCUSSION OF RESULTS

The various charts show that the analysis using FORM produces more non-linear results when plotting the strength multiplier, M_S/M_R, versus the unstrengthened beams utilization ratio, UR. In more than half the cases, the FORM analysis yields both more and less strengthening needed to meet the target safety index, as compared to the deterministic code approach of CSA S806:17. It can be seen for higher D/L ratios, the FORM curves become more non-linear. This causes the x-intercept to shift right, meaning the beam does not require any strengthening for utilization above unity, with curves starting as high as UR = 1.45 (See Figure 5.1b). Two general scenarios can be observed: i) times when the curve given by the FORM is below the deterministic code line for the same UR, and ii) times when the curve given by the FORM is above the deterministic code line for the same UR. The first scenario indicates times when the code's approach finds the member deficient and in need of strengthening, but the reliability-based approach finds the members capacity to be adequate for the given loads (See Figure 5.1b). The second scenario shows times, for higher UR, it is possible for the code to under-prescribe the amount of FRP needed to strengthen the section and does not meet the selected target reliability index as compared to the FORM analysis (see Figure 5.3b). It should be noted that this intersection point, where the deterministic and FORM lines intersect, varies for each set of input parameters, as shown.

Both scenarios above demonstrate that the S806 code is not sensitive to taking into account the load type and history of an existing building during assessment, and may give costly, over-conservative designs due to this. It was found that as the selected target reliability index increases, the value of the x-intercept of the design line decreases (i.e., the value of UR at which repair is first needed decreases with increasing β_t). This trend shows that choosing a higher target reliability index to meet for assessment of the deficient existing beam, means the code will find some beams

deficient when they may not be. Moreover, for deficient beams with utilization close to unity, the code approach will give highly conservative designs, meaning the amount of FRP prescribed for strengthening. Finally, the effect of ratio of measured-to-design live load experienced, ψ_L, does not affect the results significantly for any set of input parameters as shown, and thus, can be neglected.

5.9 DESIGN EXAMPLE: EB FRP STRENGTHENED RC BEAM

An example is presented to show how this framework can be applied. A strengthened simply supported rectangular RC beam designed as per S806:17 will be examined. The beam is a typical interior beam of a multistory RC building in Canada. The beam is cast-in-place and supports pre-cast double tees that sit on top to make up the floor system, having a span of 8.0 m and a tributary width of 3.5 m. The beam itself has dimensions of 300 mm x 400 mm, with the area of internal steel, $As = 1095\,mm^2$, and a depth to internal tensile rebar, $d = 365\,mm$. The material strength of the concrete and steel is 35 MPa and 400 MPa, respectively. The building is part of an ongoing structural health monitoring program, in which measurements have been taken, so that the load type and history of the structure can be known. It is reported that the live load used in design is $LL = 2.4\,kPa$, the ratio of dead-to-live load is $D/L = 1.0$, the ratio of measured-to-design live load is ψ_L= 1.0, the ratio of measured-to-design dead load is ψ_D = 0.9. A target reliability index of $\beta_t = 3.5$ is selected for assessment purposes.

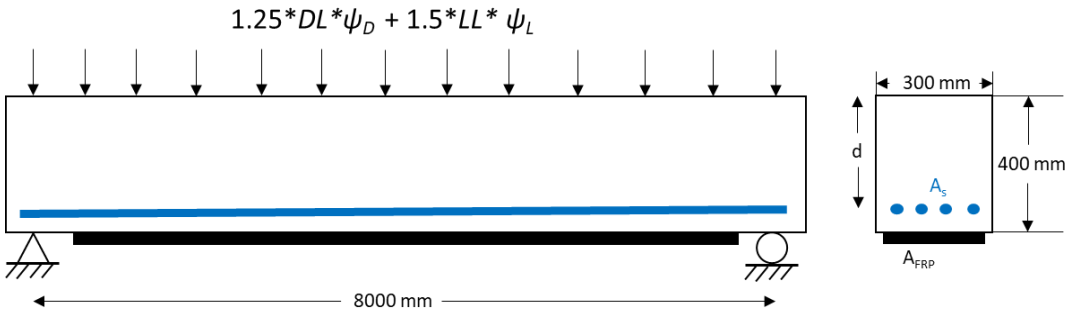

Figure 5.4. EB FRP Strengthened RC beam designed as per CSA S806:17.

Using the provisions of the CSA S806:17 standard and the governing load combinations from the NBCC 2015 ($1.25D + 1.5L$), it was found that the factored moment resistance of the section is M_r = 122 kNm and the factored demand on the beam is $M_f = 175\ kNm$. This means that the beam is deficient, with a utilization ratio of $UR = 1.43$. Using Figure 5.2b (presented in Section 5.7 of this chapter), the optimized strength multiplier, M_S/M_R, is found for the given input parameters. It was found using the reliability method, the strength multiplier needed is $M_S/M_R = 1.18$ (see Figure 5.5). Conversely, applying the deterministic CSA S806:17 approach yields a strength multiplier of $M_S/M_R = 1.43$. The calibration of the resistance and load factors in current codes are conducted to ensure that a design meets a pre-determined target safety level (Allen 1975). Code calibration is conducted for new construction and does not consider that the structure is service proven for a certain portion of the design loads. The resulting design becomes over-conservative for the amount of FRP needed for repair, as shown by the difference in strength multiplier found.

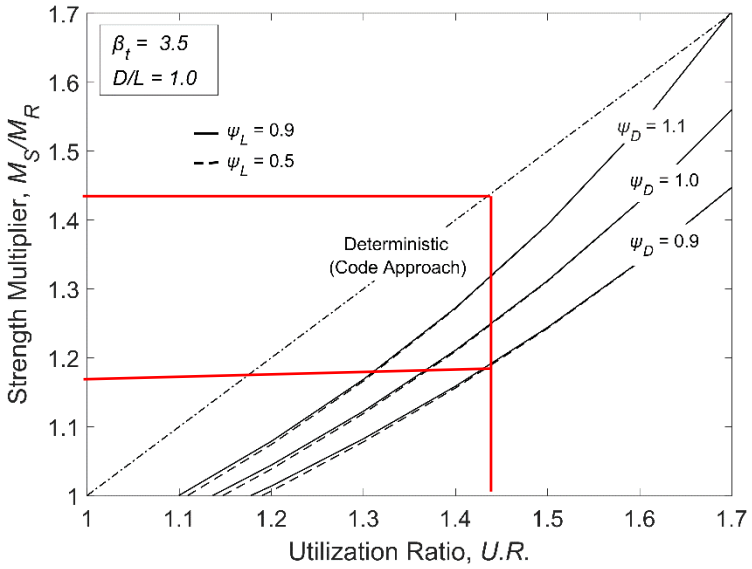

Figure. 5.5. Strengthening chart: M_S/M_R versus UR for $\beta_t = 3.5$ and $D/L = 1.0$.

Carbon fiber-reinforced polymer (CFRP) is used for repair. A common, industry found type of CFRP composite will be used, having properties of one-layer thickness, t_{frp}, equal to 0.33 mm, a modulus of elasticity, E_{frp}, equal to 227 GPa and an ultimate strength, f_{frp}, equal to 3,800 MPa. The number of FRP layers needed to meet the selected reliability is calculated by multiplying the value of M_S/M_R found, by the unstrengthened moment resistance, M_R, to get the required strengthened moment resistance, M_S. Results show that the code approach requires 50% more material than required by FORM to achieve the code target safety limit; with the code requiring two-layers of CFRP, while the reliability analysis conducted in this research requires only one-layer of CFRP.

5.10 Conclusions

The present study introduces a framework to optimize the repair of existing RC beams deficient in flexure, with EB FRP, using load type and history to reduce the uncertainty. Review of available literature was completed to establish a database of experimental tests of beams failing in flexure

(FRP rupture or concrete crushing). Bias and COV values are obtained for the strengthened beams from the database. These values are used in combination with the load statistics used to calibrate the NBCC 2015 to preform reliability analysis. As part of the solution scheme, unstrengthened beams are evaluated based on input parameters of load history and type, to determine if they meet a predetermined target reliability index given by the code, using FORM to conduct the reliability analysis. Should the beam be deficient, an optimized strength multiplier, M_S/M_R, is calculated. This multiplier is the minimum amount of additional material needed to meet the selected target reliability index. It was found that M_S/M_R is most sensitive to input parameters of i) target reliability index β_t, ii) ratio of measure-to-design dead load, ψ_D, and iii) dead-to-live load ratio, D/L; while the effect of the ratio of measure-to-design dead load, ψ_L can be neglected. It should be noted for lower UR closer to unity, the code tends to give over-conservative amounts of FRP needed to strengthen, whereas, at higher UR, the opposite effect is found. Both trends show the poor sensitivity of the CSA S806:17 standard to parameters of load type and history.

The inclusion of load type and history into a basic reliability framework for assessing existing beams will further aid in reducing the over-conservative designs given by the CSA S806:17 design standard, in some cases, when choosing FRP as a means for external strengthening. The charts generated are derived to be compatible with the Canadian building codes (NBCC 2015; CSA S806:17) and show the proposed framework can produce safe, economical designs. Further work is needed to include the partial resistance factors in analysis by use of more robust reliability techniques, such as MCS. Furthermore, a recommendation for a larger database of experimentally tested beams, so more accurate updated reliability statistics can be calculated and used in the calibration of the design charts.

CHAPTER 6 CONCLUSIONS AND RECOMMENDATIONS

6.1 SUMMARY

With material cost still being a major factor in choosing FRP in Canada, further research into the optimization of design for strengthening members using reliability is key to furthering the competitiveness of EB FRP with conventional repair techniques in today's market. The objective of this research program was to investigate the safety of EB FRP strengthened flexural members when the existing condition of the beam prior to strengthening is considered. Two research gaps identified surrounding the existing conditions of the RC beam prior to strengthening have been chosen for investigation: i) the effect of the spatial variability of the existing concrete and the effect on the bond during debonding failure modes, and ii) the effect of considering the load history of the beam on the strengthened reliability. No consideration of these existing conditions prior to strengthening is stipulated by a clause in the North American FRP design standards such as the CSA S806:17, CSA S6:19, and ACI440.2R:17.

The project was undertaken in four phases: i) literature review to identify research gaps and collect relevant statistics (bias, COV, and distribution type) of the random variables used in reliability analysis; ii) investigate the effect of considering the spatial variability of the concrete strength and its effect on the strengthened reliability when subject to IFC debonding using SFE-MCS; iii) investigate the effect of active-learning kriging (AK) reliability framework on optimizing the computational cost of assessing the strengthened beam reliability, and iv) investigate the effect of considering the load type and history of the unstrengthened beam on the strengthened reliability. Each phase is a chapter within the thesis and each chapter is written as a standalone research paper.

All frameworks of analysis developed are to assess the reliability of the strengthened beam given the identified existing conditions have been developed to investigate the optimization of the design of flexural EB FRP upgrades. Stochastic FE has been used to capture the spatial variation in the concrete. Due to the computational burden of SFE simulation, active-learning kriging (AK) metamodeling technique has been implemented to investigate if a reduction in the number of SFE models is possible. A total of 4,066 stochastic FE strengthened beam models have been generated and evaluated to establish the resistance statistics using the proposed interface. The principals of conditional probability are used to update the reliability of the unstrengthened beam considered load history.

It should be noted that this work has examined a limited number of strengthened beam configurations. The results and recommendations given are for the beams considered in the study and may not be applicable to other geometries or strengthening configurations.

6.2 CONCLUSIONS

The following thesis is a paper-based work with Chapter 2, 3, 4, and 5 being stand alone research papers. The research gaps identified in the literature review of Chapter 2 are provided in Section 2.6 and propose several research directions based on the identified gaps. The following summarizes the major findings of Chapter 3, 4, and 5 (the reader is referred to the respective chapters' conclusion sections for the detailed findings of the research):

6.2.1 Chapter 3 – Stochastic FE MCS Analysis:

- The use of stochastic FE to capture the spatial variability in the concrete volume of an RC beam is feasible through an LSDYNA-Python-MATLAB interface. Analysis results

indicated a minor impact of varying the stochastic input parameters (correlation length and stochastic mesh density) and the material input parameters (coefficient of variation of concrete) on the reliability index evaluated using MC simulation.

- Results of considering the spatial variability of the concrete and bond strength show little change in the safety of the strengthened beams when the spatial variability of the concrete increased (i.e., increased coefficient of variation due to poor quality concrete quality or degradation) for tension-controlled sections. A more significant effect was reported for compression-controlled sections. The more prevalent change in reliability is seen between the chosen design standard used for designing the member. The design standards considered showed large reliability index values for all sample beams.
- The use of the random field to capture the spatial variability of the concrete needs to be properly calibrated through experimental work to recommend a suitable range for the autocorrelation lengths. In this work, a constant correlation length was used in all directions but may not be necessarily representative of the true spatial variability in a concrete volume.
- Parametric analysis of the stochastic inputs shows an increase in computational burden when a finer stochastic mesh is used but may be needed to ensure proper propagation of the cracks in the concrete to initiate debonding. An optimal stochastic configuration is one that will balance computational cost with a practical range of autocorrelation lengths, SEM/EM ratio, and the number of terms kept in the truncation of the eigenvalues/vectors when producing the random field.
- The larger issue highlighted in this work is the conservative nature of the North American FRP design standards when prescribing EB FRP upgrades. The codes are producing

beams that have high-reliability index values in most designs (compression- and tension-controlled). Increasing the strain limit prescribed by codes shows little effect on reducing these bias values, indicating other factors compounding the conservatism that needs to be understood. One indication of this is the fact of the ACI 440.2R using a range of member reduction factors, depending on the ductility of the member determined based on the strain in the internal rebar, saw the largest range of reliability index values for the beams considered. Investigation into the possible reasons for the conservatism is needed and re-calibration of the material and overall strength reduction factors should be done to account for these factors when strengthening flexural members using EB FRP.

6.2.2 Chapter 4 – Stochastic FE-AK-MCS Analysis:

- Comparing the two reliability frameworks considered (SFE-MCS and AK-SFE-MCS) shows that the AK framework requires more calibration to be representative. Convergence was achieved using the AK framework in fewer calls than the SFE model but did not yield matching reliability index values. This could be due to the combination of regression and correlation function used to train the kriging predictor. Other studies have shown the accuracy of the AK method is affected by the choice of AK configuration (Buckley et al. 2020).
- The computer available in this work can run up to 10 SFE models in parallel in LS-DYNA. This allowed 9 simulations to be run in parallel for the SFE-MCS analysis in chapter 3. Compared to the clustering AK method which limits the number of parallel simulations to the number of clusters for each enrichment iteration means that the SFE-MCS method can run more SFE simulations than the AK-SFE-MCS method for the same

timeframe. This savings in time may offset the reduction in calls to the SFE model by the AK once the AK configuration is properly calibrated.

6.2.3 Chapter 5 – Application of Conditional Probability Analysis:

- The inclusion of load type and history into a reliability framework for assessing existing beams further aids in reducing the over-conservative designs given by the CSA S806:17 design standard, in some cases, when choosing FRP as a means for external strengthening. This is due to accounting for the load history of the existing member can improve the reliability of the unstrengthened member by truncating the uncertainty in the design loads.
- Design charts accounting for load history show instances where the CSA S806:17 standard is both conservative and un-conservative in the amount EB FRP prescribed for strengthening, showing a general insensitivity to design parameters.

6.3 RECOMMENDED FUTURE RESEARCH

The following are recommended future research directions based on the work done in this thesis:

1. Consideration of a larger design space of beams for the reliability analysis including a wide range of geometries and material properties.
2. Investigation into the source of the high bias given by the codes for the ultimate moment resistance. Re-calibration of the resistance factors is recommended for all codes to account for the effect of the addition of the EB FRP.
3. Investigation into the stochastic parameters that make up the random field (correlation length, correlation function, SEM density, SEM/EM ratio, truncation value).

Calibration of experimental work to recommend a practical range of autocorrelation lengths to yield representative fields of the degraded concrete volume spatially.

4. Investigation into the role of both EM and SEM mesh density in the propagation of cracks in the SFE model as this is integral to understanding IFC debonding failure modes.
5. Parametric analysis of the different AK configurations to recommend an optimal configuration based on an accurate and efficient solution.
6. Investigation into the use of clustering using a different number of clusters into the efficiency of the AK method is recommended as the parallelization saw the most gains in reducing the time of computation.
7. Expansion of Chapter 5 to include all design standards and provide a complete set of load history based design aids for all North American FRP design codes.
8. Incorporation of both the load history and spatial variability into a single robust framework considering the existing conditions of the member and the combined effect on the strengthened reliability after application of EB FRP.

BIBLIOGRAPHY

AASHTO. (2004). “LRFD bridge design specifications” American Association of State Highway and Transportation Officials, Washington, DC.

Alabdulhady, M. Y., and Sneed, L. H. (2019). “Torsional strengthening of reinforced concrete beams with externally bonded composites: A state of the art review.” *Construction and Building Materials*, Elsevier Ltd, 205, 148–163.

ACI 318, Building Code Requirements for Structural Concrete. (2019). Farmington Hills, MI: American Concrete Institute.

ACI 440.2R, Guide for the Design and Construction of Structural Concrete Reinforced with Fiber-Reinforced Polymer (FRP) Bars. (2017). Farmington Hills, MI: American Concrete Institute.

Ali, O. (2017). “Structural reliability of biaxial loaded Short/Slender-Square FRP-confined RC columns.” *Construction and Building Materials*, 151, 370–382.

Ali, O., Bigaud, D., and Ferrier, E. (2012). “Comparative durability analysis of CFRP-strengthened RC highway bridges.” *Construction and Building Materials*, 30, 629–642.

Ali, O., Bigaud, D., and Riahi, H. (2018). “Seismic performance of reinforced concrete frame structures strengthened with FRP laminates using a reliability-based advanced approach.” *Composites Part B: Engineering*, 139 (November 2017), 238–248.

Almusallam, T. H., Elsanadedy, H. M., and Al-Salloum, Y. A. (2015). “Effect of Longitudinal Steel Ratio on Behavior of RC Beams Strengthened with FRP Composites: Experimental and FE Study.” *Journal of Composites for Construction*, 19(1), 04014028.

Alsayed, S. H., and Siddiqui, N. A. (2013). “Reliability of shear-deficient RC beams strengthened with CFRP-strips.” *Construction and Building Materials*, 42, 238–247.

Andrieu-Renaud C, Sudret B, Lemaire M. (2004) "The PHI2 method: a way to compute time-

variant reliability." *Reliability Engineering and Systems Safety*, 84:75‑86.

Atadero, R. A., and Karbhari, V. M. (2008). “Calibration of resistance factors for reliability based design of externally-bonded FRP composites.” *Composites Part B: Engineering*, 39(4), 665–679.

Atadero, R., Lee, L., and Karbhari, V. M. (2005). “Consideration of material variability in reliability analysis of FRP strengthened bridge decks.” *Composite Structures*, 70(4), 430–443.

Aurenhammer, F. (1991). “Voronoi Diagrams - A Survey of a Fundamental Data Structure.” *ACM Computing Surveys (CSUR)*, 23(3), 345–405.

Bagheri, M., Chahkandi, A., and Jahangir, H. (2019). “Seismic Reliability Analysis of RC Frames Rehabilitated by Glass Fiber-Reinforced Polymers.” *International Journal of Civil Engineering*, 17(11), 1785–1797.

Baji, H., Ronagh, H. R., and Li, C. Q. (2016). “Probabilistic Design Models for Ultimate Strength and Strain of FRP-Confined Concrete.” *Journal of Composites for Construction*, 20(6).

Bakis, C. E., Bank, L. C., Brown, V. L., Cosenza, E., Davalos, J. F., Lesko, J. J., Machida, A., Rizkalla, S. H., and Triantafillou, T. C. (2002). “Fiber-reinforced polymer composites for construction - State-of-the-art review.” *Journal of Composites for Construction*, 6(2), 73–87.

Bartlett, Michael, Hong, Han Ping, and Zhou, Wenxing, (2003a), “Load factor calibration for the proposed 2005 edition of the National Building Code of Canada: statistics of loads and load effects", Canadian Journal of Civil Engineering, Vol. 30, No. 2, pp. 429-439.

Bartlett, Michael, Hong, Han Ping, and Zhou, Wenxing, (2003b), “Load factor calibration for the proposed 2005 edition of the National Building Code of Canada: companion-action load combinations", Canadian Journal of Civil Engineering, Vol. 30, No. 2, pp. 440-448.

BIBLIOGRAPHY

Bharil, R. K. (2020). “Time-Dependent Reliability Framework for Durability Design of FRP Composites.”

Bigaud, D., and Ali, O. (2014). “Time-variant flexural reliability of RC beams with externally bonded CFRP under combined fatigue-corrosion actions.” *Reliability Engineering and System Safety*, 131, 257–270.

Buckley, E., Khorramian, K., and Oudah, F. (2021). “Application of adaptive kriging method in bridge reliability analysis.” *CSCE 2021 Annual Conference Inspired*, (May), 1–8. (Virtual Conference).

Bukhari, I. A., Vollum, R., Ahmad, S., and Sagaseta, J. (2013). “Shear Strengthening of Short Span Reinforced Concrete Beams with CFRP Sheets.” *Arabian Journal for Science and Engineering*, 38(3), 523–536.

Castaldo, P., Gino, D., and Mancini, G. (2019). “Safety formats for non-linear finite element analysis of reinforced concrete structures: discussion, comparison and proposals.” *Engineering Structures*, Elsevier, 193(May), 136–153.

Chen, J. F., and Teng, J. G. (2003). “Shear capacity of FRP-strengthened RC beams: FRP debonding.” *Construction and Building Materials*, 17(1), 27–41.

CSA S806, Design, and construction of building structures with fibre-reinforced polymers. (2012); Re-approved (2017). Mississauga (Ontario): Canadian Standards Association.

CSA S6, Canadian Highway Bridge Design Code. (2019). Canadian Standards Association, Mississauga, Ontario.

CSA A23.3/A23.4 (2019), Concrete materials and methods of concrete construction/Test methods and standard practices for concrete, Mississauga (Ontario): Canadian Standards Association.

D’Antino, T., Sneed, L. H., Carloni, C., and Pellegrino, C. (2016). “Effect of the inherent

eccentricity in single-lap direct-shear tests of PBO FRCM-concrete joints." *Composite Structures*, Elsevier Ltd, 142, 117–129.

Dehghani, H., and Fadaee, M. J. (2014). "Probabilistic assessment of torsion in concrete beams externally strengthened with CFRP composites." *Materials and Structures/Materiaux et Constructions*, 47(5), 885–894.

Deniaud, C., and Cheng, J. J. R. (2001). "Review of shear design methods for reinforced concrete beams strengthened with fibre reinforced polymer sheets." *Canadian Journal of Civil Engineering*, 28(2), 271–281.

Dias-da-Costa, D., Neves, L. A. C., Gomes, S., Hadigheh, S. A., and Fernandes, P. (2019). "Time-dependent reliability analyses of prestressed concrete girders strengthened with CFRP laminates." *Engineering Structures*, Elsevier, 196(February), 109297.

Diez, C. (2018). "Build your own LD-DYNA Tools Quickly in Python," In the proceedings of the *15th international LS-DYNA Users Conference* 2018.

Echard, B., Gayton, N., and Lemaire, M. (2011). "AK-MCS: An active learning reliability method combining Kriging and Monte Carlo Simulation." *Structural Safety*, Elsevier Ltd, 33(2), 145–154.

Ellingwood, B., Galambos, T. V, MacGregor, J. G., and Cornell, C. A. (1980). *Development of a Probability Based Load Criterion for American National Standard A58 - Report 577. NBS Special Pulication 577*.

Ellingwood, B. R. (2003). "Toward load and resistance factor design for fiber-reinforced polymer composite structures." *Journal of Structural Engineering*, 129(4), 449–458.

Elsanadedy, H. M., Almusallam, T. H., Alsayed, S. H., and Al-Salloum, Y. A. (2013). "Flexural strengthening of RC beams using textile reinforced mortar - Experimental and numerical

study.” *Composite Structures*, Elsevier Ltd, 97, 40–55.

Firouzi, A., Taki, A., and Mohammadzadeh, S. (2019). “Time-dependent reliability analysis of RC beams shear and flexural strengthened with CFRP subjected to harsh environmental deteriorations.” *Engineering Structures*, 196 (June), 109326.

El Haj, A. K., and Soubra, A. H. (2020). “Efficient estimation of the failure probability of a monopile foundation using a Kriging-based approach with multi-point enrichment.” *Computers and Geotechnics*, Elsevier, 121(November 2019), 103451.

Hao, H., Li, Z.-X., and Shi, Y. (2016). “Reliability Analysis of RC Columns and Frame with FRP Strengthening Subjected to Explosive Loads.” *Journal of Performance of Constructed Facilities*, 30(2).

Hasofer, A.M., and N.C. Lind. (1974). “An Exact and Invariant First Order Reliability Format.” *Journal Eng. Mech. Division (ASCE)* 100 (July): 111–21.

Helton, J. C., and Davis, F. J. (2003). “Latin hypercube sampling and the propagation of uncertainty in analyses of complex systems.” *Reliability Engineering and System Safety*, 81, 23–69.

Hong, H. P. (1998). “Reliability of existing structures.” *Civil Engineering and Environmental Systems*, 15(3), 187–206.

Hong, H. P., and Lind, N. C. (1991). “Proof load test levels by exact integration.” *Canadian journal of civil engineering*, 18(2), 297–302.

Huang, L., Gao, C., Yan, L., Kasal, B., and Ma, G. (2016). "Reliability assessment of confinement models of carbon fiber reinforced polymer-confined concrete." *Journal of Reinforced Plastics and Composites*.

Huang, X., Sui, L., Xing, F., Zhou, Y., and Wu, Y. (2019). “Reliability assessment for flexural

FRP-Strengthened reinforced concrete beams based on Importance Sampling." *Composites Part B: Engineering*, Elsevier, 156(August 2018), 378–398.

Huang, X., Zhou, Y., Xing, F., Wu, Y., Sui, L., and Han, N. (2020). "Reliability-based design of FRP flexural strengthened reinforced concrete beams: Guidelines assessment and calibration." *Engineering Structures*, 209 (October 2019).

ISO 13822:2010, Bases for Design of Structures – Assessment of Existing Structures. (2010). International Organization for standardization.

J. Chen, and Teng. (2001). "Anchorage strength models for frp and steel plates bonded to concrete." *Journal of Structural Engineering*, 127(c), 784–791.

Kalfat, R., Al-Mahaidi, R., and Smith, S. T. (2013). "Anchorage devices used to improve the performance of reinforced concrete beams retrofitted with FRP composites: State-of-the-art review." *Journal of Composites for Construction*, 17(1), 14–33.

Kalfat, R., Gadd, J., Al-Mahaidi, R., and Smith, S. T. (2018). "An efficiency framework for anchorage devices used to enhance the performance of FRP strengthened RC members." *Construction and Building Materials*, Elsevier Ltd, 191, 354–375.

Kaymaz, I. (2005). "Application of kriging method to structural reliability problems." *Structural Safety*, 27(2), 133–151.

Khalifa, A., Gold, W. J., Nanni, A., and M.I., A. A. (1998). "Contribution of Externally Bonded FRP to Shear Capacity of RC Flexural Members." *Journal of Composites for Construction*, 2(4), 195–202.

Khalifa, A., and Nanni, A. (2002). "Rehabilitation of rectangular simply supported RC beams with shear deficiencies using CFRP composites." *Construction and Building Materials*, 16, 135–146.

Khorramian, K., Alhashmi, A.E., and Oudah, F. (2022). "Effect of random fields in stochastic FEM on the structural reliability assessment of pile groups in soil." *Canadian Society of Civil Engineering Annual Structural Specialty Conference (CSCE 2022)*, Whistler, BC, Canada, May 25th to 27th.

Khorramian, K. and Oudah, F., (2022). "Active Learning Kriging-Based Reliability for Assessing the Safety of Structures: Theory and Application." In: *Leveraging Artificial intelligence into Engineering, Management, and Safety of Infrastructure.* s.l.:Taylor and Francis (CRC), p. (Accepted).

Khorramian, K., Oudah, F., Sadeghian, P. (2019). Calibration of reduction factor for concrete columns strengthened with unidirectional fiber-reinforced wrapping. *The 14th Conference on Fiber Reinforced Polymer for Reinforced Concrete Structures (FRPRCS 14)*, Queen's University, Belfast, UK, June 4-7th.

Kroetz, H. M., Moustapha, M., Beck, A. T., and Sudret, B. (2020). "A Two-Level Kriging-Based Approach with Active Learning for Solving Time-Variant Risk Optimization Problems." *Reliability Engineering and System Safety*, Elsevier Ltd, 203(April), 107033.

Lophaven, S. N., Nielsen, H. B. and Søndergaard, J., (2002). "A Matlab Kriging Toolbox," *Technical Report No. IMM-TR-2002-12.* s.l.: Technical University of Denmark, Kongens Lyngby.

Lophaven, S. N., Nielsen, H. B. and Søndergaard, J., (2002). "DACE: a Matlab kriging toolbox." *Vol. 2. IMM Informatics and Mathematical Modelling*. The Technical University of Denmark, pp. 1-34.

Lelièvre, N., Beaurepaire, P., Mattrand, C., and Gayton, N. (2018). "AK-MCSi: A Kriging-based method to deal with small failure probabilities and time-consuming models." *Structural*

Safety, 73, 1–11.

Li, C., and Der-Kiureghian, A. (1993). “Optimal discretization of random fields.” *ASCE-ASME Journal of Mechanical Engineering*, 119(6), 1136–1154.

Li, Y., Liu, K., Zhang, B., and Xu, N. (2020). “Reliability of Shape Factors for Bearing Capacity of Square Footings on Spatially Varying Cohesive Soils.” *International Journal of Geomechanics*, 20(3), 1–13.

Liang, H., Li, S., Lu, Y., and Yang, T. (2018). “Reliability analysis of bond behaviour of CFRP-Concrete interface under wet-dry cycles.” *Materials*, 11(5).

Lu, X. Z., Teng, J. G., Ye, L. P., and Jiang, J. J. (2005). “Bond-slip models for FRP sheets/plates bonded to concrete.” *Engineering Structures*, 27(6), 920–937.

Madsen H, Tvedt L. (1990). “Methods for time-dependent reliability and sensitivity analysis.” *Journal of Engineering Mechanics*, 116(10):2118‑35.

Mahdavipour, M. A., Eslami, A., and Jehel, P. (2020). “Seismic evaluation of ordinary RC buildings retrofitted with externally bonded FRPs using a reliability-based approach.” *Composite Structures*, 232 (October 2019).

Melchers, R. (1989). "Importance sampling in structural systems." *Structural Safety*, 6, 3-10.

Melchers, R. (1992). "Load-space formulation for time-dependent structural reliability." *Journal of Engineering Mechanics*, 118(5):853‑70.

Melchers, R., Beck A., (2018). Structural reliability analysis and prediction. John Wiley and Sons.

Monti, G., and Liotta, M. (2007). “Tests and design equations for FRP-strengthening in shear.” *Construction and Building Materials*, 21(4), 799–809.

Monti, G., and Santini, S. (2002). “Reliability-based calibration of partial safety coefficients for fiber-reinforced plastic.” *Journal of Composites for Construction*, 6(3), 162–167.

Narváez, N. S., Rojas, N. R., and Evangelista, F. (2020). “Reliability analyses of shear strengthened RC beams with externally bonded fiber reinforced polymer.” *Materials and Structures/Materiaux et Constructions*, 53(2).

Nataf, A. (1962). "Determination des distribution dont les marges sont donnees." *Comptes Rendus de l'Academie des Sciences,* Volume 225, pp. 42-43.

NBCC, National building code of Canada. (2015). Ottawa (Ontario): National Research Council.

Neale, K. W., Ebead, U., Abdel Baky, H., Elsayed, W., and Godat, A. (2005). “Modelling of Debonding Phenomena in FRP-Strengthened Concrete Beams and Slabs.” *Proceedings of the International Symposium on Bond Behaviour of FRP in Structures (BBFS 2005)*, (Bbfs), 10.

Noël, M. (2019). “Special Issue 4th Brazilian Conference on Composite Materials (2018) Probabilistic fatigue life modelling of FRP composites for construction.” *Construction and Building Materials*, 206, 279–286.

Nowak, A., and Collins, K. (2000). *Reliability of Structures by Nowak and Collins.pdf*. The McGraw-Hill Companies.

Nowak, A. S., Nowak, S., and Szerszen, M. M. (2003). “Calibration of design code for buildings (ACI 318): Part 1 - Statistical models for resistance.” *ACI Structural Journal*, 100(3), 377–382.

Okeil, A. M., Belarbi, A., and Kuchma, D. A. (2013). “Reliability assessment of FRP-strengthened concrete bridge girders in shear.” *Journal of Composites for Construction*, 17(1), 91–100.

Okeil, A. M., El-Tawil, S., and Shahawy, M. (2002). “Flexural reliability of reinforced concrete bridge girders strengthened with carbon fiber-reinforced polymer laminates.” *Journal of Bridge Engineering*, 7(5), 290–299.

Oudah, F., and Alhashmi, A. (2022). “Time-dependent reliability analysis of degrading structural

elements using stochastic fe and lstm learning." *Canadian Society of Civil Engineering Annual Structural Specialty Conference (CSCE 2022)*, Whistler, BC, Canada, May 25th to 27th.

Oudah, F. and El-Hacha, R. (2014). Seismic evaluation of concrete buildings reinforced using FRP – Capacity spectrum method. *The 7th International Conference on FRP Composites in Civil Engineering (CICE)*, Vancouver, Canada, August 20-22.

Oudah, F. and Hassan, A. (2022). "Reliability of compression controlled FRP RC flexural members designed using North American codes and standards: Comparison and FRP material resistance/strength reduction factor calibration." *ACI Special Publications*. (Accepted)

Pellegrino, C., and Modena, C. (2008). "An experimentally based analytical model for the shear capacity of FRP-strengthened reinforced concrete beams." *Mechanics of Composite Materials*, 44(3), 231–245.

Peng, F., and Xue, W. (2019). "Reliability-based design provisions for flexural strength of fiber-reinforced polymer prestressed concrete bridge girders." *ACI Structural Journal*, 116(1), 251–260.

Petrie, C. and Oudah, F. (2021). "Examining the effect of load type and history using reliability on optimizing the design of FRP strengthened RC members in flexure." *In 8th International Conference on Advanced Composite Materials in Bridges and Structures (ACMBC 2021)*, Sherbrooke, Quebec, Canada August 5-7, 2021.

Plevris, B. N., Member, S., Triantafillou, T. C., Veneziano, D., and Member, A. (1995). "Reliability of rc members strengthened with cfrp laminates" 121 (July), 1037–1044.

Poli, R., Kennedy, J., and Blackwell, T. (2007). "Particle swarm optimization: An overview." *Swarm Intelligence*, 1(1), 33–57.

Rackwitz R, Fiessler B. (1978). "Structural reliability under combined random load sequences." *Comput Struct*; 9(5):489–94.

Rahman, S. (2008). "A polynomial dimensional decomposition for stochastic computing." *International journal for numerical methods in engineering*, 76(July), 2091–2116.

Said, H., and Wu, Z. (2008). "Evaluating and Proposing Models of Predicting IC Debonding Failure." *Journal of Composites for Construction*, 12(June), 284–299.

Sayed, A. M., Wang, X., and Wu, Z. (2013). "Modeling of Shear Capacity of RC Beams Strengthened with FRP Sheets Based on FE Simulation." *Journal of Composites for Construction*, 17(5), 687–701.

Sendeckyj, G.P. (1981). "Fitting models to composite materials fatigue data" ASTM STP 734. 245–260.

Schöbi, R., Sudret, B., and Marelli, S. (2017). "Rare Event Estimation Using Polynomial-Chaos Kriging." *ASCE-ASME Journal of Risk and Uncertainty in Engineering Systems, Part A: Civil Engineering*, 3(2), 1–12.

Shahriari, S., and Naderpour, H. (2020). "Reliability assessment of shear-deficient reinforced concrete beams externally bonded by FRP sheets having different configurations." *Structures*, 25(March), 730–742.

Shi, J., Wu, Z., Wang, X., and Noori, M. (2015). "Reliability analysis of intermediate crack-induced debonding failure in FRP-strengthened concrete members." *Structure and Infrastructure Engineering*, 11(12), 1651–1671.

Smith, S. T., and Teng, J. G. (2002a). "FRP-strengthened RC beams. I: Assessment of debonding strength models." *Engineering Structures*, 24(4), 397–417.

Smith, S. T., and Teng, J. G. (2002b). "FRP-strengthened RC beams. II: Assessment of debonding

strength models." *Engineering Structures*, 24(2), 397–417.

Souza, O. L. D. C., Sánchez Filho, E. D. S., Vaz, L. E., and Silva Filho, J. J. H. (2013). "Reliability analysis of RC beams strengthened for torsion with carbon fibre composites." *Structural Concrete*, 15(1), 38–44.

Stefanou, G. (2009). "The stochastic finite element method: Past, present and future." *Computer Methods in Applied Mechanics and Engineering*, Elsevier B.V., 198(9–12), 1031–1051.

Sudret, B., and Der-Kiureghian, A. Der. (2000). "Stochastic Finite Elements and Reliability - A state-of-the-art report". Univ. of California, Berkeley, CA: Dept. of Civil and Environmental Engineering.

Sudret B. (2008). "Analytical derivation of the outcrossing rate in time-variant reliability problems." *Structure and Infrastructure Engineering,* 4(5):353‑62.

Taki, A., Firouzi, A., and Mohammadzadeh, S. (2018). "Life cycle reliability assessment of reinforced concrete beams shear-strengthened with carbon fiber reinforced polymer strips in accordance with fib bulletin 14." *Structural Concrete*, 19(6), 2017–2028.

Täljsten, B. (2003). "Strengthening concrete beams for shear with CFRP sheets." *Construction and Building Materials*, 17(1), 15–26.

Tanarslan, H. M., and Altin, S. (2010). "Behavior of RC T-section beams strengthened with CFRP strips, subjected to cyclic load." *Materials and Structures/Materiaux et Constructions*, 43(4), 529–542.

Triantafillou, T., and Antonopoulos, C. (2000). "Design of concrete flexural members strengthened in shear with FRP." *ASCE Journal of Materials in Civil Engineering*, 11(4), 325–330.

Triantafillou, T. C. (1998). "Shear strengthening of reinforced concrete beams using epoxy-bonded

FRP composites." *ACI Structural Journal*, 95(2), 107–115.

Val, D. V. (2003). "Reliability of fiber-reinforced polymer-confined reinforced concrete columns." *Journal of Structural Engineering*, 129(8), 1122–1130.

Wang, N., and Ellingwood, B. R. (2015). "Limit state design criteria for FRP strengthening of RC bridge components." *Structural Safety*, 56, 1–8.

Wang, N., Ellingwood, B. R., and Zureick, A. (2010). "Reliability-Based Evaluation of Flexural Members Strengthened with Externally Bonded Fiber-Reinforced Polymer Composites." *Journal of Structural Engineering*, 136(September), 1151–1160.

Wen, Y., and Chen, H. (1987). "On fast integration for time variant structural reliability." *Probability Engineering Mechanics*, 2(3):156-162.

Wieghaus, K. T., and Atadero, R. A. (2011). "Effect of existing structure and FRP uncertainties on the reliability of FRP-based repair." *Journal of Composites for Construction*, 15(4), 635–643.

Wu, Z., and Niu, H. (2007). "Prediction of Crack-Induced Debonding Failure in R/C Structures Flexurally Strengthened With Externally Bonded Frp Composites." *JSCE Journal of Materials, Concrete Structures and Pavements*, 63(4), 620–639.

Wu, Z., Wang, X., Zhao, X., and Noori, M. (2014). "State-of-the-art review of FRP composites for major construction with high performance and longevity." *International Journal of Sustainable Materials and Structural Systems*, 1(3), 201.

Xiao-ling, Z., Bo-han, J., Yan, H., Shong-loong, C., and Xiu-yu, L. (2021). "Random field model of soil parameters and the application in reliability analysis of laterally loaded pile." *Soil Dynamics and Earthquake Engineering*, Elsevier Ltd, 147(March), 106821.

Yang, D. Y., Frangopol, D. M., and Teng, J. G. (2019). "Probabilistic life-cycle optimization of

durability-enhancing maintenance actions: Application to FRP strengthening planning." *Engineering Structures*, 188(February), 340–349.

Zhang, A. H., Jin, W. L., and Li, G. B. (2006). "Behavior of preloaded RC beams strengthened with CFRP laminates." *Journal of Zhejiang University: Science*, 7(3), 436–444.

Zhang, Z., and Hsu, C.-T. T. (2005). "Shear Strengthening of Reinforced Concrete Beams Using Carbon-Fiber-Reinforced Polymer Laminates." *Journal of Composites for Construction*, 9(2), 158–169.

Zhou, Y., Zhang, J., Li, W., Hu, B., and Huang, X. (2020). "Reliability-based design analysis of FRP shear strengthened reinforced concrete beams considering different FRP configurations." *Composite Structures*, Elsevier, 237(October 2019), 111957.

Zou, X., Wang, Q., and Wu, J. (2018). "Reliability-based performance design optimization for seismic retrofit of reinforced concrete buildings with fiber-reinforced polymer composites." *Advances in Structural Engineering*, 21(6), 838–851.

Zou, Y., and Hong, H. P. (2011). "Reliability assessment of FRP-confined concrete columns designed for buildings." *Structure and Infrastructure Engineering*, 7(3), 243–258.

APPENDIX A: MOMENT RESISTANCE DESIGN EQUATIONS FOR CSA AND ACI CODES

A.1 Design Equations for the Ultimate Moment Resistance as per the CSA Design Standards.

$$R = M_r = C_s(\frac{\beta_1 c}{2} - d') + \sum_{i=1}^{N} T_i \left(d_i - \frac{\beta_1 c}{2}\right) + T_f(h - \frac{\beta_1 c}{2})$$

$Where,$

$$T_{fi} = \phi_f A_{fi} E_{frp} \varepsilon_{fi}; \quad \varepsilon_{frp} = \varepsilon_{frpu} \leq \varepsilon_{FRPt}$$

$$T_{si} = \phi_s A_{si} f_{si}; \quad f_{si} = \varepsilon_{si} E_s \leq f_y$$

$$C_s = \phi_s A'_{si} f'_{si}; \quad f'_{si} = \varepsilon_{si} E_s \leq f_y$$

$$\beta_1 = 0.97 - 0.0025 f'_c \geq 0.65$$

A.2 Design Equations for the Ultimate Moment Resistance per ACI440.2R Design Standards.

$$\phi R = \phi M_n = \phi[C_s(\frac{\beta_1 c}{2} - d') + \sum_{i=1}^{N} T_i \left(d_i - \frac{\beta_1 c}{2}\right) + T_{frp}(d_{frp} - \frac{\beta_1 c}{2})]$$

$$T_{fi} = \Psi_{frp} A_{fi} E_f \varepsilon_{fe_i}; \quad \varepsilon_{fi} = \varepsilon_{fe} \leq \varepsilon_{fd}$$

$$T_{si} = A_{si} f_{si}; \quad f_{si} = \varepsilon_{si} E_s \leq f_y$$

$$C_s = A'_{si} f'_{si}; \quad f'_{si} = \varepsilon_{si} E_s \leq f_y$$

$$\beta_1 = 0.97 - 0.0025 f'_c \geq 0.65$$

Effective Strain to mitigate debonding, ε_{fd}:

$$\varepsilon_{fd} = 0.41 \sqrt{\frac{f'_c}{n E_{frp} t_{frp}}} \leq 0.9 \varepsilon_{frpu}$$

APPENDIX B: SAMPLE CALCULATIONS OF EB FRP STRNEGHTNED BEAM TF25C01 FOR THE CSA AND ACI CODES

B.1 General Beam Information

Table B1 summarizes the strengthened beam inputs used in the calculation of the moment resistance. See Figure 3.20 for overview of the beam geometry.

Table B1. Sectional properties of strengthened beam TF25C01

Variable	Mean Value	Units
	Concrete	
b	120	mm
h	250	mm
d	225	mm
d'	25	mm
L	2500	mm
f'_c	25	MPa
	Steel	
f_y	335	MPa
A_s (T)	260	mm^2
A_s' (C)	80	mm^2
A_v	100	mm^2
E_s	200	GPa
	FRP	
f_{frpu}	3350	MPa
E_{frp}	235	GPa
t_{frp}	0.222	mm
w_{frp}	120	mm
A_{frp}	26.6	mm^2
L_{frp}	1800	mm

b = beam width; h = beam height; d = depth to extreme tensile rebar; L = length of beam; f'_c = concrete strength; f_y = steel yield strength; A_v = Area of shear rebar; E_s = modulus of elasticity of steel; f_{frpu} = FRP ultimate tensile strength; $Efrp$ = FRP modulus; t_{frp} = FRP thickness; w_{frp} = FRP width; A_{frp} = Area of FRP; L_{frp} = Length of bonded FRP

B.2 CSA S806:17 and S6:19 Ultimate Moment Resistance of EB FRP Strengthened RC Beam

CSA S806:17	CSA S6:19
• FRP Strain Limit, $\varepsilon_{frpu} = 0.007$ • $\phi_c = 0.65$ (Cl 6.5.3.2, CSA S806:17) • $\phi_s = 0.85$ (Cl 6.5.4, CSA S806:17) • $\phi_{frp} = 0.65$ (Cl 7.2.7, CSA S806:17) • $\alpha 1 = 0.85 - 0.0015(25) = 0.813$ (Cl 8.4.1.5, CSA S806:17) • $\beta_1 = 0.97 - 0.0025(25) = 0.908$ (Cl 8.4.1.5, CSA S806:17)	• FRP Strain Limit, $\varepsilon_{frpu} = 0.006$ • $\phi_c = 0.75$ (Table 8.1, CSA S6:19) • $\phi_s = 0.90$ (Table 8.1, CSA S6:19) • $\phi_{frp} = 0.80 * 0.75 = 0.60$ (Table 16.2, CSA S6:19) • $\alpha 1 = 0.85 - 0.0015(25) = 0.813$ (Cl 8.8.3, CSA S6:19) • $\beta_1 = 0.97 - 0.0025(25) = 0.908$ (Cl 8.8.3, CSA S6:19)

1. Start by assuming the section is Tension Controlled. Establish location of Neutral axis, c, assuming tension rebar yields and compression rebar does not yield. Solving the balance of forces will give a quadratic equation to solve:

$$C_c + C_s = T_s + T_{frp}$$

Subbing in the design variables for the internal forces:

$$\alpha_1 \phi_c f_c' \beta_1 bc + \phi_s E_s \varepsilon_{frpu} \left(\frac{c - d'}{h - c}\right) A_s' = \phi_s f_y A_s + \phi_{frp} E_{frp} \varepsilon_{frpu} A_{frp}$$

Re-arranging into a quadratic equation:

$$\alpha_1 \phi_c f_c' \beta_1 bc^2 - \left[\alpha_1 \phi_c f_c' \beta_1 bh + \phi_s E_s \varepsilon_{frpu} A_s' + \phi_s f_y A_s + \phi_{frp} E_{frp} \varepsilon_{frpu} A_{frp}\right] c + \left[\phi_s E_s \varepsilon_{frpu} A_s' d' + \phi_s f_y A_s h + \phi_{frp} E_{frp} \phi_{frp} E_{frp} \varepsilon_{frpu} A_{frp}{}_{frpu} A_{frp} h\right] = 0$$

Subbing in the values presented above and solving for the neutral axis, c:

$$c = 58.86mm \quad \text{[CSA S806:17]}$$

$$c = 55.82mm \quad \text{[CSA S6:17]}$$

2. The strain in the internal steel rebar can be checked to verify assumptions made in step 1 using the following equations:

$$\varepsilon_s = \varepsilon_{frp}\left(\frac{d-c}{h-c}\right)$$

$$\varepsilon_s' = \varepsilon_{frp}\left(\frac{c-d'}{h-c}\right)$$

Looking first at the S806:17 code:

$$\varepsilon_s = 0.007\left(\frac{225-58.70}{250-58.70}\right) = 0.0061 > \varepsilon_y$$

$$\varepsilon_s' = 0.007\left(\frac{25-58.86}{250-58.86}\right) = 0.0012 < \varepsilon_y$$

Looking next at the S6:19 code:

$$\varepsilon_s = 0.007\left(\frac{225-58.70}{250-58.70}\right) = 0.0052 > \varepsilon_y$$

$$\varepsilon_s' = 0.007\left(\frac{25-58.70}{250-58.70}\right) = 0.0011 < \varepsilon_y$$

The assumptions of strain are correct and the value of c can be used to calulate the moment resistance, Mr.

3. Using the design equations presented in Appendix A, calculate the factored moment resistance , Mr.

$$R = M_r = C_s\left(\frac{\beta_1 c}{2} - d'\right) + T_s\left(d_i - \frac{\beta_1 c}{2}\right) + T_f\left(h - \frac{\beta_1 c}{2}\right)$$

Subbing in the design variables for the internal forces:

$$M_r = \phi_s A_s' E_s \varepsilon_s'\left(\frac{\beta_1 c}{2} - d'\right) + \phi_s A_{si} f_{si}\left(d_i - \frac{\beta_1 c}{2}\right) + \phi_f A_{frp} E_{frp} \varepsilon_{frpu}\left(h - \frac{\beta_1 c}{2}\right)$$

Subbing in the values for all variables yields the factored moment resistance:

$$\boldsymbol{M_r = 21.48\ kNm} \quad \textbf{[CSA S806:17]}$$

$$\boldsymbol{M_r = 21.91\ kNm} \quad \textbf{[CSA S6:17]}$$

B.3 ACI 440.2R:17 Ultimate Moment Resistance of EB FRP Strengthened RC Beam

ACI 440.2R:17
• $\varepsilon_{fd} = 0.41\sqrt{\frac{f_c^{'}}{nE_{frp}t_{frp}}} \leq 0.9\varepsilon_{frpu}$ (Eq.[10.1.1], ACI440.2R:17) • ϕ factor given in Table B2. • $\Psi_{frp} = 0.85$ (Cl 10.2.10, ACI 440.2R:19) • $\alpha 1 = 0.85 - 0.0015(25) = 0.813$ • $\beta_1 = 0.97 - 0.0025(25) = 0.908$

Table B2. Phi Factors for the ACI 440.2R:17 Design Standard (Eq.[10.2.7] , ACI 440.2R:17).

ϕ	Range
0.90	$\varepsilon_t > 0.005$
$0.65 + \frac{0.25(\varepsilon_t - \varepsilon_y)}{0.005 - \varepsilon_y}$	$\varepsilon_y < \varepsilon_t < 0.005$
0.65	$\varepsilon_t < \varepsilon_y$

1. Start by assuming the section is Tension Controlled. Determine the limit on the maximum tensile FRP strain.

$$\varepsilon_{fd} = 0.41\sqrt{\frac{23}{2 * 235{,}000 * 0.111}} = 0.009 \leq (0.9 * 0.0143) = 0.012$$

The debonding strain of 0.009 is smaller of the two limits and will be used for analysis.

2. Establish location of Neutral axis, c, assuming tension rebar yields and compression rebar does not yield. Solving the balance of forces will give a quadratic equation to solve:

$$C_c + C_s = T_s + T_{frp}$$

Subbing in the design variables for the internal forces:

$$\alpha_1 f_c' \beta_1 bc + E_s \varepsilon_{frpu}\left(\frac{c - d'}{h - c}\right)A_s' = f_y A_s + E_{frp}\varepsilon_{frpu}A_{frp}$$

Re-arranging into a quadratic equation:

$$\alpha_1 f_c' \beta_1 b c^2 - \left[\alpha_1 f_c' \beta_1 b h + E_s \varepsilon_{frpu} A_s' + f_y A_s + E_{frp} \varepsilon_{frpu} A_{frp}\right] c + \left[E_s \varepsilon_{frpu} A_s' d' + f_y A_s h + E_{frp} E_{frp} \varepsilon_{frpu} A_{frp} h\right] = 0$$

Subbing in the values presented above and solving for the neutral axis, c:

$$c = 51.07mm \quad \text{[ACI 440.2R:17]}$$

3. The strain in the internal steel rebar can be checked to verify assumptions made in step 2 using the following equations and the ultimate strain found in step 1:

$$\varepsilon_s = \varepsilon_{frp}\left(\frac{d-c}{h-c}\right) = 0.009\left(\frac{225-51.07}{250-51.07}\right) = 0.0078 > \varepsilon_y$$

$$\varepsilon_s' = \varepsilon_{frp}\left(\frac{c-d'}{h-c}\right) = 0.009\left(\frac{51.07-25}{250-51.07}\right) = 0.0012 < \varepsilon_y$$

The assumptions of strain are correct and the value of c can be used to calulate the moment resistance, Mr.

4. Using the design equations presented in Appendix A, calculate the unfactored moment resistance , M_u.

$$M_u = C_s\left(\frac{\beta_1 c}{2} - d'\right) + T_s\left(d_i - \frac{\beta_1 c}{2}\right) + T_f\left(h - \frac{\beta_1 c}{2}\right)$$

Subbing in the design variables for the internal forces:

$$M_r = A_s' E_s \varepsilon_s'\left(\frac{\beta_1 c}{2} - d'\right) + A_{si} f_{si}\left(d_i - \frac{\beta_1 c}{2}\right) + \psi_{frp} A_{frp} E_{frp} \varepsilon_{fd}\left(h - \frac{\beta_1 c}{2}\right)$$

Subbing in the values for all variables yields the factored moment resistance:

$$M_u = 27.91\ kNm \quad \text{[ACI 440.2R:17]}$$

The strain in the rebar must be checked in order to choose the Phi factor. The strain in the most extreme tensile internal steel rebar is found to be 0.0078 at ultimate limit state. Based on the range in table B2, a Phi factor of 0.9 is chosen.

$$M_r = \phi M_u = 0.9*27.91 \text{ kNm}$$

$$\boldsymbol{M_r = 25.12\ kNm} \quad \textbf{[ACI 440.2R:17]}$$

APPENDIX C: ULTIMATE RESPONSE AT FAILURE OF 'MESH20' SFE STRENGTHENED BEAM CONFIGURATION (IFC DEBONDING FAILURE)

Figure C.1)

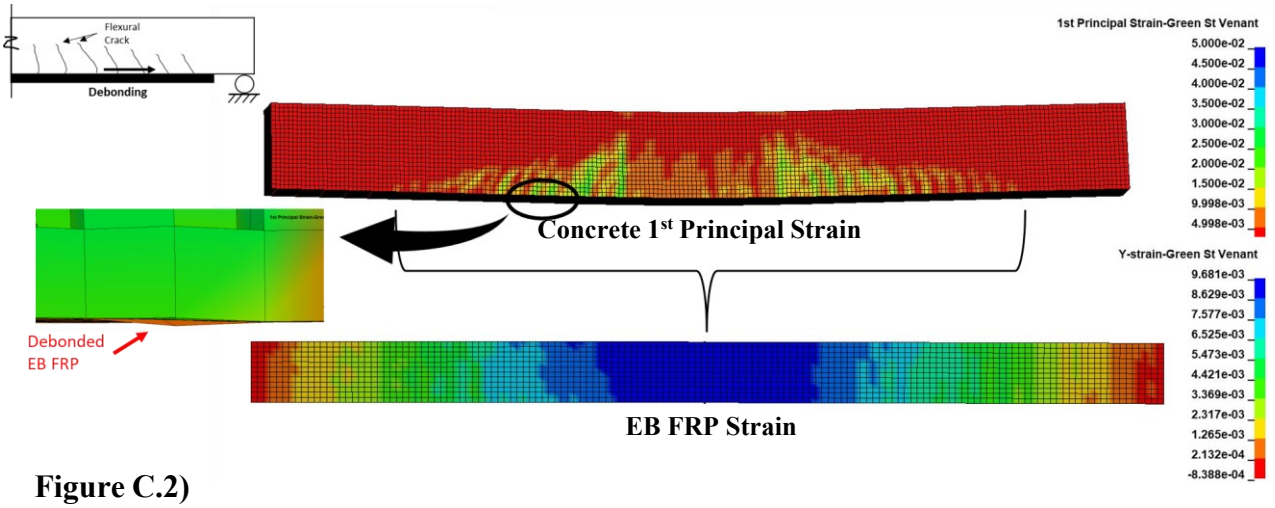

Figure C.2)

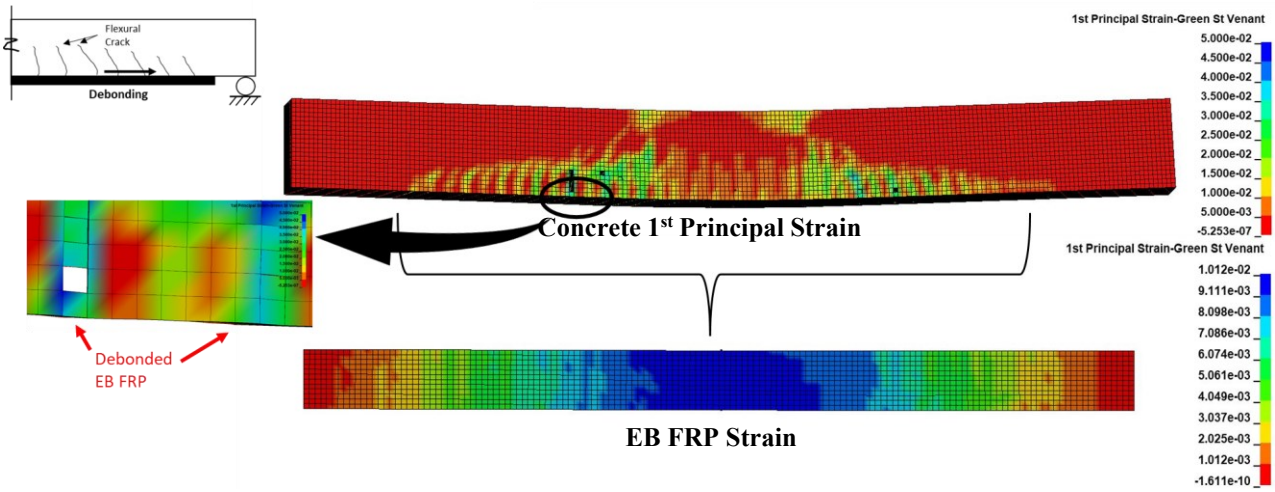

Figure C.3)

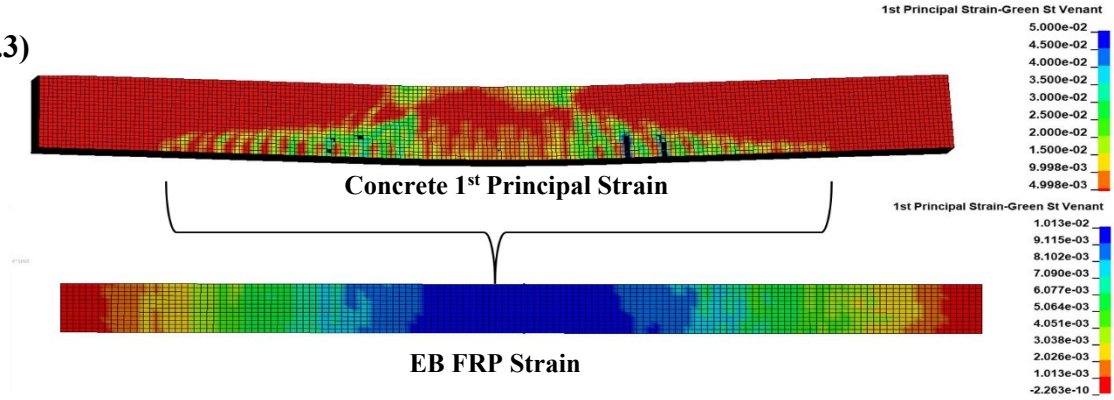

APPENDIX C: ULTIMATE RESPONSE AT FAILURE OF 'MESH20' SFE STRENGTHENED BEAM CONFIGURATION (IFC DEBONDING FAILURE)

Figure C.4)

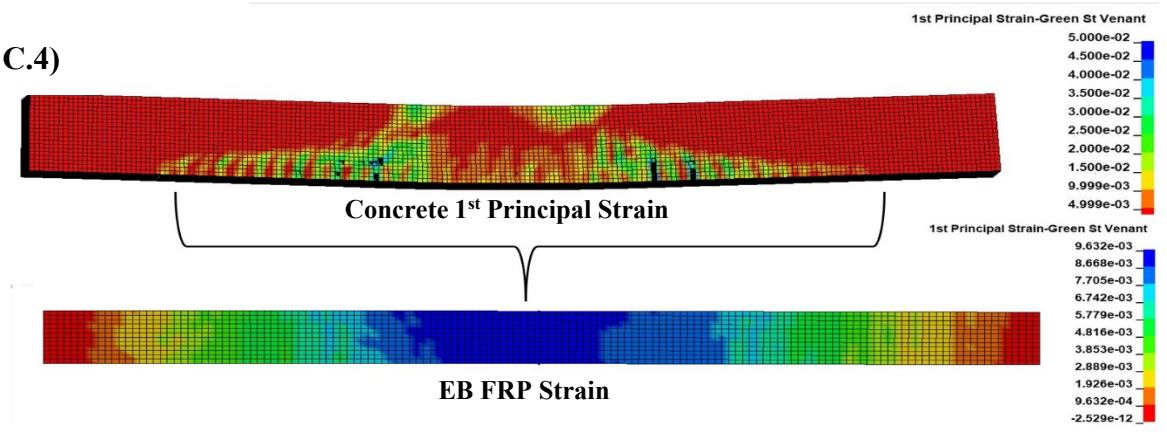

Figure C.5)

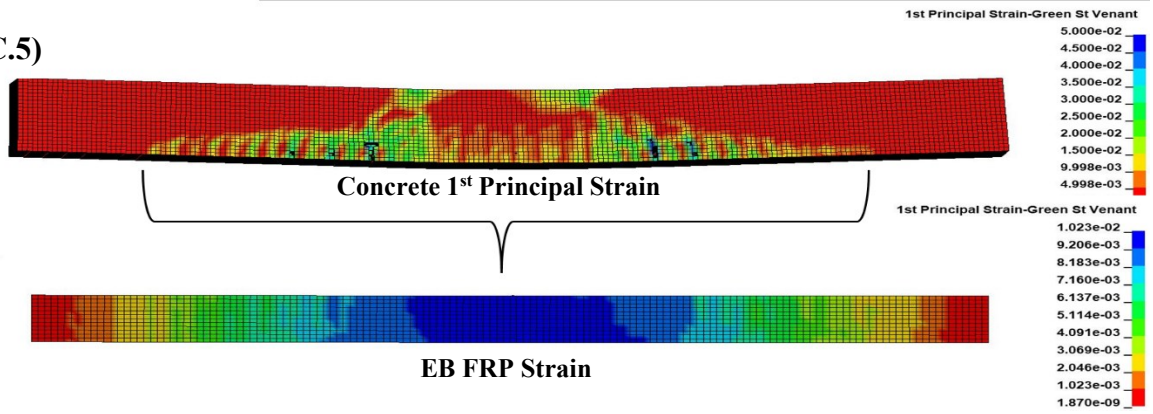

Figure C.6)

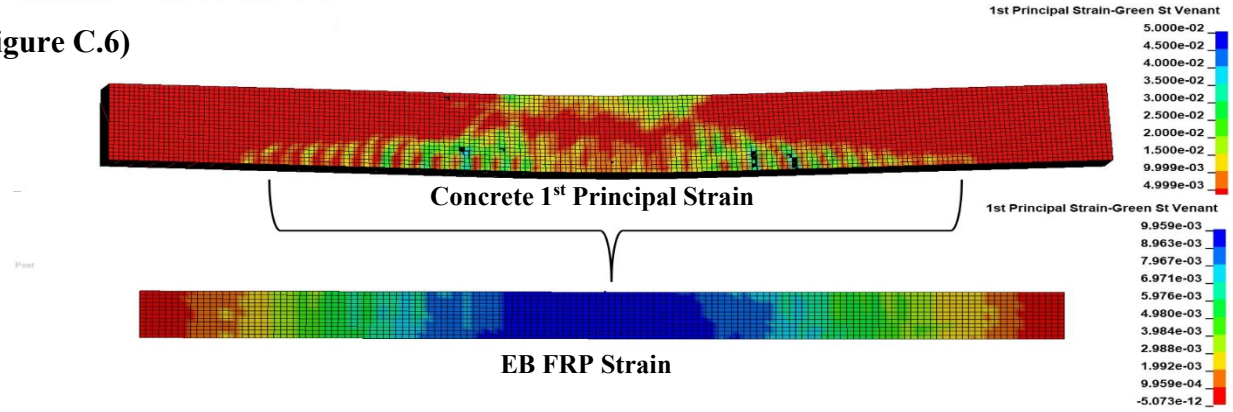

Figure C.7)